Oncolytic Reovirus Induces Intracellular Redistribution of Ras to Promote Apoptosis and Progeny Virus Release

by

Katy Garant

Submitted in partial fulfilment of the requirements
for the degree of Doctor of Philosophy

at

Dalhousie University
Halifax, Nova Scotia
August 2014

To my husband, Rémi

TABLE OF CONTENTS

LIST OF TABLES

LIST OF FIGURES

ABSTRACT

Ras is a dynamic protein capable of interacting with plasma membrane microdomains and intracellular membranes. Its activity, as controlled by post-translational modifications, is essential in regulating cell growth, differentiation, and death. Consequently, mutations that result in constitutive Ras activity lead to cell transformation, and are associated with over 30% of all human cancers. Reovirus is a naturally oncolytic virus that preferentially replicates in Ras-transformed cells and is currently undergoing clinical trials as a cancer therapeutic. It was previously demonstrated that Ras transformation promotes uncoating of the parental virion during entry, production of infectious viral progeny, and virus release through apoptosis; however, the mechanism behind the latter is not well understood. This study set out to determine whether reovirus alters the intracellular location of oncogenic Ras to induce apoptosis of H-RasV12-transformed fibroblasts. Here, I show that reovirus decreases palmitoylation levels of H-RasV12 and causes accumulation of the oncogenic protein in the Golgi body through Golgi fragmentation. With the Golgi body being the site of Ras palmitoylation, treatment of target cells with the palmitoylation inhibitor, 2-bromopalmitate (2BP), prompts a greater accumulation of H-RasV12 in the Golgi body, as well as a dose-dependent increase in reovirus release and spread. Use of 2BP on cell lines expressing H, N, or K-Ras oncogenic isoforms causes an increase in reovirus release that correlates with the palmitoylation status of the respective Ras protein. Alternatively, tethering H-RasV12 to the plasma membrane, and preventing its movement back to the Golgi, allows for efficient virus production, but results in basal levels of reovirus-induced cell death. Furthermore, treatment of H-RasV12 cells with the FKBP12 inhibitor, FK506, which is known to retain Ras at the plasma membrane, reduces virus-related death and plaque size. Analysis of Ras downstream signalling reveals that cells expressing cycling H-RasV12 have elevated levels of phosphorylated JNK, and that Ras retained at the Golgi body by 2BP increases activation of the MEKK1/MKK4/JNK signalling pathway to promote cell death. Collectively, the data suggests that reovirus induces Golgi fragmentation of target cells, and the subsequent accumulation of oncogenic Ras in the Golgi body initiates apoptotic signalling events required for virus release.

LIST OF ABBREVIATIONS AND SYMBOLS USED

˚C - Degrees Celsius

2BP - 2-Bromohexadecanoic Acid / 2-Bromopalmitate

AA - Antibiotic-Antimycotic

AF - Alexa Fluor

Alk P - Alkaline Phosphatase

ANOVA - Analysis of Variance

APT-1 - Acyl-Protein Thioesterase 1

ATCC - American Type Culture Collection

βME - Beta Mercaptoethanol

BSA - Bovine Serum Albumin

C - Cysteine

CAAX - Cysteine, Aliphatic residue, Aliphatic residue, Any amino acid

CD8 - Cluster of Differentiation 8

CO_2 - Carbon Dioxide

Cy - Cyanine

DHHC9 - DHHC Domain-Containing 9

Diablo - Direct Binding of IAP binding protein with low isoelectric point, PI

DMEM - Dulbucco's Modified Eagle Medium

DMSO - Dimethyl Sulfoxide

DNA - Deoxyribonucleic Acid

DNase - Deoxyribonuclease

dsRNA - Double-stranded RNA

DPI - Dual Prenyltransferase Inhibitor

EDTA - Ethylenediaminetetraacetic acid

EGF - Epidermal Growth Factor

EGFR - Epidermal Growth Factor Receptor

ER - Endoplasmic Reticulum

ERK 1/2 - Extracellular Signal-Regulated Kinases 1 and 2

FACS - Fluorescence-Activated Cell Sorting

FC - Flow Cytometry

FKBP12 - FK506-Binding Protein 12

FTase - Farnesyltransferase

FTI - Farnesyltransferase Inhibitor

FTS - Farnesylthiosalicylic Acid

G - Glycine

GAP - GTPase Activating Protein

GAPDH - Glyceraldehyde 3-Phosphate Dehydrogenase

GCP16 - Golgi Complex-Associated Protein of 16 kDa

GDP - Guanosine Diphosphate

GEF - Guanine Nucleotide Exchange Factor

GGTase-I - Geranylgeranyltransferase Type I

GGTIs - Geranylgeranyltransferase Inhibitors

Grb2 - Growth Factor Receptor-Bound 2

GSK-3 - Glycogen Synthase Kinase 3

GTP - Guanosine Triphosphate

GTPase - Guanosine Triphosphatase

h - Hour(s)

HA - Hemagglutinin

hpi - Hours Post-Infection

H-Ras - Harvey Rat Sarcoma Viral Oncogene Homolog

HRP - Horseradish Peroxidase

HVR - Hypervariable Region

ICC - Immunocytochemistry

Icmt - Isoprenylcysteine Carboxylmethyltransferase

IF - Immunofluorescence

IFN-β - Interferon Beta

IgG - Immunoglobulin G

IP - Immunoprecipitation

ISVP - Intermediate Subviral Particle

JAM - Junctional Adhesion Molecule

JMEM - Joklik's Modified Eagle Medium

K - Lysine

kD - Kilodaltons

KDEL - Lysine, Aspartic Acid, Glutamic Acid, Leucine

K-Ras - Kirsten Rat Sarcoma Viral Oncogene Homolog

MAPK - Mitogen-Activated Protein Kinase

MEM - Modified Eagle Medium

MEK 1/2 - MAPK/ERK Kinase

MEKK1 - MEK Kinase 1

MLB - Mg^{2+} Lysis Buffer

MOI - Multiplicity of Infection

NEAA - Non-Essential Amino Acids

NEM - N-Ethylmaleimide

NF-κB - Nuclear Factor Kappa B

NMS - Normal Mouse Serum

N-Ras - Neuroblastoma Rat Sarcoma Viral Oncogene Homolog

NT - No Treatment

P - Proline

PAT - Palmitoyl Acyltransferase

PBS - Phosphate Buffered Saline

PDK1 - Phosphoinositide Dependent Protein Kinase-1

pfu - Plaque Forming Unit

PH - Pleckstrin Homology

PI3K - Phosphoinositide 3-Kinase

PIC - Protease Inhibitor Cocktail

PIP_2 - Phosphatidylinositol (4,5)-Bisphosphate

PIP_3 - Phosphatidylinositol (3,4,5)-Trisphosphate

PKB - Protein Kinase B (also known as Akt)

PKC - Protein Kinase C

PKR - dsRNA-Activated Protein Kinase

PMSF - Phenylmethylsulfonyl Fluoride

PTB - Phosphotyrosine Binding

PTEN - Phosphatase and Tensing Homolog

PTKR - Protein Tyrosine Kinase Receptor

qRT-PCR - Quantitative Real-Time Polymerase Chain Reaction

RA - Ras Association

Ral - Ras-like

RalBP1 - Ral Binding Protein 1

Ras - Rat Sarcoma

RasGRP - Ras Guanyl Nucleotide-Releasing Protein

RASSF - Ras Association Domain-Containing Family

RBD - Ras Binding Domain

Rce1 - Ras Converting Enzyme 1

RE - Recycling Endosome

Reovirus - Respiratory Enteric Orphan Virus

RIG-1 - Retinoic Acid-Inducible Gene 1

Rin1 - Ras Interaction/Interference Protein-1

RKTG - Raf Kinase Trapping to Golgi

RNA - Ribonucleic Acid

RNAi - RNA Interference

rpm - Revolutions Per Minute

RT - Room Temperature

S - Serine

SAPK/JNK - Stress Activated Protein Kinase/Jun N-Terminal Kinase

SDS-PAGE - Sodium Dodecyl Sulfate Polyacrylamide Gel Electrophoresis

SH2 - Src Homology Region 2

Smac - Second Mitochondria-Derived Activator of Caspases

SOS - Son of Sevenless

T3D - Type 3 Dearing

TBK1 - Tank Binding Kinase 1

TBST - Tris-Buffered Saline Tween

TGN - Trans Golgi Network

Tiam1 - T-Cell Lymphoma Invasion and Metastasis-Inducing Protein 1

TRAIL - Tumor Necrosis Factor-Related Apoptosis-Inducing Ligand

UI - Uninfected

V - Valine

WB - Western Blot

ACKNOWELDGEMENTS

Foremost, I would like to thank my supervisor, Dr. Patrick Lee, for giving me the opportunity to develop my own research project, and work independently in pursuit of my Ph.D. degree. I have the utmost respect for you and appreciate your continued enthusiasm in research. Many thanks to two former Lee Lab members: Dr. Maya Shmulevitz and Dr. Luzhe Pan, who provided amazing guidance, scientific expertise, silliness, and life-long friendship. You are both such wonderful people and I wish the absolute best for you and your families. I miss having you both around very much. Also, to former member, Dr. Da Pan, I admire your work ethic, crazy memory skills, and willingness to help anyone. Thank you for all of your help and heartfelt discussions over the years. I would also like to thank the rest of the Lee Lab: Cheryl for putting up with all of us and lending a kind listening ear; Derek for ridiculous impressions and making me smile; and Dan and Tanveer for both your honesty and discussions on life (I hope things turn out amazing for both of you).

I would like to thank the members of my supervisory committee: Dr. Roy Duncan, Dr. Chris Richardson, Dr. Neale Ridgway, and Dr. Kirill Rosen for providing excellent discussion, suggestions, and guidance throughout the years. It was nice to gain different perspectives on my research and I know my work is better because of you all. Many thanks to the wonderful administration at Dalhousie University. Specifically, Susan White, Donalda Mitchell-Snell, and Christine Anjowski in the Department of Microbiology and Immunology, and Danielle Pottie in the Faculty of Graduate Studies. Also, a big thank you to Stephen Whitefield in the Cellular & Molecular Digital Imaging

Facility and to Mary-Ann Trevors in the flow cytometry facility for their fantastic technical support.

Also, thank you to the various funding agencies that have supported me and my research over the years. These include personal scholarships and fellowships from NSERC, Killam, and NSHRF, as well as, in-house graduate scholarships and President's awards.

Last, but certainly not the least, I would like to thank all of my family and friends. I know my work has been hard on all of you, and has made me miss out on a lot of things, but I sincerely appreciate all of your support and understanding over the years, and cherish the times when we could get together. I could not have finished this degree without the support, laughter, and love from my husband, Rémi. I am so lucky to have you in my life, and I cannot wait for the next chapter of our lives to begin. You mean the world to me.

CHAPTER 1: INTRODUCTION

1.1. Ras

The rat sarcoma (Ras) superfamily consists of over 150 human members that exist as small guanosine triphosphatases (GTPases) (Wennerberg et al., 2005). Due to their critical role in cellular function, these genes have remained evolutionarily conserved with orthologs identified in several eukaryotes, including *Drosophila melanogaster*, *Saccharomyces cerevisiae*, *Caenorhabditis elegans*, and *Danio rerio* (Colicelli, 2004; Cox and Der, 2010). Based on sequence and functional similarities, the human Ras superfamily is subdivided into five main branches: Ras, Rho, Rab, Ran, and Arf. These small GTPases or monomeric G-proteins are approximately 20 to 25 kilodaltons (kD) in size and function as binary molecular switches. Structural differences, post-translational modifications, and specific regulatory and effector proteins enable these small GTPases to control a wide array of cellular processes, such as proliferation, motility, vesicular trafficking, polarity, differentiation, and death.

Some of the most extensively studied small GTPases are the Ras family of proteins. This heightened interest stems from initial observations made during the 1960s which concluded that viral oncogenes (*v-H-ras* and *v-K-ras*) derived from rat sarcoma viruses contributed to cellular transformation and cancer development (Harvey, 1964; Kirsten and Mayer, 1967). Further inquiries led to the discovery of human Ras oncogene homologs and their involvement in human oncogenesis and disease (Malumbres and Barbacid, 2003). The following will focus on Ras and its role in cancer development while highlighting a virus that utilizes aspects of the Ras pathway for its own propagation.

1.1.1. Structure and Function

There are three human *ras* genes that encode four protein products: Harvey (H)-Ras, Neuroblastoma (N)-Ras, Kirsten (K)-Ras4A, and K-Ras4B, with the latter two resulting from alternative splicing of the *K-ras* locus at exon 4 (Der et al., 1982; Shimizu et al., 1983; Wang et al., 2001). These 21 kD proteins function as molecular switches and bind guanosine diphosphate (GDP) or guanosine triphosphate (GTP) to cycle between inactivated and activated states, respectively (Prior and Hancock, 2012). The highly conserved Ras sequence is 188 to 189 amino acids in length and is comprised of a G domain and hypervariable region (HVR). The G domain, which represents the first 165 amino acids, is nearly identical between isoforms (> 90%) and contains the effector and switch regions (Figure 1.1A). The effector domain, which is also located in the switch I region, enables binding of activated Ras to its downstream effectors, while the switch I and II domains are responsible for conformational changes during GTP binding and hydrolysis (Johnson and Mattos, 2013). Ras mainly exists in its GDP-bound form in inactive and non-dividing cells. In the presence of certain extracellular stimuli, Ras quickly cycles into its GTP-bound state with the help of guanine nucleotide exchange factors (GEFs), such as son of sevenless (SOS) and Ras guanyl nucleotide-releasing protein (RasGRP) (Vigil et al., 2010). The switch domains alter the structure of Ras to increase its affinity for downstream effectors and as a result, certain signalling pathways are initiated. Although Ras possesses its own intrinsic GTPase activity, it is relatively inefficient and GTPase activating proteins (GAPs), such as neurofibromin and p120, promote GTP hydrolysis and return Ras back to its inactive, GDP-bound state. Single amino acid substitutions, typically at sites 12, 13, and 61, result in mutated Ras proteins

(Bos, 1989). Consequently, these proteins remain GTP-bound and constitutively activated; rendering RasGAPs ineffective and leaving signalling to downstream effectors unregulated. These mutations give rise to the oncogenic form of Ras and unsurprisingly, are found in over 30% of all human cancers.

Since the isoforms display a high degree of sequence homology within their G domains, and interact with common upstream activators and downstream effectors, it was originally presumed that H-, N-, and K-Ras were functionally redundant. However, increasing scientific evidence supports the notion that the isoforms have specific functional roles (Castellano and Santos, 2011). While essentially ubiquitous, the expression levels of H-, N-, and K-Ras actually vary depending on cell type and developmental stage (Leon et al., 1987). If murine tissue is considered, *K-ras* transcripts are prevalent in the gut and thymus, but are infrequently detected in skeletal muscle, ovary, liver, and skin. *N-ras* transcripts are abundant in the thymus and testes, but scarce in the kidney and liver, while *H-ras* transcripts are highest in the skin, skeletal muscle, and brain, but lowest in the ovary and liver. In regards to the K-Ras variants, expression of K-Ras4B dominates over K-Ras4A in the majority of tissues, and is also critical to murine development (Pells et al., 1997). Mice deficient in K-Ras4A are able to develop normally if they are in the presence of a functioning K-Ras4B isoform, while those harboring a homozygous *K-ras* null mutation are incapable of survival (Koera et al., 1997; Plowman et al., 2003). *H-* and/or *N-ras* knock-out mice develop and reproduce normally (Esteban et al., 2001). Interestingly, replacing *K-ras* with the *H-ras* coding sequence while still under the control of the *K-ras* promoter results in normal embryonic development, but cardiomyopathies in adult mice; suggesting some overlap between the

isoforms (Potenza et al., 2005). The variation in expression between the isoforms also extends to their prevalence in certain human cancers (Fernández-Medarde and Santos, 2011). For instance, *K-ras* mutations frequently occur in lung (>20%), colon (>40%), and pancreatic (>95%) cancers. *N-ras* mutations are commonly associated with melanomas (~20%), thyroid (~17%), and hematological malignancies, such as leukemias and lymphomas (10-20%). *H-ras* mutations are not as frequent, but have been linked to bladder (~12%) and thyroid (<16%) cancers. While some cancers have a clear association with a specific Ras isoform, other tumors will form in the presence of any oncogenic Ras or in some cases, will even contain all three activated forms (ie. thyroid malignancies) (Garcia-Rostan et al., 2003). Despite some redundancy, it is evident that Ras isoforms have specific functional roles. This is attributed to the hypervariable region in the C-terminus; the site of essential post-translational modifications (Figure 1.1A).

Figure 1.1: Ras sequence comparison and post-translational modifications. (A) A schematic representing a typical Ras sequence. Numbers above and below indicate amino acid number and sequence homology between isoforms, respectively, while roman numerals designate the locations of switch I and II domains. The enlarged hypervariable region (HVR) highlights the functional differences between isoforms. The shaded grey region represents the CAAX box while the bolded amino acids (red) indicate sites within the HVR that enable correct membrane binding and intracellular localization. (B) Newly synthesized Ras undergoes prenylation by cytosolic farnesyltransferases (FTase). The addition of a farnesyl lipid group (F) to the cysteine residue within the CAAX motif targets Ras to the ER for cleavage by Ras converting enzyme 1 (Rce1) and subsequent carboxylmethylation by isoprenylcysteine carboxylmethyltransferase (Icmt). At this point, K-Ras4B deviates from the pathway and is shuttled to the plasma membrane by an unknown mechanism. The polybasic lysine (K^+) residues in its C-terminus enable stable membrane binding. Phosphorylation of the HVR or calcium/calmodulin complex binding releases K-Ras4B from the plasma membrane, and allows it return to the endomembranes. In contrast, H- and N-Ras are palmitoylated (P) by the palmitoyl acyltransferase (PAT), DHHC9-GCP16, at the surface of the Golgi apparatus and sent to the plasma membrane via vesicle transport. Depalmitoylation by the acyl-protein thioesterase 1 (APT-1) releases H- and N-Ras from the plasma membrane and allows the proteins to move by retrograde transport back to the Golgi apparatus for subsequent palmitoylation. Image modified from Mor and Philips (2006).

A

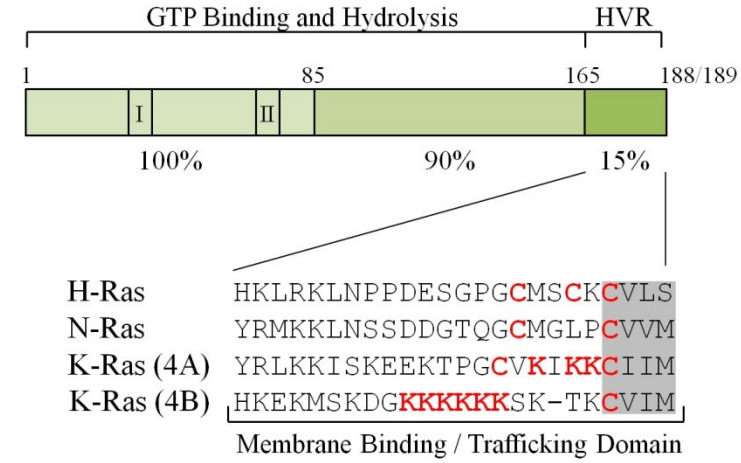
GTP Binding and Hydrolysis
HVR
1
85
165
188/189
I
II
100%
90%
15%
H-Ras HKLRKLNPPDESGPGCMSCKCVLS
N-Ras YRMKKLNSSDDGTQGCMGLPCVVM
K-Ras (4A) YRLKKISKEEKTPGCVKIKKCIIM
K-Ras (4B) HKEKMSKDGKKKKKKSK-TKCVIM
Membrane Binding / Trafficking Domain

B

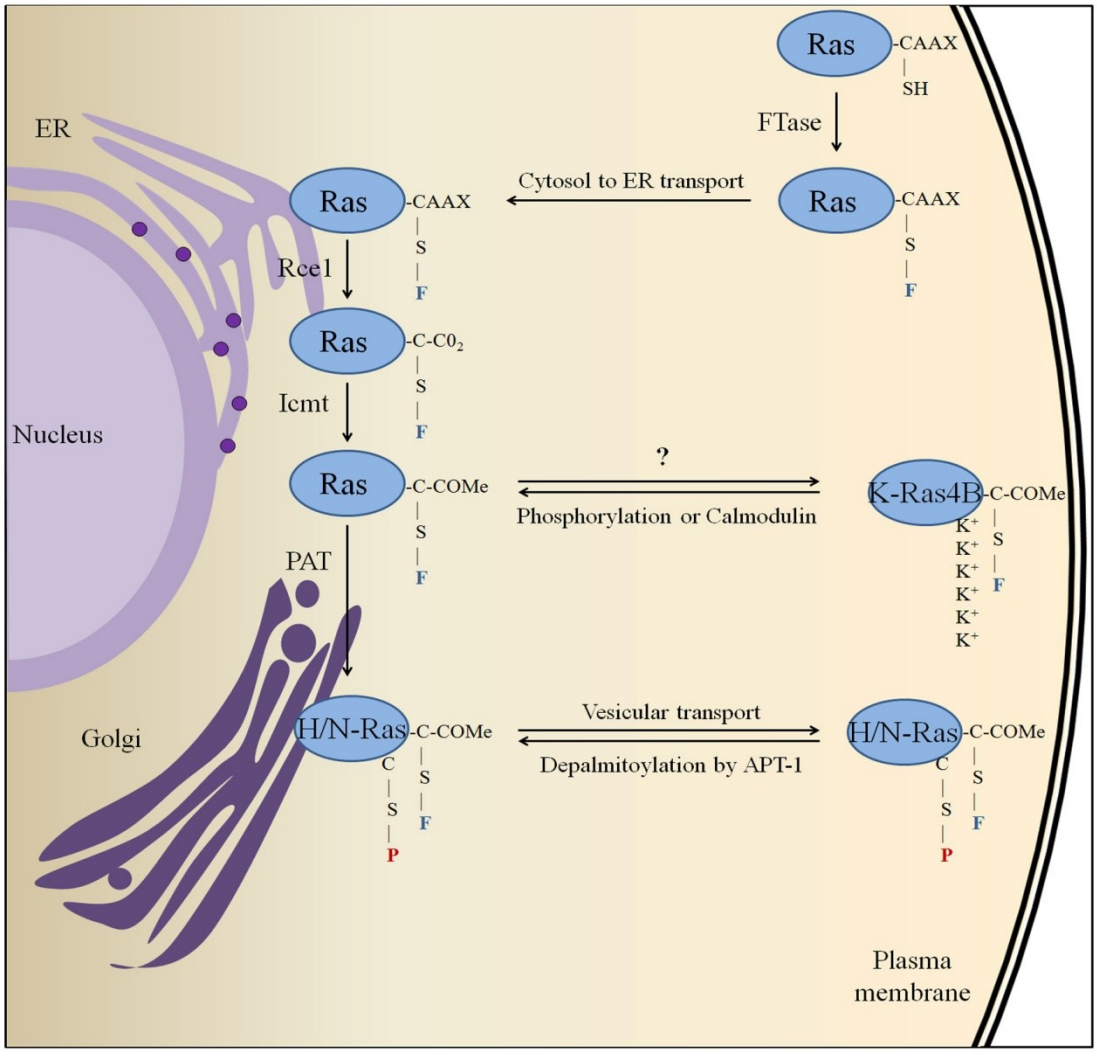
Ras
-CAAX
SH
FTase
ER
Cytosol to ER transport
Rce1
-C-C0₂
Icmt
Nucleus
-C-COMe
?
Phosphorylation or Calmodulin
K-Ras4B
PAT
Golgi
H/N-Ras
Vesicular transport
Depalmitoylation by APT-1
Plasma membrane

1.1.2. Post-Translational Modifications: Farnesylation

The hypervariable region represents the last 25 amino acids in the Ras sequence. As each isoform undergoes a series of unique post-translational modifications, sequence homology within this region is extremely low (15%) (Prior and Hancock, 2001). The post-translational modifications increase the hydrophobicity of Ras and enable an otherwise globular and hydrophilic protein to effectively participate in intracellular trafficking, membrane binding, and biological activation (Ahearn et al., 2012). A diagram illustrating Ras post-translational modifications can be found in Figure 1.1B. The HVR terminates with a CAAX motif; a sequence belonging to a large family of proteins and an indicator of prenylation (Figure 1.1A). The CAAX box, which consists of cysteine (C), two aliphatic (A) amino acids, and any (X) amino acid residue, is the location of the first set of post-translational modifications to Ras. Newly synthesized and inactive Ras is targeted by cytosolic farnesyltransferases (FTases) for prenylation (Casey et al., 1989). The FTase attaches a 15-carbon isoprenoid lipid using a thioether linkage to the cysteine residue in the CAAX motif, rendering Ras with a weak affinity for membranes and causing it to accumulate on the surface of the endoplasmic reticulum (ER). ER-resident endoprotease, Ras converting enzyme 1 (Rce1), recognizes farnesylated Ras as its substrate and cleaves the remaining -AAX amino acids from the motif (Boyartchuk et al., 1997). Further modification occurs by another ER membrane-bound enzyme, isoprenylcysteine carboxylmethyltransferase (Icmt), which methylates the carboxyl group of the lipidated cysteine residue (Dai et al., 1998). The activities of the FTase and Rce1 result in permanent modifications to Ras, whereas methylation is considered reversible. CAAX prenylation, proteolysis, and methylation are designed to increase the

hydrophobicity of the C-terminus and facilitate Ras to transiently interact with cellular membranes. Ras isoforms require a second signal to stably associate with membranes and obtain full biological activity. This occurs in the form of an additional lipid modification or inherent amino acid charge within their sequence (Hancock et al., 1990).

1.1.3. Post-Translational Modifications: Palmitoylation

At this point in Ras intracellular processing, the pathways diverge. H-, N-, and K-Ras4A travel to the Golgi apparatus for modification by the palmitoyl acyltransferase (PAT), DHHC domain-containing 9 - Golgi complex-associated protein of 16 kD (DHHC9-GCP16) (Hancock et al., 1989, 1990; Swarthout et al., 2005). DHHC9-GCP16 is one of 25 human PAT family members (Mitchell et al., 2006). These PATs share a common DHHC motif, but differ with respect to their location and substrates within the cell. Interestingly, knockdown of DHHC9 has no effect on Ras palmitoylation, suggesting that additional PATs are capable of exerting their activity on Ras (Rocks et al., 2010). DHHC9-GCP16 palmitoylates Ras on the cytosolic face of the Golgi apparatus through the addition of a 16-carbon palmitoyl group via thioester linkage to the HVR. In H-Ras, there are two cysteine residues (C181 and C184) that can be palmitoylated (Choy et al., 1999; Roy et al., 2005). Palmitoylation of C181 is required for efficient intracellular trafficking from the Golgi apparatus to the plasma membrane, while palmitoylation of C184 is important for H-Ras microlocalization within the plasma membrane itself. In contrast, N-Ras and K-Ras4A are monopalmitoylated at C181 and C180, respectively. Surprisingly, the latter two isoforms also possess a basic region of

amino acids upstream to their HVR that they require for additional membrane binding and stabilization (Laude and Prior, 2008).

While Ras incurs a weak affinity for membranes through farnesylation, the addition of one or two palmitoyl groups increases this affinity (>100-fold) and allows Ras to transit via Golgi budded vesicles to the plasma membrane for activation (Shahinian and Silvius, 1995). Other than vesicles, recycling endosomes (REs) have recently been identified as a stopover for H- and N-Ras during their Golgi to plasma membrane transition, and it appears to be regulated by palmitoylation (Misaki et al., 2010). Monopalmitoylated H-Ras (C181) is directly transported to the plasma membrane, whereas dually palmitoylated H-Ras (C181 and C184) associates with REs. Unexpectedly, monopalmitoylated N-Ras also localizes to REs, as its slightly upstream basic region provides enough electrostatic interaction between the protein and the endosomal membrane to incur stability. Once at the plasma membrane, Ras localizes to different membrane microdomains based on its palmitoylation and GTP-loading status (Roy et al., 2005). The plasma membrane is not a homogeneous structure, and is subdivided into lipid rafts and disordered membranes (Rajendran and Simons, 2005). Lipid rafts are highly ordered and tightly packed structures that float freely throughout the plasma membrane and are rich in cholesterol and glycosphingolipids. If they contain any of the caveolin family of proteins, they are referred to as caveolae. In contrast, the disordered membrane refers to highly fluid domains that are full of unsaturated phospholipids. N-Ras has been detected in both caveolin-positive and negative rafts, while H-Ras associates with lipid rafts and the disordered membrane (Kranenburg et al., 2001; Prior et al., 2001). Interesting, these microdomains can be further subdivided into

nanoclusters. A Ras nanocluster is an area of less than 20 nm in diameter that contains approximately seven spatially concentrated Ras proteins and serves as a platform for downstream effector recruitment and efficient signal propagation (Cho and Hancock, 2013). Ras must first interact with the galectin family of carbohydrate-binding proteins in order to form a nanocluster. Activated H-Ras recruits galectin-1 from the cytosol to the plasma membrane where they form a complex in microdomains lacking cholesterol (Belanis et al., 2008). Acting as a scaffold, galectin-1 stabilizes GTP-bound Ras, and the resulting nanoclusters serve as a platform for Ras downstream signalling. Suppression of galectin-1 forces H-Ras out of the plasma membrane and causes its activity to be inhibited, while overexpression of galectin-1 increases the level of activated H-Ras nanoclustering (Paz et al., 2001). In addition to directing protein trafficking and conferring stability to protein-membrane interactions, palmitoylation also dictates plasma membrane microlocalization (Misaki et al., 2010; Roy et al., 2005). As previously mentioned, monopalmitoylated H-Ras (C181) is directly shuttled to the plasma membrane, and once there, it is confined to lipid rafts. N-Ras, which can transit via REs, also localizes to lipid rafts. H-Ras requires palmitoylation at C184 to move from lipid rafts to raft-free regions. Furthermore, only GDP-bound H-Ras interacts with lipid rafts, while activated H-Ras complexes with galectin-1 to form nanoclusters in the bulk plasma membrane (Rotblat et al., 2004, 2010). Overall, the post-translational modifications, activation status, and structure of the individual Ras isoforms determine which membranes they interact with on their way to the plasma membrane and their lateral movements within it.

1.1.4. Post-Translational Modifications: Depalmitoylation

Unlike farnesylation, palmitoylation is a readily reversible process. While palmitoylation only occurs at the Golgi, depalmitoylation has been detected throughout the cell (Rocks et al., 2005). In order for depalmitoylation to proceed, a small peptidyl-prolyl isomerase known as FK506-binding protein 12 (FKBP12) must first bind the C-terminus of H- or N-Ras (Ahearn et al., 2011). FKBP12 catalyzes the *cis-trans* isomerization of proline (P179) within the HVR and this conformational change primes Ras for depalmitoylation by the putative acyl-protein thioesterase 1 (APT-1) (Duncan and Gilman, 1998). The resulting depalmitoylated Ras cycles back to the Golgi apparatus for another round of palmitoylation and subsequent vesicular transport to the plasma membrane (Rocks et al., 2005). Galectin-1, which was previously mentioned for its involvement in H-Ras nanoclustering, also acts as a molecular chaperone and returns depalmitoylated H-Ras to the Golgi complex (Belanis et al., 2008). Inhibition of FKBP12 by FK506 results in plasma membrane accumulation of H- or N-Ras (Ahearn et al., 2011). This is also the case for short-term inhibition of APT-1 by palmostatin B (Dekker et al., 2010). Long-term inhibition of APT-1 causes a re-distribution of H- and N-Ras to the endomembranes and a reversion of the transformed phenotype in MDCK cells. Ras itself has a half-life of 24 h, but its palmitoyl groups have a half-life of 20 min to 2.4 h for N- and H-Ras, respectively (Lu and Hofmann, 1995; Magee et al., 1987). N-Ras goes through the deacylation cycle faster than H-Ras since only one palmitoyl group needs to be removed, and as a result, it is also more abundant in the Golgi apparatus (Rocks et al., 2005). Intriguingly, GTP-loaded Ras is depalmitoylated faster than GDP-bound Ras (Baker et al., 2003). This further extends to the constitutively active form, as the

palmitate turnover of oncogenic H-Ras is significantly reduced (<10 min) when compared to its wild-type counterpart. The altered conformation of the mutated H-Ras causes the palmitoylated cysteine residues to become more accessible to the palmitoyl thioesterase.

1.1.5. Post-Translational Modifications: K-Ras4B

As opposed to the other Ras isoforms, K-Ras4B does not require palmitoylation as its second signal. Slightly upstream of its farnesylated cysteine residue and still within its HVR, is a string of polybasic lysine residues (Hancock et al., 1990). K-Ras4B gets shuttled directly from the ER to the plasma membrane by a poorly understood mechanism that potentially involves the use of microtubules and/or cytosolic chaperones (Nancy et al., 2002; Thissen et al., 1997). The positively charged lysine residues of K-Ras4B interact with the negatively charged phospholipid heads of the plasma membrane inner leaflet (Hancock et al., 1990). The electrostatic interaction provided by the lysine residues coupled with the initial farnesylation modification establishes stable membrane association and allows K-Ras4B to obtain full biological activity. K-Ras4B preferentially associates with the disordered microdomain of the plasma membrane, and uses galectin-3 and actin to form nanoclusters (Elad-Sfadia et al., 2004; Shalom-Feuerstein et al., 2009). In order to leave the plasma membrane, K-Ras4B utilizes phosphorylation as a farnesyl-electrostatic switch (Ballester et al., 1987; Bivona et al., 2006). Phosphorylation of serine (S181) by protein kinase C (PKC) neutralizes the net charge of the polybasic region and causes K-Ras4B to lose membrane affinity and localize to endomembranes. Alternatively, it has been shown that glutamate stimulated hippocampal neurons can

recruit calcium/calmodulin complexes to the plasma membrane and sequester the K-Ras4B farnesylated membrane anchor and polybasic region (Fivaz and Meyer, 2005). Similar to above, the ability to stably interact with membranes is lost and dissociated K-Ras4B returns back to internal membranes, such as the Golgi complex and endosomes. In either case, only one modification can occur at a time (Alvarez-Moya et al., 2010). Phosphorylation and calmodulin binding both involve the K-Ras4B polybasic region and consequently, the presence of one prevents the other from occurring.

Taken collectively, it is clear that the HVR is modified by specific post-translational modifications to each of the Ras isoforms. These modifications facilitate the movement of Ras to the plasma membrane, stabilize its interaction for activation, and when its activity is no longer required, release Ras back to intracellular membranes. The following section will discuss Ras activation and highlight the main signalling pathways and biological outcomes initiated by the activated protein.

1.1.6. Ras Activation and Downstream Signalling

To recall, activated Ras binds to downstream effectors and initiates signalling cascades, which in turn, regulate numerous and essential cellular processes. The effectors are identified by the presence of Ras association (RA) or Ras-binding domains (RBD) that preferentially interact with GTP-bound Ras (Wohlgemuth et al., 2005). These domains lack primary sequence homology, but share a common tertiary structure known as an ubiquitin superfold (ββαββαβ). While not all proteins containing these domains are Ras effectors, the ones that interact with Ras are well characterized. The three main Ras effectors are Raf, phosphoinositide 3-kinase (PI3K), and Ras-like guanine nucleotide

exchange factor (RalGEF). A simplified version of Ras downstream signalling can be found in Figure 1.2.

Of these effectors, the Raf family (A-Raf, B-Raf, and Raf-1) of serine/threonine kinases was the first to be identified in mammalian cells, and their activity is dependent on Ras activation (Barnier et al., 1995). The pathway is first set in motion when growth factors, such as epidermal growth factor (EGF), bind to their associated protein tyrosine kinase receptors (PTKR) (Lemmon and Schlessinger, 2000; Pawson, 2002). In response, the receptors dimerize and phosphorylate the tyrosine residues within their cytosolic domains. The residues now act as docking sites for proteins containing an SH2 (Src homology region 2) or PTB (phosphotyrosine binding) domain. The SH2 domain of the adaptor protein, growth factor receptor-bound 2 (Grb2), binds the activated receptor and recruits SOS to the plasma membrane where it constitutively binds SOS using its SH3 domains (McKay and Morrison, 2007). Acting as a RasGEF, SOS removes the GDP from post-translationally modified and plasma membrane-associated Ras, thereby allowing GTP, which is more plentiful in the cytoplasm than GDP (10-fold), to take its place (Colicelli, 2004). Activated Ras recruits Raf to the plasma membrane where it interacts with the Ras binding domain of Raf (Marais et al., 1995). Subsequent phosphorylation events lead to Raf activation, and as a serine/threonine kinase, it phosphorylates and activates MAPK/Erk 1 and 2 (MEK1/2) (Santarpia et al., 2012). In turn, MEK1/2 phosphorylates and activates extracellular signal-regulated kinase 1 and 2 (Erk1/2), which are also mitogen-activated protein kinases (MAPKs). Erk1/2, with over 200 downstream targets, can interact with cytoskeletal elements, membrane receptors, cytosolic proteins (ie. p90 ribosomal S6 kinase), and can even pass through the cytoplasm

to the nucleus to phosphorylate transcription factors, such as Elk-1, c-Fos, and c-Jun (Wortzel and Seger, 2011). With its plethora of protein interactions, the Raf/MEK/Erk signalling pathway is implicated in various biological outcomes, including cell proliferation, differentiation, and death. Therefore, it is no surprise that this pathway is linked to human oncogenesis. Activating mutations, typically in the *ras* or *B-raf* genes, lead to deregulation of this pathway and result in uncontrolled cell growth and survival. Early studies demonstrated that introducing activated Raf into murine cell lines induced transformation, and subsequent *in vivo* mouse models reinforced this pathway in tumorigenesis (Cleveland et al., 1986; Cowley et al., 1994; Davies et al., 2002). Mutations in the *ras* and *raf* genes rarely overlap in human cancers. For instance, *N-ras* and *B-raf* mutations are each associated with melanomas, but tumors rarely contain both mutated forms (Akslen et al., 2005). This suggests a level of redundancy between the activities of Ras and Raf, and stresses the importance of the Raf/MEK/Erk pathway in human oncogenesis.

The second most extensively studied Ras effector is PI3K. Class I PI3Ks consist of a regulatory p85 subunit and a catalytic p110 subunit (Jimenez et al., 2002). In response to growth factors, SOS-activated Ras activates the p110 subunit of PI3K, which catalyzes the conversion of phosphatidylinositol (4,5)-bisphosphate (PIP_2) to phosphatidylinositol (3,4,5)-trisphosphate (PIP_3) (Cantley, 2002). PIP_3 directly binds proteins containing a pleckstrin homology (PH) domain, such as phosphoinositide-dependent kinase 1 (PDK1) and Akt, and recruits them to the plasma membrane. Activation of Akt, which is also known as protein kinase B (PKB), by PDK1 promotes cell growth and survival by regulating several downstream effectors. For instance, Akt

phosphorylates and inhibits glycogen synthase kinase 3 (GSK-3), thereby preventing cyclin D from degradation and allowing cell cycle progression (Diehl et al., 1998). Akt promotes cell survival by inhibiting the pro-apoptotic factor, BAD, causing the release of anti-apoptotic proteins Bcl-2 and Bcl-XL (Datta et al., 1997). The PI3K pathway is regulated by the tumor suppressor, phosphatase and tensing homolog (PTEN), which dephosphorylates PIP_3 to PIP_2 to terminate PI3K signalling (Maehama and Dixon, 1998). The PI3K pathway is also associated with Ras-mediated oncogenesis. In a study by Gupta et al. (2007), mice were generated with point mutations in *pik3ca* to prevent the p110α subunit from interacting with Ras. When they were crossed with mice carrying the oncogenic *K-ras* allele, which normally causes lung adenocarcinoma development, there was almost no tumor formation. This exemplifies how important the Ras/PI3K interaction can be in Ras-associated tumorigenesis. In addition to mutations in Ras, PI3K itself can harbor activating mutations. This has been observed in numerous human cancers, including but not limited to, breast, colon, endometrial, liver, lung, brain, stomach, and ovarian tumors (Samuels and Waldman, 2010). Similar to Raf, Ras and PI3K mutations tend to occur independently of one another, but some overlap has been detected in endometrial and colorectal cancers (Oda et al., 2008; Velho et al., 2005). Furthermore, PTEN is one of the most commonly mutated tumor suppressors, and loss of its function leads to unregulated PI3K signalling, abnormal growth, and cancer development (Rodríguez-Escudero et al., 2011).

RalGEF is another well characterized Ras downstream effector. It serves as a link between Ras and Ral, and consists of four human family members (RalGDS, Rgl1, Rgl2, and Rgl3) (Neel et al., 2011). RalGEFs interact with Ras using their RA domains, and

subsequently activate RalA and RalB small GTPases by exchanging GDP to GTP. Similar to Ras, Ral can be inactivated by RalGAPs (Shirakawa et al., 2009). Activated Ral binds to downstream targets, such as Ral binding protein 1 (RalBP1), filamin, and components of the exocyst complex (Sec5 and Exo84) to control endocytosis, actin organization, and exocytosis, respectively (Moskalenko et al., 2002; Nakashima et al., 1999; Ohta et al., 1999). In addition to vesicular trafficking, Ral also associates with transcription factors to regulate cell proliferation and survival. RalB can cause its downstream effector, Sec5, to complex with and activate the atypical IκB kinase, Tank binding kinase 1 (TBK1) (Chien et al., 2006). TBK1 phosphorylates and activates the nuclear transcription factor, NF-κB, to promote cell survival. In terms of Ral's transforming potential, it was originally believed to be limited and likely vary between species. For instance, an H-Ras effector mutant (12V/37G) that can only interact with Ral, and not PI3K or Raf, is unable to transform rodent fibroblasts, but can transform primary human embryonic kidney cells, astrocytes, and fibroblasts (Hamad et al., 2002). More recent studies indicate that the effector plays a strong role in human cancers and their metastasis (Smith et al., 2012). Elevated levels of Ral have been detected in metastatic bladder, pancreatic, and prostate cancers, which is likely attributed to its involvement in cytoskeletal organization and cell motility. Furthermore, since Ral is associated with activation of the anti-apoptotic transcription factor, NF-κB, deregulation of this pathway can lead to tumor cell survival (Henry et al., 2000).

In addition to Raf, PI3K, and RalGEF, Ras interacts with numerous other downstream effectors. These include, but are not limited to: Tiam1, MEKK1, Rin1, PLCε and RASSF; all of which have been linked to Ras-mediated oncogenesis (Karnoub and

Weinberg, 2008). In brief, T-cell lymphoma invasion and metastasis-inducing protein 1 (Tiam1) acts as a GEF to facilitate Ras-dependent activation of Rac (Lambert et al., 2002). Activated Rac is involved in actin organization, cell migration, and cell death, and can also be activated by PI3K and RalGEFs. The Ras downstream effector, MEK kinase 1 (MEKK1), is also involved in cell death (Fuchs et al., 1998; Russell et al., 1995). Once activated, MEKK1 phosphorylates MKK4, which in turn activates p38/JNK (c-jun N-terminal kinase) signalling pathways to promote cell apoptosis. The Ras interaction/ interference protein-1 (Rin1) is capable of blocking Ras activity (Hu et al., 2005; Wang et al., 2002). Rin1 competes with Raf for Ras binding and mediates the endocytosis of PTKRs to inhibit Ras signalling and cell transformation. Lastly, members of the Ras association domain-containing family (RASSF) function as tumor suppressors and play a role in cell cycle arrest, microtubule stabilization, and apoptosis (Richter et al., 2009). While the above demonstrates the importance of Ras activation and downstream signalling from the plasma membrane, the reality is that there is an enormous amount of cross-talk between signalling pathways, and that Ras activation and signalling is further regulated by spatially distinct GEFs, GAPs, effectors, and even the Ras isoforms themselves.

Figure 1.2: Ras activation and signalling to downstream effectors. Growth factors bind to protein tyrosine kinase receptors (PTKR) and cause phosphorylation of tyrosine residues and receptor activation. Grb2 binds to the activated receptor and recruits the RasGEF, SOS, to activate Ras through a GDP to GTP exchange. Activated Ras interacts with its effectors and initiates signalling to downstream pathways. The most studied pathways include Raf, PI3K, and RalGEF. RasGAPs inactivate Ras by returning the protein to its GDP-bound state.

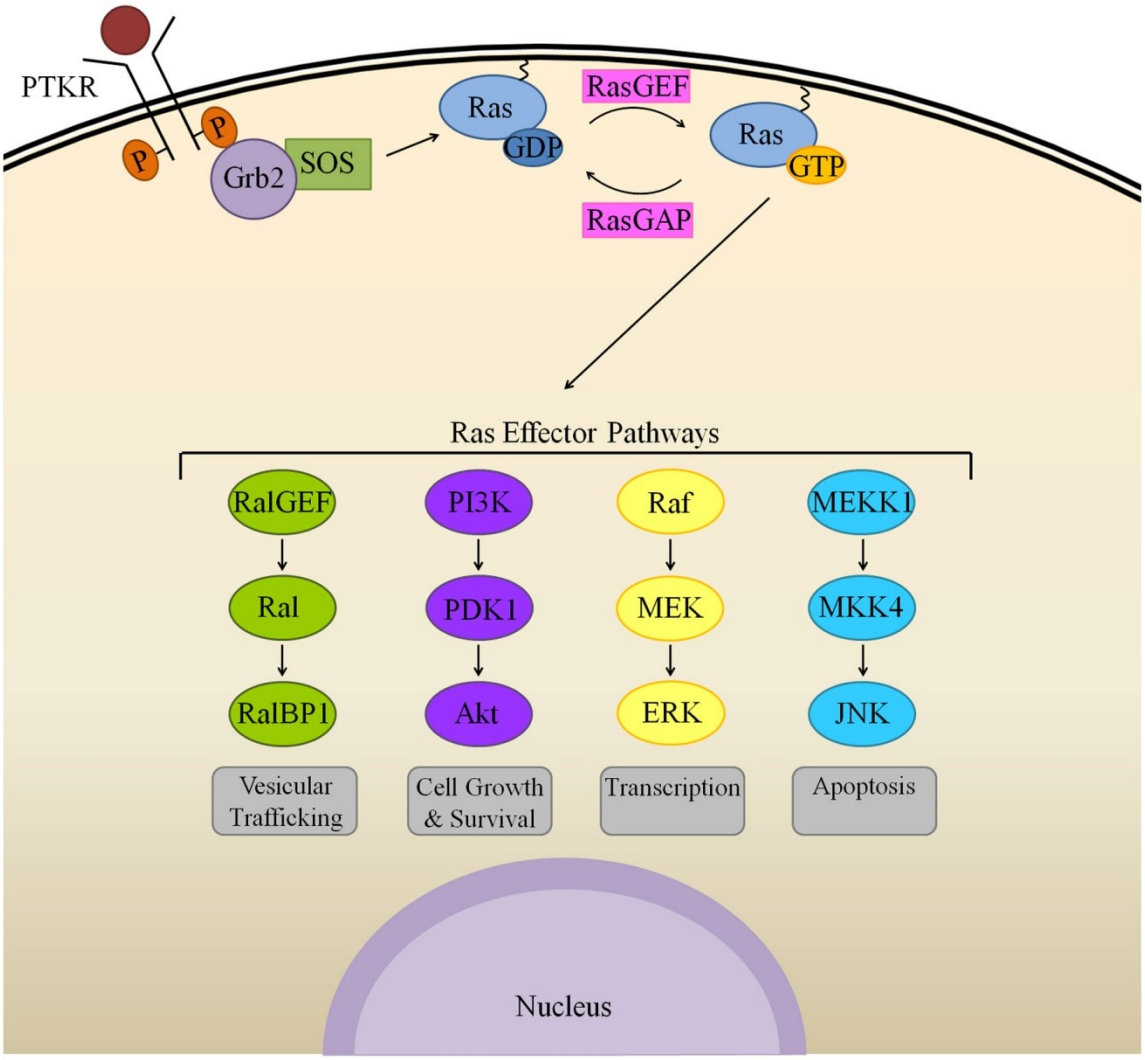
PTKR
P
P
Grb2
SOS
Ras
GDP
RasGEF
Ras
GTP
RasGAP
Ras Effector Pathways
RalGEF
Ral
RalBP1
PI3K
PDK1
Akt
Raf
MEK
ERK
MEKK1
MKK4
JNK
Vesicular Trafficking
Cell Growth & Survival
Transcription
Apoptosis
Nucleus

1.1.7. Compartmentalized Signalling: Plasma Membrane

It was initially thought that the plasma membrane was the only membrane that Ras could associate with for activation. Recent work has demonstrated that Ras is not only functional in plasma membrane microdomains, but that it is active in subcellular locations, such as the ER, mitochondria, Golgi, and endosomes (Bivona et al., 2006; Chiu et al., 2002; Lu et al., 2009; Prior et al., 2001; Wolfman et al., 2006). Ras activation at the plasma membrane is known to be transient and rapid, whereas activation at the endomembranes is sustained and slow. Most of what is known about Ras compartmentalized signalling comes from artificially tethered constructs and mutating amino acid residues that are essential to Ras post-translational modifications. As previously mentioned, the plasma membrane is subdivided into lipid rafts and disordered membrane microdomains, in which Ras associates with in an isoform-specific manner (Hancock, 2003; Hancock and Parton, 2005; Rajendran and Simons, 2005; Roy et al., 2005). H-, N-, and K-Ras form non-overlapping, spatially distinct nanoclusters to serve as signalling platforms within these microdomains, and also move laterally within the plasma membrane based on their GTP status. Nanoclusters serve as the only site in the plasma membrane where Ras activates the Raf/MEK/Erk signalling cascade (Tian et al., 2007). At the plasma membrane, H-Ras preferentially activates the PI3K/Akt signalling pathway, while K-Ras is more likely to activate Raf-1. This also extends to their constitutively activated forms (Yan et al., 1998). In response to B-Raf inhibition, oncogenic N- and K-Ras nanoclustering is upregulated, while no change is observed in oncogenic H-Ras nanoclustering (Cho and Hancock, 2013). Interestingly, phosphorylation of oncogenic K-Ras was shown to prevent K-Ras nanocluster formation

in BHK and PC12 rodent cell lines (Plowman et al., 2008). The same study concluded that galectin-3 and phosphorylation have separate roles in K-Ras nanoclustering. In contrast, a more recent study noted that phosphorylated and non-phosphorylated forms of oncogenic K-Ras4B segregate into distinct and non-overlapping nanoclusters in HeLa and HEK293 cells (Barceló et al., 2013). The phosphorylated forms were primarily located at the plasma membrane and generated oncogenic K-Ras nanoclusters to signal preferentially to Raf-1 and PI3K. These differences are likely attributed to variations in cell type and experimental conditions.

While oncogenic H-Ras can localize to endomembranes, it primarily signals from the plasma membrane (Lommerse et al., 2005). As such, tethered constructs tend to elicit a similar response (Matallanas et al., 2006). H-RasV12 tethered to lipid rafts or the bulk membrane efficiently transforms murine fibroblasts and can activate RalGEF, Erk, and PI3K; however, JNK activation is diminished in both cases. Tethering is achieved by incorporating an N-terminal LCK myristoylation signal (lipid raft associated) or cluster of differentiation 8 alpha (CD8α) transmembrane domain (bulk membrane associated) and further mutating the sites of palmitoylation (C181S and C184S). Therefore, mutating Ras lipidation sites causes differential localization. Ras is confined to the cytosol in farnesylation deficient constructs (Cadwallader et al., 1994; Miyake et al., 1996). Palmitoylation deficient N-Ras accumulates in the ER and Golgi complex, while palmitoylation deficient H-Ras exists in a dynamic equilibrium between the ER and the cytosol, but has also been detected in the Golgi body (Chiu et al., 2002; Goodwin et al., 2005; Matallanas et al., 2006). The latter is unable to stably bind membranes and exhibits decreased PI3K/Akt and Erk signalling. Furthermore, a mutation in C181 of H-Ras

restricts the isoform to the Golgi complex, whereas a mutation in C184 still allows H-Ras to traffic to the plasma membrane (Roy et al., 2005). When tethering H-Ras to a particular plasma membrane microdomain or endomembrane, both palmitoylation sites are mutated to ensure that the N-terminal tag is the primary driver in H-Ras localization.

1.1.8. Compartmentalized Signalling: ER and Mitochondria

Extending this methodology, Ras can be tethered to the ER by fusing the amino acid residues (1 to 66) of the avian infectious bronchitis virus M protein (M1) to the N-terminus of Ras (Swift and Machamer, 1991). ER-tethered H-Ras supports proliferation and transformation of murine fibroblasts, and efficiently activates RalGEF, PI3K, Raf/Erk, and JNK downstream signalling (Matallanas et al., 2006). Also at the ER, N-Ras is known to generate a strong anti-apoptotic signal, suggesting that the ER may play a role in cell survival (Wolfman and Wolfman, 2000). More commonly associated with programmed cell death is signalling from the mitochondria (Bras et al., 2005). As previously mentioned, phosphorylation of serine (S181) by PKC can cause K-Ras4B to localize to endomembranes, such as the ER, Golgi complex, and mitochondria (Bivona et al., 2006). At the mitochondrial outer membrane, K-Ras interacts with Bcl-XL to promote cell apoptosis. This exemplifies how the location of K-Ras results in completely different biological outcomes, as signalling from the plasma membrane and ER promotes cell proliferation and apoptosis, respectively (Chiu et al., 2002; Sung et al., 2013). In contrast, N-Ras associates with outer and inner mitochondrial membranes to aid in retrograde signalling of nuclear factor kappa B (NF-κB) from the mitochondria to the nucleus to promote cell survival (Wolfman et al., 2006).

1.1.9. Compartmentalized Signalling: Golgi Complex

The largest discrepancy exists from Ras tethered to the Golgi complex. Tethering is achieved by fusing the KDEL receptor to the N-terminus of Ras (Caloca et al., 2003; Cole et al., 1996). The KDEL receptor normally functions as a chaperone to transport proteins from the Golgi complex back to the ER, but mutating amino acid N193 inhibits this movement and renders the receptor as a resident Golgi protein. Chiu et al. (2002) demonstrated that H-Ras tethered to the Golgi complex transformed rodent fibroblasts and efficiently activated PI3K/Akt and Erk signalling. The tethered construct caused low JNK activation when compared to the plasma membrane associated control. On the other hand, Matallanas et al. (2006) established that Golgi-tethered Ras was not capable of transforming murine fibroblasts and supported Ral and JNK downstream signalling. In support of this, Ras tethered to the Golgi complex by the avian bronchitis virus E1 protein is unable to induce cell transformation (Hart and Donoghue, 1997). Negative regulators, such as Raf kinase trapping to Golgi (RKTG) and retinoic acid-inducible gene 1 (RIG-1) also exist to down-regulate the Ras/Raf/Erk signalling pathways at the Golgi (Fan et al., 2008; Feng et al., 2007; Tsai et al., 2006). RKTG localizes to the Golgi complex and sequesters Raf-1 and B-Raf, thereby blocking Ras downstream signalling. RIG-1 resides at the ER and Golgi body, and functions by forming a complex with Ras to prevent its activation. Another inconsistency exists with the activation of Ras at the Golgi complex. Some studies suggest that Ras can be activated directly at the Golgi complex, while others indicate that Ras must first travel to the plasma membrane and then retrograde traffic back to the Golgi complex before initiating associated downstream signalling pathways (Fehrenbacher et al., 2009; Mayinger, 2011). Even though some of

the results are conflicting, the notion of compartmentalized signalling is well supported. The variation may be explained through Ras nanoclustering and the idea that distinct microdomains may also exist in intracellular endomembranes.

1.1.10. Compartmentalized Signalling: Endosomes

Instead of trafficking back to the Golgi complex, palmitoylated Ras can accumulate on endosomes through clathrin-mediated endocytosis. H- and N-Ras localize to endosomes through a conditional modification known as ubiquitination (Jura et al., 2006). While poly-ubiquitination of any Ras isoform leads to proteasomal degradation, mono- or di-ubiquitination by the E3 ubiquitin ligase, Rabex-5/RabGEF1, causes anchoring of palmitoylated H- and N-Ras to endosomal membranes (Kim et al., 2009; Xu et al., 2010). It is also regulated by the Ras effector, Rin1, suggesting that Ras may regulate its own ubiquitination. Since Ras/Raf/Erk signalling primarily occurs at the plasma membrane, redirecting H- and N-Ras to endosomes by ubiquitination reduces Erk activation (Jura et al., 2006; Tian et al., 2007). In support of this, mutations that prevent ubiquitination of H-Ras result in enhanced H-Ras plasma membrane localization and Erk activation. As opposed to using ubiquitination to alter Ras intracellular localization, the deubiquitination enzyme, USP17, can indirectly sequester H- and N-Ras to the cytosol and ER by reducing the activity of the protease, Rce1 (Burrows et al., 2009). Interestingly, USP17, does not block K-Ras trafficking to the plasma membrane, and may serve as a means of promoting K-Ras downstream signalling over H- and N-Ras (De-La Vega et al., 2010). K-Ras is rarely retained on endosomes; however, it can be internalized by clathrin-mediated endocytosis, and initiate MAPK signalling from late endosomes

before lysosomal degradation (Lu et al., 2009; Roy et al., 2002). Furthermore, K-Ras also undergoes mono-ubiquitination, but instead of endosomal localization, it results in enhanced GTP loading and binding affinity for Raf and PI3K downstream effectors (Sasaki et al., 2011).

As demonstrated above, Ras subcellular localization leads to variation in signalling to downstream effectors. As expected, site-specific GEFs and GAPs exist to regulate this response. For example, RasGRF activates Ras in epithelial cells based on the type of stimulus present. Calcium causes RasGRF to activate Ras at the plasma membrane, while lysophosphatidic acid promotes its activation at the ER (Arozarena et al., 2004). In lymphocytes, calcium triggers recruitment of the Golgi-specfic GEF, RasGRP1, to the Golgi complex where it binds diacylglycerol and activates Ras (Bivona et al., 2003). At the same time, plasma membrane associated Ras is inactivated by the calcium-reactive RasGAP, CAPRI. Modifying GEF or GAP function can also regulate Ras signalling. The previously mentioned scaffold protein, galectin-3, which functions in K-Ras nanocluster formation, prevents RasGRP4 from activating H- and N-Ras isoforms (Shalom-Feuerstein et al., 2008). As a result, signalling from GTP-loaded K-Ras nanoclusters is promoted, and the activity of the other isoforms is suppressed. Likewise, phosphorylation of GTP-bound K-Ras sustains its activity to PI3K and Erk downstream effectors, while also preventing the RasGAP, p120, from inactivating the isoform (Elad-Sfadia et al., 2004). Taken collectively, Ras signalling to downstream effectors is highly regulated, and not only varies by Ras subcellular localization, which is mainly attributed to post-translational modifications, but also by the stimulus and accessory proteins present, and the type of cell in question. With constitutively activated Ras involved in

30% of all human cancers, and associated downstream pathways increasing that frequency to 50%, it is no surprise that many strategies have been developed to inhibit Ras activity (Calvo et al., 2010).

1.1.11. Targeting Ras for Cancer Therapy

The concept of inhibiting Ras signalling lends itself to the notion of oncogene addiction (Torti and Trusolino, 2011). The term refers to cancer cells which, despite having numerous genetic mutations, become dependent on the activity of a single oncogene for their continued proliferation and/or survival. There are three recognized models for oncogene addiction. The first, known as genetic streamlining, suggests that non-essential cellular pathways are inactivated over time as the tumor relies on the signalling from the oncogenic protein (Kamb, 2003). Termination of signalling leads to an attempt of cellular recovery, which ultimately fails, and ends in cell cycle arrest or apoptosis. The second, termed oncogenic shock, postulates that oncogenes simultaneously stimulate both pro-survival and pro-apoptotic signals, with the former pathways dominating in the tumor cell environment (Sharma et al., 2006). Disruption of the oncogenic protein leads to a rapid decline in pro-survival signals and shifts the balance in favour of death promoting signalling pathways. Lastly, the synthetic lethal model describes a situation in which the activities of two oncogenes function towards a common downstream effector (Kaelin, 2005). When one is lost, the other is still capable of maintaining cell survival; however, the loss of both proves fatal.

Unfortunately, finding ways to target oncogenic Ras and interrupt its associated downstream signalling is no small endeavor. If the direct approach is considered, the

binding pocket or active site of Ras is made inaccessible due to the continuous occupancy of GDP or GTP; essentially deeming Ras "undruggable" (Mattingly, 2013). Nonetheless, some inhibitors do exist. The Schering-Plough inhibitors, such as SCH-54292, are small molecules that can bind in the active site without displacing GDP and likely function by preventing the interaction of Ras with the RasGEF, SOS (Taveras et al., 1997). Furthermore, newly discovered small binding pockets in K-Ras have also led to the development of compounds that block SOS-mediated Ras activation (Maurer et al., 2012). Alternatively, small molecules which promote GTP hydrolysis of oncogenic Ras are also under consideration (Ahmadian et al., 1999). Another direct approach in targeting oncogenic Ras is silencing its expression through RNA interference (RNAi). Small interfering RNAs have been shown to silence oncogenic K-Ras expression in tumor cell lines and inhibit their growth (Smakman et al., 2005). Interestingly, another study showed that tumor cell lines were sensitive to K-Ras RNAi depending on their degree of epithelial to mesenchymal transition (Singh et al., 2009). Epithelial tumor cell lines expressing mutant K-Ras were good candidates for RNAi, while those expressing mesenchymal markers were not. This technique shows promise, but lacks in efficient delivery, uptake by target cells, and effective gene silencing.

With direct targeting being rather unsuccessful, indirect methods stem from inhibiting Ras downstream effectors or its association with membranes. The list of inhibitors for Raf, MEK, Erk, PI3K, Akt, and RalGEFs is vast and because of their efficacy as cancer therapeutics, numerous clinical trials are currently underway. An extensive review can be found in select chapters of The Enzymes, Vol. 34 (Cooper et al., 2013; Gentry et al., 2013; Sheridan and Downward, 2013). The discovery that Ras

requires post-translational modifications for membrane association and activation prompted an inhibition of the enzymes responsible (Casey et al., 1989; Hancock et al., 1990). The cytosolic farnesyltransferase was one of the first enzymes to be targeted. Farnesyltransferase inhibitors (FTIs) suppressed a wide array of tumor cells both *in vitro* and *in vivo*, and were extremely effective in preventing H-Ras farnesylation and reverting cell transformation (Appels et al., 2005; Basso et al., 2006). Furthermore, orally developed FTIs, such as Tipifarnib and Lonafarnib, were also well tolerated by experimental groups. Unfortunately, clinical trials revealed that FTIs were unable to target tumors driven by N- or K-Ras; the latter of which dominates in human cancers (Fernández-Medarde and Santos, 2011). As it turns out, if the farnesylation of N- or K-Ras is inhibited, the proteins can undergo alternate prenylation by the geranylgeranyltransferase type I (GGTase-I) (Whyte et al., 1997). Instead of farnesylation, the GGTase-I adds a 20-carbon geranylgeranyl isoprenoid lipid group to the CAAX motif of N- or K-Ras. This led to the development of GGTase-I inhibitors (GGTIs), which were also tried in combination with FTIs, and the development of compounds that served as dual prenyltransferase inhibitors (DPIs) (Tamanoi and Lu, 2013; Tucker et al., 2002). Either treatment has shown promise, but the concern lies with dose-limiting cytotoxicity. In order to achieve a significant reduction in K-Ras prenylation, high doses are required. Unfortunately, *in vivo* studies revealed zero survivability in mice at these levels. Future endeavors with FTIs, GGTIs, and DPIs may rest in the delivery system, where tumor cells are specifically targeted by antibodies or nanoparticles.

Palmitoylation is not considered an appropriate target for Ras inhibition as K-Ras4B does not require palmitoylation for activity, and palmitoylation mutants for the other Ras isoforms are still capable of GTP activation and some downstream signalling (Fotiadou et al., 2007; Hancock et al., 1989; Matallanas et al., 2006). Palmitoylation inhibitors, such as 2-bromopalmitate (2BP), cerulenin, and tunicamycin are broad spectrum inhibitors and serve more as a molecular tool, than a cancer therapeutic (Resh, 2006). Other targets include the post-prenylation processing enzyme, Icmt, and the galectin family of Ras chaperones (Kloog et al., 2013; Tamanoi and Lu, 2013). Knockout of *Icmt* causes K-Ras to accumulate in the cytoplasm, prevents K-Ras induced oncogenic transformation, and improves myeloproliferative disease in mice (Bergo et al., 2000, 2004; Wahlstrom et al., 2008). Chemical compound screening has led to the identification of a potent Icmt inhibitor, known as cysmethynil (Winter-Vann et al., 2005). Cysmethynil is highly specific for Icmt and causes growth inhibition or death in colon, prostate and liver cancer cells (Wang et al., 2008, 2010). The main concern with Icmt inhibitors is that the enzyme methylates many other proteins, including the Ras downstream effector, B-Raf (Bergo et al., 2004). It is therefore important to determine whether or not the inhibition of Ras or other Icmt substrates are behind the anti-tumor effects. As opposed to targeting Ras modification enzymes, a relatively new approach is the inhibition of Ras chaperones. The inhibitor, farnesylthiosalicylic acid (FTS, Salirasib®) and its derivatives selectively interfere with GTP-bound Ras and its interaction with galectins to prevent Ras nanoclustering and signalling to downstream effectors (Kloog et al., 2013). FTS can be taken orally and lacks clinical toxicity in mice and humans. In terms of clinical efficacy, FTS has successfully targeted pancreatic and

non-small cell lung carcinomas in patients participating in phase II clinical trials (Bustinza-Linares et al., 2010). Furthermore, the majority of studies assessing the effects of FTS in combination with current cancer therapeutics have shown synergistic results (Kloog et al., 2013). Whether direct or indirect, individual or in combination, targeting a dynamic protein like Ras for cancer therapy is extremely difficult and filled with countless obstacles. Fortunately, there is another avenue under consideration that utilizes biological agents as a therapeutic platform.

1.1.12. Oncolytic Viruses

Oncolytic virotherapy refers to the use of live viruses in cancer therapy (Russell et al., 2012). The approach is based on the notion that certain viruses can selectively target, replicate in, and destroy cancer cells. Oncolytic viruses have unique advantages over conventional radiotherapy and chemotherapy (Kim et al., 2011). They generally target cancer cells because of their reduced pathogenicity in normal cells, and in comparison to replication-incompetent vectors, can disseminate their viral progeny to neighbouring or distant cancer cells; thereby, distributing a potent anti-tumor response. Despite the above, there are concerns with this approach. Firstly, to ensure that the virus efficiently targets all cancer cells including those at sites of metastasis. Secondly, to minimize damage to proliferating cells and normal tissues, and lastly, to evade the natural immune response of the host such that the virus is not eradicated before the cancer is destroyed. Regardless of these challenges, many viruses are currently under investigation as a cancer therapeutic, and due to their demonstrated safety and effectiveness in clinical trials will likely result in future commercialization and combination therapies (Russell et al., 2012). These include

adenovirus, herpes simplex virus, measles virus, and vaccinia virus, which have been genetically engineered to target tumor cells while reducing their pathogenicity to normal tissues, as well as naturally oncolytic viruses, such as Newcastle disease virus, coxsackie A virus, and reovirus. When considering oncolytic viruses which target Ras, reovirus is the top contender. Its affiliation with Ras and associated downstream pathways has led to its use in phase I, II, and III clinical trials (Coffey et al., 1998; Oncolytics Biotech Inc, 2014; Strong et al., 1998). As such, the remainder of this chapter will focus on reovirus and its interaction with Ras.

1.2. Reovirus

The *Reoviridae* family is made up of small, non-enveloped, double-stranded RNA (dsRNA) viruses that are ubiquitously found in the environment and infect a wide range of hosts (Gomatos and Tamm, 1963; Stanley, 1961). Mammalian REO (respiratory enteric orphan) virus is a member of this family, and derives its name from its ability to target human upper respiratory and gastrointestinal tracts and generate a relatively benign, and often asymptomatic, infection (Sabin, 1959). Under the orthoreovirus genus, mammalian reovirus is classified into four main serotypes and five strains by neutralization and hemagglutination-inhibition assays (Attoui et al., 2001; Ramos-Alvarez and Sabin, 1954; Rosen et al., 1960; Sabin, 1959). These include: Type 1 Lang (T1L), Type 2 Jones (T2J), Type 3 Abney (T3A), Type 4 Ndelle (T4N), and the focus of this study, Type 3 Dearing (T3D).

1.2.1. Structure and Life Cycle

The reovirus genome consists of ten dsRNA segments, which are divided into large (L), medium (M), and small (S) classes based on their size (Ward et al., 2007). Each of the segments encodes a single viral protein, with the exception of M3 and S1, which each encode two. A list of reovirus dsRNA segments and their respective protein products can be found in Figure 1.3A. The reovirus genome is encompassed by two concentric, icosahedral protein capsids. The outer capsid is comprised of σ1, σ3, μ1, and λ2 structural proteins, and the inner capsid is made up of σ2 and λ1, as well as the viral replication enzymes, μ2 and λ3. The remaining four proteins are non-structural (NS) and play a role in reovirus replication. The formation of viral inclusion bodies is aided by σNS, μNS, and μNSC, while σ1s has recently been implicated in reovirus-induced cell cycle arrest and apoptosis (Boehme et al., 2013; Kobayashi et al., 2009). During its life cycle, reovirus particles exist in three forms: mature virions, intermediate subviral particles (ISVPs), and core particles (Borsa et al., 1973; Smith et al., 1969).

The reovirus life cycle begins with the binding of σ1 to cell surface glycans (Figure 1.3B) (Lee et al., 1981). These have been identified as *α*- linked 5-N-acetyl neuraminic acid / sialic acid and ganglioside GM2 glycan for T3D and T1L strains, respectively (Barton et al., 2001b; Reiss et al., 2012). Acting as co-receptors, the cell surface glycans allow reovirus to move laterally across the cell surface until it can bind with higher affinity to its main receptor, junctional adhesion molecule-A (JAM-A) (Barton et al., 2001a). Following attachment, reovirus is internalized via receptor-mediated, clathrin-dependent endocytosis (Ehrlich et al., 2004). This requires the interaction of outer capsid protein, λ2, and β1-integrins (Maginnis et al., 2006). Caveolin-

mediated endocytosis may also be involved in entry (Schulz et al., 2012). After reovirus enters the cell, it begins to disassemble in acidified late endosomes (Mainou and Dermody, 2012; Sturzenbecker et al., 1987). Cysteine proteases, such as cathepsin B, L, or S, enable the virus to uncoat by digesting σ3 to reveal μ1N and μ1C (Ebert et al., 2002; Golden et al., 2004). The former undergoes myristoylation, while the latter is digested into hydrophobic δ and φ fragments (Chandran et al., 2003; Tillotson and Shatkin, 1992). These conformation changes give rise to ISVPs, which penetrate the endosomal membrane and cause transcriptionally active core particles to be released into the cytosol (Mendez et al., 2008). ISVPs can also be generated by intestinal proteases, and by trypsin and chymotrypsin *in vitro* (Bodkin et al., 1989). As such, it is believed that ISVPs may directly penetrate the plasma membrane to enter the cytoplasm, thereby bypassing the endocytic process (Borsa et al., 1979; Chandran et al., 2002). Disassembly of the ISVP also causes activation of the RNA-dependent RNA polymerase, λ3, and primary transcription is initiated in the core particles (Yamakawa et al., 1982). Capped mRNAs are released into the cytoplasm where they serve as templates for host cell translational machinery. At this point, reovirus non-structural proteins (σNS, μNS, and μNSC) and structural protein, μ2, form the viral inclusion bodies or factories in the cytoplasm (Becker et al., 2001; Kobayashi et al., 2006). These factories incorporate cellular cytoskeletal structures, such as microtubules and intermediate filaments, and function as the main site of viral replication and assembly (Babiss et al., 1979; Parker et al., 2002; Sharpe et al., 1982). Progeny core particles begin to assemble, and within the cores, the positive-sense RNAs help to complete the reovirus genome by serving as templates for minus strand synthesis (Schonberg et al., 1971). The addition of the outer

capsid generates mature virions, and subsequent reovirus-induced apoptosis results in the release of viral progeny (Oberhaus et al., 1997). In addition to infecting mucosal epithelial cells, reovirus is a naturally oncolytic virus that preferentially targets cells harboring constitutively activated Ras or one of its downstream effectors (Hashiro et al., 1977; Strong et al., 1998). As a result, reovirus exploits certain aspects of Ras signalling to enhance its own replication.

Figure 1.3: Reovirus structure and life cycle. (A) Structure of a typical reovirus (left). Translated products from the individual RNA strands of the reovirus genome (right). (B) Reovirus life cycle begins by (1) attaching to host cell receptors, sialic acid and JAM-A, using σ1 to induce receptor-mediated endocytosis. (2) Outer capsid proteins, σ1 and σ3, are shed and (3) the virus penetrates through the endosomal membrane resulting in core particles in the cytoplasm. (4) Primary transcription of viral mRNA occurs within these core particles, and capped mRNAs are released and (5) translated by host cell machinery. (6) As viral proteins accumulate in viral factories, new core particles are formed. (7) Secondary transcription and (8) translation occur, and (9) assembly of the outer capsid results in mature virions. (10) The virus is released via cell apoptosis. (11) Direct penetration of the cell membrane by reovirus ISVPs. Images modified from Shmulevitz et al. (2005).

A

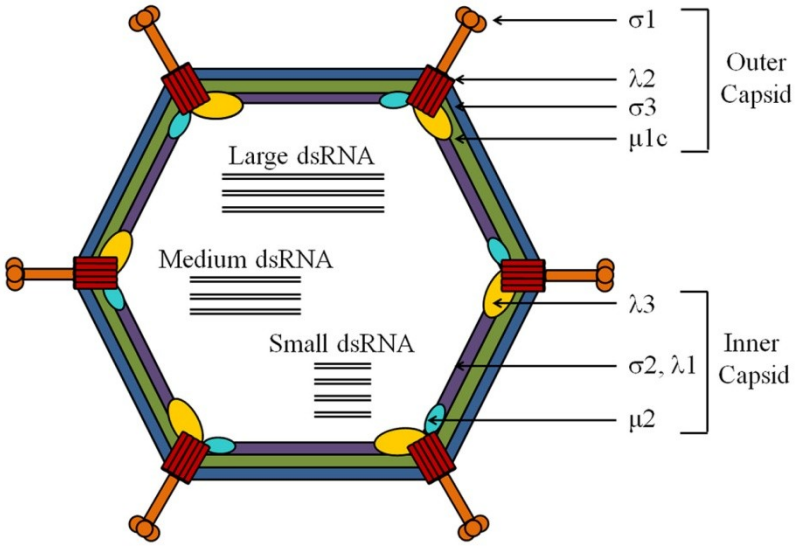

RNA	Protein
S1	σ1, σ1s
S2	σ2
S3	σNS
S4	σ3
M1	μ2
M2	μ1
M3	μNS, μNSC
L1	λ3
L2	λ2
L3	λ1

B

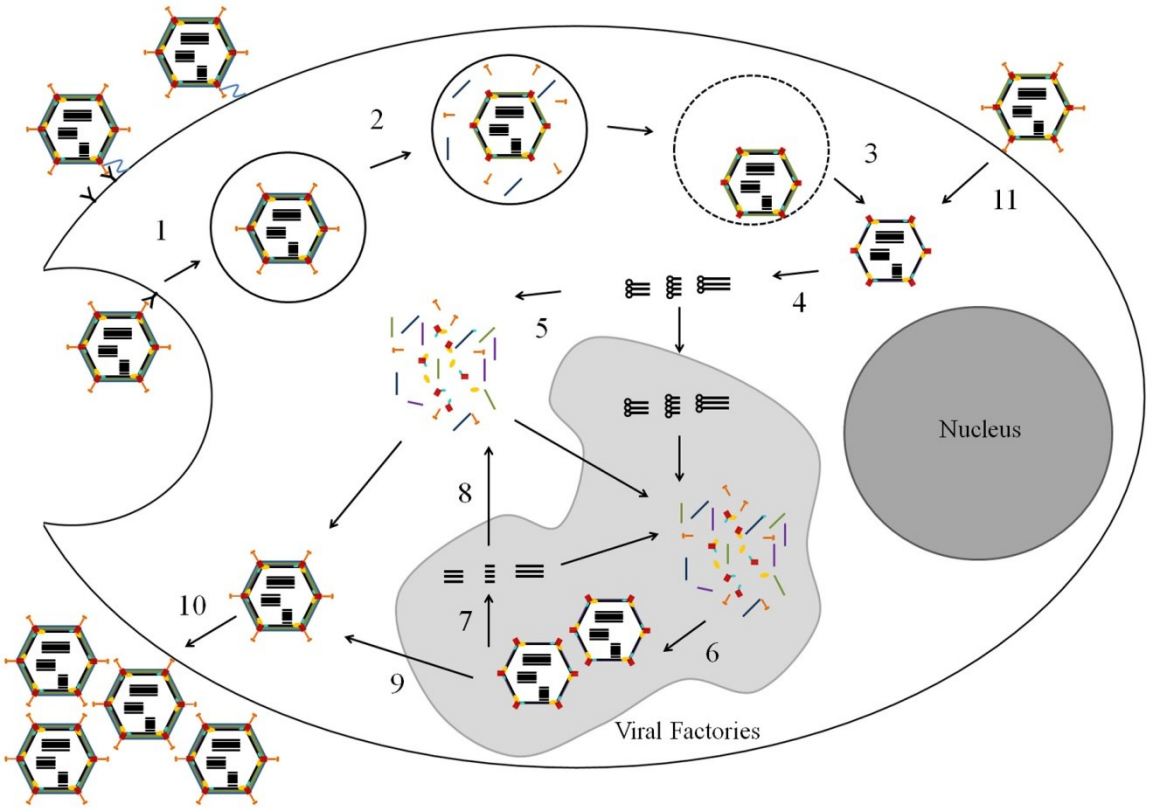

1.2.2. Reovirus Utilizes the Ras Signalling Pathways

It has long been demonstrated that reovirus is able to selectively infect and kill a wide variety of transformed cells; however, it was not until the 1990s that the link between reovirus and Ras was established (Duncan et al., 1978; Hashiro et al., 1977). Introduction of the epidermal growth factor receptor (EGFR), or in a later study, its constitutively activated and truncated form, rendered reovirus-resistant cells permissible to reovirus infection (Strong and Lee, 1996; Strong et al., 1993). These findings suggested that the signalling pathways downstream of EGFR, which include Ras, may play a role in reovirus oncolysis. In light of these findings, subsequent studies showed that murine cells transformed by SOS or Ras increased their permissiveness to reovirus infection and death (Strong et al., 1998). With Ras implicated in efficient reovirus oncolysis, researchers set out to determine which steps in the reovirus life cycle were enhanced by the presence of an activated Ras protein (Marcato et al., 2007). Constitutively activated Ras contributed to reovirus replication by increasing the efficiency of (1) reovirus proteolytic disassembly during entry, (2) infectious progeny virion production, and (3) reovirus release by caspase-dependent apoptosis. Furthermore, Ras-transformed cells are compromised in their ability to induce and respond to interferon beta (IFN-β) (Shmulevitz et al., 2010). During infection, pattern recognition receptors, such as RIG-1-like receptors, toll-like receptors, and dsRNA-activated protein kinase (PKR) recognize viral RNAs. In response, IFN-α and IFN-β are upregulated, which in turn stimulate genes that inhibit virus replication. In Ras-transformed cells, the MEK/Erk pathway blocks signalling from RIG-1 to inhibit IFN-β production, and as a result, allows for efficient spread of the virus. Additionally, a similar situation may exist

for PKR (García et al., 2006). Upon binding viral dsRNA, PKR dimerizes and autophosphorylates itself for activation. PKR functions by inhibiting host cell translational machinery through eIF2α, which ceases reovirus protein synthesis in normal cells (Bischoff and Samuel, 1989). In Ras-transformed cells, PKR phosphorylation is not detected during reovirus infection (Strong et al., 1998). Therefore, Ras-transformed cells not only encourage certain steps in the reovirus life cycle, but also reduce the antiviral response of the host cell to enable efficient virus replication and spread.

1.2.3. Reovirus-Induced Apoptosis

With the link between reovirus and Ras firmly established, it was imperative to understand the mechanisms behind its apoptosis of target cells. Reovirus triggers caspase-dependent cell death by utilizing both extrinsic and intrinsic apoptosis pathways. In the extrinsic pathway, tumor necrosis factor-related apoptosis-inducing ligand (TRAIL), binds death receptors and recruits the adaptor protein Fas-associated death domain (FADD). FADD activates caspase-8, which activates downstream caspases to initiate apoptosis. Inhibiting TRAIL, FADD or caspase-8 negatively affects reovirus oncolysis (Clarke et al., 2000, 2001a). Furthermore, it has been shown that reovirus infected cells release TRAIL and downregulate the expression of cFLIP, a competitive inhibitor of caspase-8 for FADD binding (Clarke and Tyler, 2007). The extrinsic pathway actually feeds into the intrinsic pathway through caspase-8, which reovirus also requires for its pathogenesis (Kominsky et al., 2002a, 2002b). Caspase-8 cleaves the pro-apoptotic protein, Bid. Bid translocates to the mitochondria to release cytochrome C and Smac/Diablo (second mitochondria-derived activator of caspases / direct binding of

inhibitor of apoptosis binding protein with low isoelectric point, PI), which activate caspase-3 for cleavage of downstream apoptotic targets.

Other death-related signalling pathways are also activated by reovirus. These include stress activated protein kinase / c-jun N-terminal kinase (SAPK/JNK) pathways and the transcription factor NF-κB. A typical reovirus infection results in the phosphorylation and activation of JNK (Clarke et al., 2001b). In turn, JNK translocates to the nucleus and activates c-jun; thereby, upregulating the expression of pro-apoptotic genes. JNK can also translocate to the mitochondria where it can suppress anti-apoptotic proteins, such as Bcl-2 or Bcl-XL, through direct phosphorylation or BAD-mediated neutralization. Furthermore, JNK can stimulate the release of cytochrome C or Smac/Diablo which are involved in activation of the caspase cascade and cell death. In the context of reovirus infection, JNK inhibition blocks reovirus-induced cell death by delaying the release of cytochrome C and Smac/Diablo (Clarke et al., 2004). T3 reoviruses tend to induce more apoptosis than T1 reoviruses, and the ability to activate JNK is linked to strain differences in S1 and M2 reovirus genes; both of which are critical for triggering apoptosis following virus disassembly (Tyler et al., 1996, 1995). As previously mentioned, S1 encodes the attachment protein σ1 and the non-structural protein σ1s, while M2 encodes the outer capsid protein μ1. T3 reoviruses null for σ1s are unable to cause cell cycle arrest and induce lower levels of apoptosis when compared to the wild-type virus both *in vitro* and *in vivo* (Boehme et al., 2013). More work is needed to determine how σ1s is connected to the JNK or NF-κB apoptotic pathways. Slightly upstream of JNK is the Ras downstream effector, MEKK1. MEKK1 activates MKK4, which in turn phosphorylates and activates JNK. Consequently, reovirus infection of

murine embryonic fibroblasts that are null for MEKK show diminished caspase-3 activity and reduced apoptosis (Clarke et al., 2004).

In addition to JNK, the reovirus μ1C components, δ and φ, are also important in activating caspase-8 and NF-κB pathways (Coffey et al., 2006; Wisniewski et al., 2011). During reovirus infection, NF-κB signalling is required for Bid activation, which as mentioned above, is involved in the intrinsic apoptosis pathway (Danthi et al., 2010). Interestingly, many reovirus infected cells activate NF-κB early on, but in later stages of infection are found to downregulate its activity (Clarke et al., 2003). NF-κB regulates both cell survival and death, and perhaps reovirus varies its activity to achieve sufficient progeny numbers before initiating cell apoptosis. Alternatively, recent evidence suggests that NF-κB activation may not be required for reovirus-induced cell death, and that reovirus may trigger necroptosis through caspase-independent pathways (Berger and Danthi, 2013).

1.2.4. Reovirus in Cancer Therapy

The ability of reovirus to effectively induce apoptosis in a wide array of human cancers has led to the establishment of the Canadian company, Oncolytics Biotech Incorporated, which investigates the therapeutic potential of reovirus (aka REOLYSIN®) in human clinical trials. Currently, the company has thirty-one ongoing or completed phase I, II, or III clinical trials (Oncolytics Biotech Inc, 2014). In brief, early clinical trials involving the intratumoral delivery of reovirus to malignant gliomas, and subcutaneous and prostate tumors found that it was safe, well-tolerated by patients, and had no dose-limiting toxicities (Forsyth et al., 2008; Thirukkumaran et al., 2010).

Furthermore, intravenous administration of reovirus to patients with various tumors types demonstrated the ability of reovirus to reach tumors systemically, as replication-competent viral progeny were isolated from tumor biopsies (Vidal et al., 2008). Multiple doses of reovirus were also well tolerated by patients and once again, produced no observable toxicity. Showing promise, reovirus was tried in combination with standard chemo- and radiation therapies in patients with advanced cancers (Harrington et al., 2010; Karapanagiotou et al., 2012). The total clinical benefit was high in all studies, and prompted the first phase III clinical trial of reovirus with carboplatin and paclitaxel for the treatment of head and neck cancers (Oncolytics Biotech Inc, 2014). This trial is currently underway with an initial enrollment of 80 patients; however, the trial was recently expanded by an additional 160 patients after the progression free survival data was higher than expected. Therefore, in order to maximize the efficacy of reovirus as a cancer therapeutic, future trials will focus on combination therapies (ie. chemotherapy, radiation therapy, and targeted therapies) that provide synergistic anti-tumor effects.

1.3. Objectives

It is well established that reovirus preferentially targets Ras-transformed cells (Coffey et al., 1998; Strong et al., 1998). It is also known that Ras controls a wide array of downstream signalling pathways, which in turn regulate essential cellular processes, such as cell growth, differentiation, and death (Rajalingam et al., 2007). So far, studies have identified aspects of the reovirus life cycle that are enhanced in cells harboring activated Ras (Marcato et al., 2007; Shmulevitz et al., 2010), but none have focused on changes to oncogenic Ras itself in response to reovirus infection. I set out to determine

whether reovirus could alter the location of oncogenic Ras, and consequently, modify Ras activity to initiate pro-apoptotic signalling pathways required for viral progeny release. Considering that reovirus is currently undergoing clinical trials, it is more important than ever to identify the mechanism behind its oncolysis, and provide the potential to improve its efficacy as a cancer therapeutic. With Ras being a major constituent in human oncogenesis, any study that characterizes the biological outcomes of its compartmentalized signalling helps to expand the current field, and has the possibility to reinforce old, and implement new, therapeutic strategies.

CHAPTER 2: MATERIALS AND METHODS

2.1. Cell Culture and Virus Synthesis

2.1.1. Cell Culture and Reovirus Propagation

NIH3T3, L929, and 293T cell lines were purchased from the American Type Culture Collection (ATCC; Manassas, VA, USA). NIH3T3 cells were cultured in Gibco® Dulbucco's Modified Eagle Medium (DMEM, Life Technologies, Carlsbad, CA, USA) and supplemented with 10% newborn calf serum (NCS; Thermo Fisher Scientific Inc., Huntsville, AL) and 1% v/v antibiotic-antimycotic (AA; Life Technologies). L929 cells were cultured in Gibco® Modified Eagle Medium (MEM) with 5% v/v fetal bovine serum (FBS), 1 mM sodium pyruvate, 1% v/v MEM non-essential amino acids (NEAA) and 1% v/v AA (Life Technologies). 293T cells were cultured similarly to L929 cells with the exception of DMEM and 10% v/v FBS being used. All cell lines were maintained at 37˚C in a 5% CO_2 humidified incubator with cell culture medium being replaced every 2 to 3 days.

Mammalian reovirus T3D stocks were produced in L929 spinner cultures in Joklik's Modified Eagle Medium (JMEM; Sigma-Aldrich Canada, Oakville, ON, Canada) supplemented with 5% v/v FBS, 1 mM sodium pyruvate, 1% v/v MEM NEAA and 1% v/v AA. The virus was purified as previously described (Mendez et al., 2000).

2.1.2. Molecular Constructs

H-RasV12 in pBABE-puro was kindly provided by Dr. Channing Der (University of North Carolina, NC, USA). N-Ras61K and K-RasV12 (4B variant) in pBABE-puro were purchased from Addgene (Catalog #12543 and #12544; Cambridge, MA, USA).

Plasma membrane tethered CD8-HRasV12xx in pCEFL was a gift from Dr. Piero Crespo (University of Cantabria, Cantabria, Spain). CD8-HRasV12xx was cloned into the pBABE-puro vector using the primers listed in Table 2.1. N-Ras61K and CD8-HRasV12xx vectors were used as templates to clone the tethered and/or palmitoylation deficient forms of activated H- and N-Ras into pBABE-puro (Table 2.1). Palmitoylation deficient constructs, denoted with an x or xx, refer to the replacement of cysteine to serine at sites 181 and 184 within the Ras sequence (C181S and C184S in H-RasV12xx and C181S in N-Ras61Kx). All constructs were verified by sequencing.

Table 2.1: List of primers and enzymes used in the cloning of tethered and/or palmitoylation deficient Ras into the pBABE-puro retroviral vector.

Constructs	**Forward Primer 5' to 3'**	**Reverse Primer 5' to 3'**	**Restriction Enzymes**
CD8-HRasV12xx	GTACAGATCTGCCGCC ACCATGGCCTTACCAG	GAGTACGTCGACTCAG GAGAGCACACACTTGC TGCTCATGCTGCC	BglII SalI
CD8-NRas61Kx (Transmembrane portion)	GTACAGATCTGCCGCC ACCATGGCCTTACCAG	GAGTACCTCGAGCGCG GATCTCGGGAGGCT	BglII XhoI
CD8-NRas61Kx (N-Ras61Kx portion)	GAGTACCTCGAGACTG AGTACAAACTGGTGGT G	GAGTACGTCGACTTAC ATCACCACACATGGCA ATCCCATACTACCCTG	XhoI SalI
H-RasV12xx	GAGTACGGATCCGCCG CCACCATGACGGAATA TAAGCTGGTGG	GAGTACGTCGACTCAG GAGAGCACACACTTGC TGCTCATGCTGCC	BamHI SalI
N-Ras61Kx	GAGTACGGATCCGCCG CCACCATGACTGAGTA CAAACTGGTG	GAGTACGTCGACTTAC ATCACCACACATGGCA ATCCCATACTACCCTG	BamHI SalI

2.1.3. Retrovirus Synthesis, Infection and Generation of Cell Lines

To generate retroviruses encoding activated Ras mRNA sequences, 6 cm dishes of 293T cells were grown to 80% confluency in antibiotic free media. According to the manufacturer's protocol, 10 µl of Lipofectamine® 2000 transfection reagent was added to 250 µl of Opti-MEM® I reduced serum media (Life Technologies). In another 250 µl of Opti-MEM® media, 2.6 µg of the appropriate pBABE-puro retroviral vector and 1.4 µg each of plasmids MD2.G and pHIT60 were added. The reagents were incubated for 5 min at room temperature (RT). The plasmid and lipofectamine-containing media were mixed together and incubated for an additional 20 min at RT. The resulting mixture was then added to the 293T cells for 6 h, after which the DNA-containing media was replaced with complete media. Twenty-four hours later, the retrovirus-containing media was collected at 12 h intervals until the cells began to lose viability. The retrovirus-containing media was pooled and centrifuged at 1000 g for 10 min. The media was filtered (0.45 µm), aliquoted, and stored at -80˚C.

To infect NIH3T3 cells with retrovirus, the cells were first seeded at 6.25 x 10^4 cells/ml into a 6-well plate. The following day, each well received 1 ml of complete media, 1 ml of the appropriate retrovirus, and Sequa-brene to a final concentration of 8 ug/ml (Sigma-Aldrich Canada). After 4 h, the retrovirus-containing media was removed and replaced with complete media. Twenty-four hours later, the cells were given selection media containing 2 µg/ml of puromycin. Mock-infected NIH3T3 cells were used as a control to monitor puromycin cytotoxicity. Once selected, the cells were maintained for 3 to 4 weeks maximum, and if necessary, were grown on 2% gelatin-coated plates.

2.2. Inhibitors

Unless otherwise indicated, inhibitors were added to pre-warmed media at 2 hours post-infection (hpi). FK506 and FTI-277 were purchased from Sigma-Aldrich Canada (Catalog #F4679 and #F9803) and used at a concentration of 10 μM. In general, a working concentration of 50 μM was utilized for 2-bromohexadecanoic acid (2BP; Catalog #sc-251714; Santa Cruz Biotechnology, Santa Cruz, CA, USA). InSolution^{TM} Jun N-terminal kinase (JNK) inhibitor II and caspase inhibitor I Z-VAD(OMe)-FMK (ZVAD) were supplied by Calbiochem (Catalog #420128 and #627610; EMD Millipore, Billerica, MA, USA) and used at a working concentration of 50 μM. The MEK 1/2 inhibitor, U0126, was used at a concentration of 40 μM (Catalog #9903; Cell Signaling Technology, Danvers, MA, USA). Nocodazole was used at a concentration of 8 μM and added directly to the cells 2 h before collection (Catalog # R17934; BIOMOL Research Labs., Plymouth Meeting, PA, USA). All inhibitors were dissolved in dimethyl sulfoxide (DMSO), which also served as the control in samples with no inhibitor treatment.

2.3. Cell Fractionation

At the indicated times post-infection, H-RasV12 cells were washed and scraped in phosphate buffered saline (PBS) containing protease inhibitor cocktail (PIC; Sigma-Aldrich Canada). The cells were passed through a 30-gauge needle multiple times and centrifuged at 700 g for 10 min. The resulting supernatant was centrifuged at 100 000 g for 25 min to isolate the supernatant and total membrane fractions. The supernatant cytoplasmic fraction was stored at -80˚C. The membrane pellet was resuspended in 1x RIPA buffer (50 mM Tris-HCl, pH 7.4, 150 mM NaCl, 0.5% Na-deoxycholate, 1%

IGEPAL CA®630) with PIC, syringed ten times, and stored at -80˚C. The samples were later subjected to sodium dodecyl sulfate polyacrylamide gel electrophoresis (SDS-PAGE) and western blot. Antibody information can be found in Table 2.2.

2.4. Ras-Activation Assay

Samples were collected according to the suggested protocol supplied by the Ras activation assay kit (Catalog #17-218; Upstate/Millipore EMD). In brief, uninfected (UI) or reovirus-infected cells were collected at the indicated times post-infection. The cells were washed twice with ice-cold PBS, and scraped in the provided 1x Mg^{2+} lysis buffer (MLB) with PIC. The samples were syringed with a 26-gauge needle and centrifuged at 14 000 g for 5 min at 4˚C. The protein concentration of the supernatants was determined by MicroBCA (Thermo Fisher Scientific Inc).

In order to pull-down GTP bound Ras, 25 µg of total cell lysate was rotated with 10 µl of Raf-1 Ras binding domain (RBD)-agarose conjugate for 45 min at 4˚C. The beads were washed 3 times with MLB before 40 µl of 2x Laemmli sample buffer was added. The samples were heated for 3 min at 80˚C and loaded onto a 12% Tris-glycine acrylamide gel for SDS-PAGE. A proportional amount of total cell lysate was loaded as well. A western blot was then performed to probe for Ras (Table 2.2).

Table 2.2: Antibody information for various experimental assays.

Antibody	Host	Working Concentration		Supplier
Reovirus	Rabbit	1: 100 000 1: 10 000	(WB) (IF; ICC; FC)	Patrick Lee Lab
Reovirus	Rat	1: 10 000	(WB; IF)	Patrick Lee Lab
β-Actin (C4)	Mouse	1: 1000	(WB)	Santa Cruz (sc-47778)
Ras, clone RAS10	Mouse	1: 10 000 1: 400 1 µg	(WB) (IF) (IP)	Upstate/Millipore (05-516)
HA Probe (Y-11)	Rabbit	1: 1000	(WB)	Santa Cruz (sc-805)
TGN38	Rabbit	1: 400	(IF)	Abcam (ab16059)
Calnexin	Rabbit	1: 100	(IF)	Abcam (ab13504)
Golgin97	Rabbit	1: 40	(IF)	Abcam (ab33701)
Transferrin Receptor	Rabbit	1: 200	(IF)	Abcam (ab84036)
p38α (C-20)	Rabbit	1:200	(WB)	Santa Cruz (sc-535)
Phospho-p38 MAPK (Thr180/Tyr182)	Rabbit	1: 1000	(WB)	Cell Signaling (#9215)
Akt (pan) (C67E7)	Rabbit	1: 1000	(WB)	Cell Signaling (#4691)
Phospho-Akt (Ser473)	Rabbit	1: 1000	(WB)	Cell Signaling (#4060)
ERK 1 (K-23)	Rabbit	1: 800	(WB)	Santa Cruz (sc-94)
Phospho-ERK (E-4)	Mouse	1: 400	(WB)	Santa Cruz (sc-7383)
SAPK/JNK	Rabbit	1: 1000	(WB)	Cell Signaling (#9252)
Phospho-SAPK/JNK (Thr183/Try185)	Rabbit	1: 1000	(WB)	Cell Signaling (#9251)
SEK1/MKK4	Rabbit	1: 1000	(WB)	Cell Signaling (#9152)
Phospho-SEK1/MKK4 (Ser257/Thr261)	Rabbit	1: 1000	(WB)	Cell Signaling (#9156)
Cy3-conjugated Streptavidin	*S. avidinii*	1.1 µl / ml	(WB)	Jackson ImmunoResearch (016-160-084)
HRP-conjugated Goat anti-Rabbit IgG	Goat	1: 10 000	(WB)	Jackson ImmunoResearch (111-035-003)
Cy2-conjugated	Goat	1: 1000	(WB)	Jackson ImmunoResearch

Goat anti-Rabbit IgG		1: 50 1: 200	(IF) (FC)	(111-225-144)
Cy3-conjugated Goat anti-Rabbit IgG	Goat	1: 1000 1: 50	(WB) (IF)	Jackson ImmunoResearch (111-165-144)
AF647-conjugated Goat anti-Rabbit IgG	Goat	1: 1000 1: 50	(WB) (IF)	Jackson ImmunoResearch (111-605-144)
Alk P-conjugated Goat anti-Rabbit IgG	Goat	1: 1000	(ICC)	Jackson ImmunoResearch (111-055-003)
HRP-conjugated Goat anti-Rat IgG	Goat	1: 10 000	(WB)	Jackson ImmunoResearch (112-035-003)
Cy3-conjugated Goat anti-Rat IgG	Goat	1: 1000 1: 50	(WB) (IF)	Jackson ImmunoResearch (112-165-167)
DyLight 649-conjugated Goat anti-Rat IgG	Goat	1: 1000 1: 50	(WB) (IF)	Jackson ImmunoResearch (112-495-167)
HRP-conjugated Goat anti-Mouse IgG	Goat	1: 10 000	(WB)	Jackson ImmunoResearch (115-035-003)
Cy2-conjugated Goat anti-Mouse IgG	Goat	1: 1000 1: 50	(WB) (IF)	Jackson ImmunoResearch (115-225-146)
Cy3-conjugated Goat anti-Mouse IgG	Goat	1: 1000 1: 50	(WB) (IF)	Jackson ImmunoResearch (115-165-146)
Cy5-conjugated Goat anti-Mouse IgG	Goat	1: 1000 1: 50	(WB) (IF)	Jackson ImmunoResearch (115-175-146)

WB: Western Blot; IF: Immunofluorescence; ICC: Immunocytochemistry; FC: Flow Cytometry; IP: Immunoprecipitation; AF: Alexa Fluor; Cy: Cyanine; HA: Hemagglutinin; HRP: Horseradish Peroxidase; IgG: Immunoglobulin G

2.5. Acyl-Biotin Exchange Assay

H-RasV12 and H-RasV12xx transformed cells were infected with reovirus at a multiplicity of infection (MOI) of 100. After 12 hpi, the cells were washed once with ice-cold PBS, and incubated for 3 min in a palmitoylation lysis buffer (5 mM -ethylenediaminetetraacetic acid (EDTA), 1% Triton X-100, 50 mM N-ethylmaleimide (NEM), 1 mM Na_3VO_4, 1 mM NaF, and 0.1% PIC in PBS pH 7.4). The cells were scraped, passed through a 21-gauge needle, and rotated for 1 h at 4˚C. The lysates were centrifuged at 10 000 g for 10 min at 4˚C, and the protein concentration of the supernatants was determined by MicroBCA.

Cell lysates were precleared for 1 h at 4˚C using Protein G Dynabeads (Life Technologies) that were previously incubated with normal mouse serum (NMS) for 1 h at 4˚C. After 1 h, the magnetic beads were removed from the cell lysates. In order to immunoprecipitate Ras, 1 mg of protein lysate was rotated overnight at 4˚C with 40 µl of Protein G Dynabeads that were pre-bound with 2 µg of Ras antibody (Table 2.2). The beads were washed 3 times with the palmitoylation lysis buffer, once with PBS, and then incubated in 50 mM of NEM for 2 h at RT. NEM forms stable thioether bonds with reactive cysteine residues within the Ras sequence. After treatment, the beads were washed twice with PBS and then divided into two fractions. To release palmitate groups, one fraction was rotated with 1 M of hydroxylamine (pH = 7.4) for 1 h at RT. Hydroxylamine cleaves thioester bonds between Ras and its palmitoyl groups, but does not cleave thioether bonds between Ras and its farnesyl groups. The other fraction, which served as a control, was treated with PBS for the same duration. Both fractions were then washed twice with PBS and incubated with 320 µM of EZ-Link Biotin-BMCC^{TM} (Catalog #21900; Thermo Fisher Scientific Inc.) for 1 h at RT with rotation. EZ-Link Biotin-BMCC^{TM} forms a stable thioether linkage with any reactive cysteine residues within the Ras sequence. The samples were washed twice with PBS, and the beads were resuspended in 30 µl of 2x Laemmli sample buffer. The samples were heated for 3 min at 80˚C and resolved on a 12% Tris-glycine acrylamide gel by SDS-PAGE. Total Ras was detected by western blot using an anti-Ras primary antibody and horseradish peroxidase (HRP)-conjugated goat anti-mouse secondary antibody. Biotinylated protein, which represents palmitoylated protein, was detected using Cy3-conjugated Streptavidin. All

antibody information can be found in Table 2.2. Procedure modified from Dekker et al. (2010).

2.6. Immunoprecipitation

In order to immunoprecipitate Ras or reovirus proteins, the infected cells were first lysed and collected according to the palmitoylation lysis conditions described in Section 2.5. The protein concentration of the supernatants was determined by MicroBCA, and the cell lysates were precleared for 1 h at 4˚C using Protein G Dynabeads (Life Technologies) that were previously incubated with normal mouse, rat, or rabbit serum for 1 h at 4˚C. After 1 h, the magnetic beads were removed from the cell lysates, and 1 mg of the precleared lysates were rotated overnight at 4˚C with 20 µl of Protein G Dynabeads that were pre-bound with antibodies raised against Ras or reovirus (Table 2.2). The beads were washed 3 times with palmitoylation lysis buffer, and resuspended in 30 µl of 2x Laemmli sample buffer. The samples were heated for 3 min at 80˚C and resolved on a 12% Tris-glycine acrylamide gel by SDS-PAGE. To determine if the immunoprecipitation was successful, the membranes were probed using anti-Ras or anti-reovirus primary antibodies and HRP-conjugated goat anti-mouse, rabbit, or rat secondary antibodies. The membranes were re-probed to establish if co-immunoprecipitation occurred. All antibody information can be found in Table 2.2.

2.7. SDS-PAGE and Western Blotting

The cells were collected at the indicated time-points and lysed accordingly. Samples destined for standard SDS-PAGE and western blot were lysed in 1x RIPA buffer

with 0.1% PIC (see Section 2.3). The lysates were placed on ice for 20 min, and centrifuged at 14 000 rpm for 5 min at 4˚C to collect the supernatant. When examining protein phosphorylation, samples were washed twice with ice-cold PBS and lysed in 1x RIPA buffer (see Section 2.3) supplemented with 0.1% PIC, 1 mM Na_3VO_4, 5 mM NaF, 1 mM PMSF (phenylmethylsulfonyl fluoride), and 0.1% phosphatase inhibitor cocktail III. The cells were scraped, sonicated, placed on ice for 10 min, and centrifuged at 14 000 rpm for 15 min at 4˚C to collect the supernatant. In either case, the protein concentration from the supernatant was determined by MicroBCA. The cell lysates were resuspended in a 1:1 ratio of 2x Laemmli sample buffer containing β-mercaptoethanol (βME) and boiled for 5 min at 95˚C. Alternatively, lysates that were to be probed for Ras proteins were resuspended in a 1:1 ratio of 2x Laemmli sample buffer and boiled for 3 min at 80˚C. The proteins were separated using 10-15% Tris-glycine polyacrylamide gels by SDS-PAGE at 100 V for approximately 2 h. Depending on the molecular weight of the target protein, the gels were transferred for 30 min to 1 h at 100 V onto PVDF membranes. The membranes were incubated for 1 h at RT or overnight at 4˚C in blocking buffer (5% w/v bovine serum albumin (BSA) in Tris-buffered saline with 1% Tween®20 (TBST) or 3% w/v powdered milk in TBST). The primary antibodies were diluted in the appropriate TBST blocking buffer (see Table 2.2) and incubated on the membrane for 1 h at RT. The membranes were washed 3 times with TBST before a suitable Cy2, Cy3, Cy5, or HRP-conjugated secondary antibody was applied. After 1 h at RT, the membranes were washed again with TBST and if necessary, developed using the Pierce® ECL Plus western blotting substrate (Thermo Fisher Scientific Inc.). The western blots were visualized by the Typhoon 9410 variable mode imager (GE Healthcare Life Sciences,

Piscataway, NJ, USA), and ImageJ 1.47v (National Institutes of Health, Bethesda, MD, USA) was used for protein band quantification through densitometry.

2.8. RNA Purification and Quantitative Real-time Polymerase Chain Reaction (qRT-PCR)

Total RNA was extracted at 4 and 12 hpi using TRIzol® (Life Technologies). To isolate high quality RNA, the samples were treated with chloroform and 100% ethanol before being loaded onto the columns provided in the PureLink® RNA purification kit (Life Technologies). An on-column DNase I digestion was performed to remove any residual DNA contamination, and the RNA was recovered according to the manufacturer's protocol. In a 20 µl reaction, 250 ng of total RNA was used for cDNA synthesis using the suggested protocol for SuperScript® II reverse transcriptase (Life Technologies). The resulting cDNA was diluted with 80 µl of nuclease-free water. Each qRT-PCR reaction contained 3 µl of diluted cDNA, gene-specific primers (Table 2.3), nuclease-free water, and Promega™ GoTaq® qPCR master mix (Thermo Fisher Scientific Inc.). After the initial denaturation step at 95˚C for 5 min, the samples underwent 40 amplification cycles at 95˚C for 10 sec and 60˚C for 30 sec using the Mx3000P™ real-time PCR system (Stratagene, Agilent Technologies Canada Inc. Mississauga, ON, Canada). The samples collected at 4 and 12 hpi were used to amplify the reovirus S4(-) and IFN-β genes, respectively. Data was analyzed using MxPro qPCR software (Stratagene) and mRNA levels were normalized to the glyceraldehyde 3-phosphate dehydrogenase (GAPDH) internal control.

Table 2.3: List of qRT-PCR primers.

Target	Forward Primer 5' to 3'	Reverse Primer 5' to 3'
GAPDH	TGGCAAAGTGGAGATTGTTG	AAGATGGTGATGGGCTTCCC
Reovirus S4(-)	GGAACATTGTGAGAGCAGCA	GCAAGCTAGTGGAGGCAGTC
IFN-β	CCCTATGGAGATGACGGAGA	CTGTCTGCTGGTGGAGTTCA

2.9. Detection of Reovirus Infected Cells

Mock and reovirus infected cells that were treated with or without an inhibitor were collected at 12 hpi for fluorescence-activated cell sorting (FACS). The trypsinized cells were washed with PBS, fixed in a 4% paraformaldehyde in PBS solution, and placed on ice for 30 min. The cells were washed with PBS and left for 1 h at RT or overnight at 4˚C in blocking buffer (3% BSA, 0.1% Triton X-100 in PBS). The cells were probed using a polyclonal rabbit anti-reovirus primary antibody and a Cy2-conjugated goat anti-rabbit secondary antibody (Table 2.2). The washed cells were quantified using a FACScan flow cytometer (BD Biosciences, San Jose, CA, USA). Data was analyzed using FCS Express™ or CellQuest Pro™ software (BD Biosciences).

Alternatively, at 12 hpi the cells underwent immunocytochemistry (ICC). The plated cells were fixed and permeabilized in ice-cold methanol for 5 min. The cells were washed in PBS and left for 1 h at RT or overnight at 4˚C in blocking buffer (see above). The cells were probed using a polyclonal rabbit anti-reovirus primary antibody and an alkaline phosphatase-conjugated goat anti-rabbit secondary antibody (Table 2.2). The cells were incubated with the appropriate antibody for 1 h at RT, and washed 3 times in PBS containing 0.1% Triton X-100 after each antibody incubation. Reovirus infected

cells were visualized through the use of a BCIP/NBT alkaline phosphatase substrate kit IV (Vector Laboratories Ltd., Burlingame, CA, USA) diluted in 100 mM Tris buffer in ddH_20 (pH = 9.5). Once reovirus infected cells could be differentiated from uninfected cells, a stop solution was added (5 mM EDTA in PBS). The cells were photographed using the Nikon Eclipse TS100 microscope and Nikon Coolpix 4500 camera (Nikon Canada Inc., Mississauga, ON, Canada). Simple counting determined the number of reovirus infected cells.

2.10. Measures of Apoptosis and Cell Death

To determine the percentage of cells undergoing apoptosis and cell death, mock or reovirus infected cells that were cultured in the presence or absence of an inhibitor were collected at 24 hpi for FACS analysis. The cells were stained with Annexin V-PE and 7-AAD according to the manufacturer's instructions (BD Biosciences), and quantified using a FACScan flow cytometer. Trypan blue exclusion staining served as another means of quantifying cell death. Live cells prevent uptake of the dye, while dead cells are unable to exclude the stain and turn blue. At 24 hpi, trypsinized cells were mixed in a 1:1 ratio with 0.4% trypan blue stain (Life Technologies). The cells were visualized using the Nikon Eclipse TS100 microscope (Nikon Canada Inc.), and the number of dead to live cells was determined with the aid of a haemocytometer. In either technique, background cell death from uninfected cells was taken into account in order to provide an accurate representation of death caused by the virus and/or inhibitor.

2.11. Plaque Assay and Analysis

Non- and Ras-transformed cells were cultured to 90% confluency and infected with serial dilutions of reovirus. The cells were infected in a volume of 100 µl per well of a 12-well plate for 1 h at 37˚C. The plates were also shaken every 10 min to prevent the cells from drying out and to ensure even distribution of the virus. After 1 h, an agar mixture consisting of 2% agar (Catalog #BP1423; Thermo Fisher Scientific Inc) and 2x MEM (supplemented with 20% NCS and 2% AA) in equal volume was added to the cells and allowed to set. Depending on the experiment, this mixture sometimes contained an appropriate concentration of inhibitor or DMSO control. After the mixture solidified, the plates were placed upside down in a 37˚C incubator.

After 5 days, the cells were fixed in 10% formaldehyde (diluted in PBS) for 20 min at RT. The agar plug was popped out and the cells were permeabilized in ice-cold methanol for 5 min. The cells were washed in PBS and left for 1 h at RT or overnight at 4˚C in blocking buffer (3% BSA and 0.1% Triton X-100 in PBS). The cells were incubated with polyclonal rabbit anti-reovirus primary antibody for 1 h at RT and subsequently, alkaline phosphatase-conjugated goat anti-rabbit secondary antibody for the same duration (Table 2.2). After each of the antibody incubations, the cells were washed in PBS containing 0.1% Triton X-100. Reovirus plaques were visualized through the use of a BCIP/NBT alkaline phosphatase substrate kit IV (Vector Laboratories Ltd.) diluted in 100 mM Tris buffer in ddH_20 (pH = 9.5). Once reovirus plaques could be differentiated from uninfected cells, a stop solution was added (5 mM EDTA in PBS). The viral plaques were photographed using the Zeiss Stemi 2000-C stereoscope and

AxioCam HRC colour camera (Carl Zeiss Canada Inc., Toronto, ON, Canada). Plaque size was determined by measuring the largest diameter of every plaque within each well.

The plaque assay was also used to determine the viral titer from a reovirus stock preparation or from infected non- and Ras-transformed cells. A slightly different protocol was followed. In the former, purified reovirus from infected L929 spinner cultures was serially diluted to infect 90% confluent monolayers of highly permissive L929 cells. After determining the titer of the reovirus stock preparation on L929 cells, a higher MOI is required to infect the same number of NIH3T3 cells. Reovirus is over 10 times more effective at binding L929 cells than NIH3T3 cells, and as such, an MOI of 10 reovirus pfu/cell is needed to infect approximately 10–30% of NIH3T3 cells (Marcato et al., 2007). In the latter, reovirus infected non- and Ras-transformed cells were collected at 24 hpi to obtain total and release reovirus samples for titration. Reovirus release samples were collected by removing $1/10^{th}$ of the media volume, and centrifuging it for 5 min at 1000 g. To ensure that the sample remained cell free, only 80% of the supernatant was removed and stored at -80˚C. After reovirus release was collected, the same well received $1/10^{th}$ its original volume of 10x RIPA buffer (10% NP-40, 5% Na-deoxycholate, 1% PIC). The cells were scraped and stored at -80˚C.

Total and release reovirus samples were serially diluted to infect 90% confluent monolayers of L929 cells, and as per above, 100 µl of diluted virus was added per well of a 12-well plate for 1 h at 37˚C. The plates were shaken every 10 min. After 1 h, an agar mixture made up of 2% agar and 2x MEM (supplemented with 10% FBS, 2 mM sodium pyruvate, 2% MEM NEAA, and 2% AA) in equal volume was added to the cells and allowed to set. After the mixture solidified, the plates were placed upside down in a 37˚C

incubator for 5 days. After 5 days, the cells were fixed in 10% formaldehyde (diluted in PBS) for 20 min at RT. The agar plug was popped out and the cells were permeabilized in ice-cold methanol for 5 min. Crystal violet (5 g in 50% ethanol) was then used as a contrasting stain to highlight the viral plaques within the cell monolayer. Reovirus plaques were counted and the titer was determined. Titers are denoted as plaque forming units (pfu) / ml, or as % release.

2.12. Immunofluorescence (IF) Microscopy

Non- and Ras-transformed cells were grown overnight on gelatin-coated cover slips. To decrease the likelihood of the cells lifting off the cover slips, the cells were infected with diluted reovirus in a volume of 200 µl per cover slip for 1 h at 37˚C. The larger volume provided enough surface coverage such that the plates did not need to be shaken during infection. If required, 2BP or FTI-277 was added at 2 hpi. At 12 hpi, the cells were fixed in 4% paraformaldehyde (in PBS) for 20 min, washed in PBS, and left for 1 h at RT or overnight at 4˚C in blocking buffer (3% BSA, 0.1% Triton X-100 in PBS). Reovirus exponential growth occurs between 6 and 12 hpi, and the latter time point was chosen to assess the effect of the virus on target cells (Shmulevitz et al., 2012). Primary and Cy-conjugated secondary antibodies (see Table 2.2) were diluted in blocking buffer and incubated on the cover slips for 1 h at RT. PBS containing 0.1% Triton X-100 was used to rinse the cells. Cover slips were mounted onto slides using FluoroShield mounting medium (Sigma-Aldrich Canada) and further sealed with nail polish. The cells were visualized using the Zeiss LSM 510 Meta laser scanning confocal microscope (Carl Zeiss Canada Inc.), and later analyzed by the LSM image browser.

2.13. Statistical Analyses

All required statistical analyses were completed using SYSTAT 13 (Systat Software Inc., Chicago, IL, USA). Two sample t-tests were used to compare the effect of a single inhibitor on individual cell lines. A one-sample t-test was performed to determine whether a fold increase was greater than one. If there was a high degree of variability between individual trials, then a paired t-test was employed instead. One or two-way analysis of variance (ANOVA) was used when examining the effect of two or more factors. A nested ANOVA was utilized for plaque size analysis, which allowed the effect of individual wells within each treatment to be taken into account. Tukey's pair-wise comparisons were then used to identify significant differences between factors.

CHAPTER 3: RESULTS

Reovirus is a naturally occurring oncolytic virus that preferentially targets Ras-transformed cells (Coffey et al., 1998; Strong et al., 1998). Its genome, which is comprised of ten dsRNA segments, leaves little room for genetic manipulation in the creation of a functional virion. As such, the structure and size of the reovirus genome suggests a level of genomic and proteomic multitasking during its infection of target cells. Marcato et al. (2007) highlighted certain stages of the reovirus life cycle (ie. disassembly, virion production, and apoptosis) that were enhanced in Ras-transformed cells, but the direct relationship between reovirus and Ras has yet to be examined. Ras is a dynamic protein that functions at the center of a signalling hub to control a wide array of cellular processes, including growth, differentiation, and death (Prior and Hancock, 2012). When Ras is constitutively activated through mutation, its signalling to downstream effectors becomes deregulated and can lead to oncogenesis. With reovirus currently undergoing clinical trials and demonstrating its efficacy as a cancer therapeutic, a lot of emphasis has been placed on understanding the molecular mechanisms behind its oncolysis (Oncolytics Biotech Inc, 2014). Taken collectively, this study set out to determine whether reovirus was capable of manipulating oncogenic Ras to trigger apoptosis of target cells by altering its post-translational modifications, intracellular location, and signalling to downstream effectors.

3.1. Reovirus Infection Redistributes H-RasV12 from the Plasma Membrane

The following experiments were designed to assess any variations in Ras localization following reovirus infection. Using immunofluorescence, Ras was visualized

in non-transformed and H-RasV12 transformed cells. To recall, when Ras-transformed or non-transformed cells are mentioned throughout this chapter, it refers to NIH3T3 cells that were freshly transformed by retrovirus containing activated Ras or the vector control (pBABE-puro). Transformed NIH3T3 cells are a well established model system utilized in our lab for the past twenty years. While most cancers are of epithelial origin, the data obtained from this model system has led to a better understanding of reovirus pathogenesis and provided the basis for clinical investigation of reovirus as a cancer therapeutic. Endogenous Ras levels were faintly detected in non-transformed cells by confocal microscopy (Figure 3.1A), and as a result of the retrovirus-based cell system, H-RasV12 was clearly expressed in the Ras-transformed cells (Figure 3.1B). H-RasV12 requires post-prenylation processing and localizes to the ER and Golgi body before reaching the cell surface (Ahearn et al., 2012). As expected, H-RasV12 showed distinct plasma membrane and endomembrane localization in uninfected Ras-transformed cells (Figure 3.1B). Interestingly, reovirus infection of H-Ras transformed cells appeared to alter the normal distribution of H-RasV12. At 12 hpi, reovirus factories could clearly be seen in the perinuclear region of the host cell, however H-RasV12 seemed to lose its plasma membrane localization and accumulate in non-overlapping, punctate structures (Figure 3.1B). Furthermore, fractionation of reovirus infected cells into membrane and soluble fractions indicated an increase in soluble Ras during the first 18 hours of infection (Figure 3.2). With immunofluorescence and cell fractionation suggesting that reovirus infection alters the distribution of Ras, co-immunoprecipitations were performed to determine whether any direct interaction between oncogenic Ras and reovirus proteins occurred. Neither immunoprecipitations carried out by anti-Ras nor anti-reovirus

antibodies yielded any indication that the proteins associated with one another during infection (Figure 3.3). These results were consistent with the lack of overlap observed between reovirus factories and Ras punctate structures by confocal microscopy.

Figure 3.1: Reovirus infection results in a redistribution of H-RasV12 from the plasma membrane. (A) Non-transformed cells were stained with anti-Ras antibodies (green) and imaged at 630x magnification by confocal microscopy to visualize endogenous Ras. Scale bar: 20 μm. (B) H-RasV12 transformed cells were infected with reovirus at an MOI of 20 and fixed at 12 hpi. The cells were stained with anti-Ras (green) and anti-reovirus (red) antibodies, and visualized under 1000x magnification by confocal microscopy. White squares highlight regions that are enlarged under the "Zoom" heading. Arrows indicate plasma membrane localization in uninfected cells and punctate formation following reovirus infection. Scale bar: 10 μm. Images are representative of three independent experiments.

A

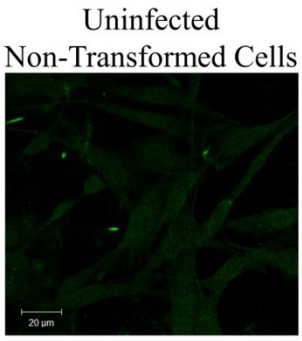
Uninfected
Non-Transformed Cells
20 µm

B

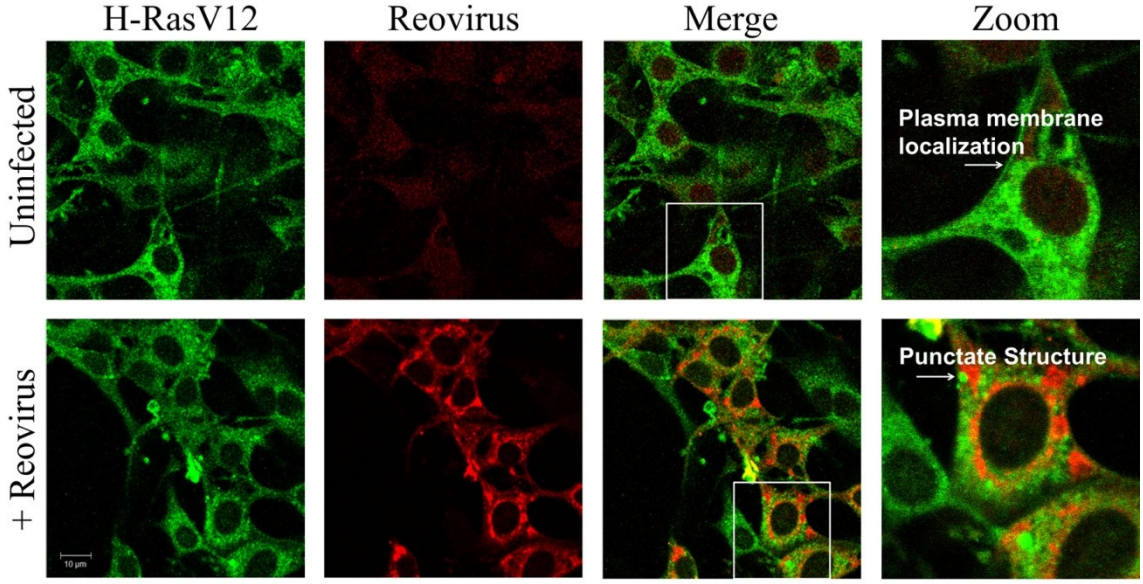
H-RasV12
Reovirus
Merge
Zoom
Uninfected
+ Reovirus
Plasma membrane localization
Punctate Structure
10 µm

Figure 3.2: Soluble Ras increases during reovirus infection. H-RasV12 transformed cells were mock or reovirus infected at an MOI of 20.(A) At the indicated times post-infection, the cells were collected and subjected to fractionation. The fractions were separated by SDS-PAGE and probed with anti-Ras and anti-β-actin antibodies. UI: uninfected. (B) Whole-cell lysates were collected at the indicated times post-infection, and following SDS-PAGE, were probed using an anti-reovirus antibody. λ, μ, and σ represent the location of reovirus proteins. Blots are representative of three independent experiments.

A

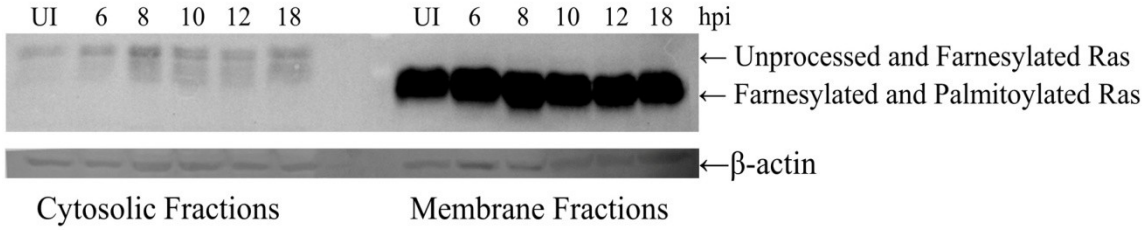
UI 6 8 10 12 18
UI 6 8 10 12 18 hpi
← Unprocessed and Farnesylated Ras
← Farnesylated and Palmitoylated Ras
←β-actin
Cytosolic Fractions
Membrane Fractions

B

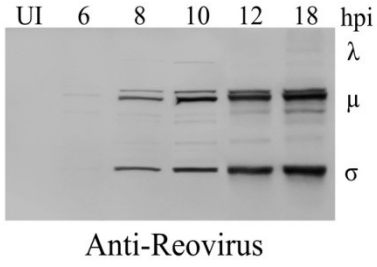
UI 6 8 10 12 18 hpi
λ
μ
σ
Anti-Reovirus

Figure 3.3: Reovirus proteins do not interact with Ras during infection. H-RasV12 transformed cells were infected with reovirus at an MOI of 100 and collected at 12 hpi. Precleared lysates were immunoprecipitated with the appropriate antibody and subjected to SDS-PAGE and western blot analysis (n = 2). (A) Ras immunoprecipitations were probed using anti-Ras, anti-reovirus (rabbit), or anti-reovirus (rat) antibodies to determine if any reovirus proteins were present in the Ras IPs. (B) Reovirus (rabbit or rat) immunoprecipitations were probed with anti-reovirus (rabbit), anti-Ras, or anti-reovirus (rat) antibodies to determine if any Ras was present in the reovirus IPs. Whole-cell lysates were used as a control. λ, μ, and σ indicate the location of reovirus proteins on the western blots. Heavy and light chains indicate antibody fragments. UI: uninfected; V: reovirus infected.

A

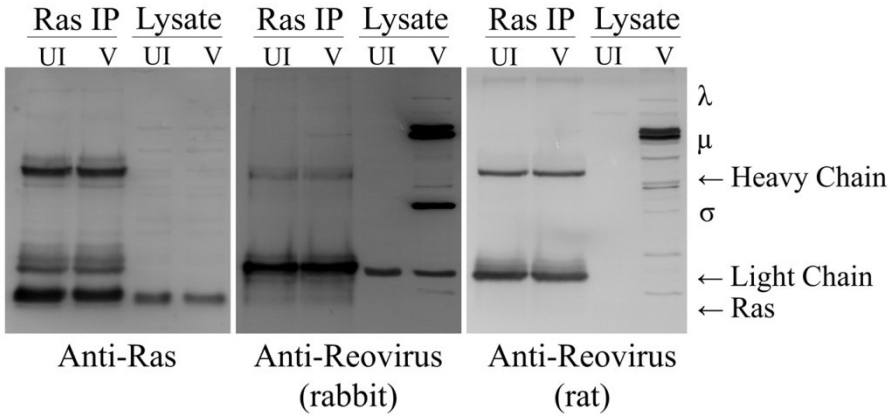
Ras IP
Lysate
UI V UI V
Ras IP
Lysate
UI V UI V
Ras IP
Lysate
UI V UI V
λ
μ
← Heavy Chain
σ
← Light Chain
← Ras
Anti-Ras
Anti-Reovirus (rabbit)
Anti-Reovirus (rat)

B

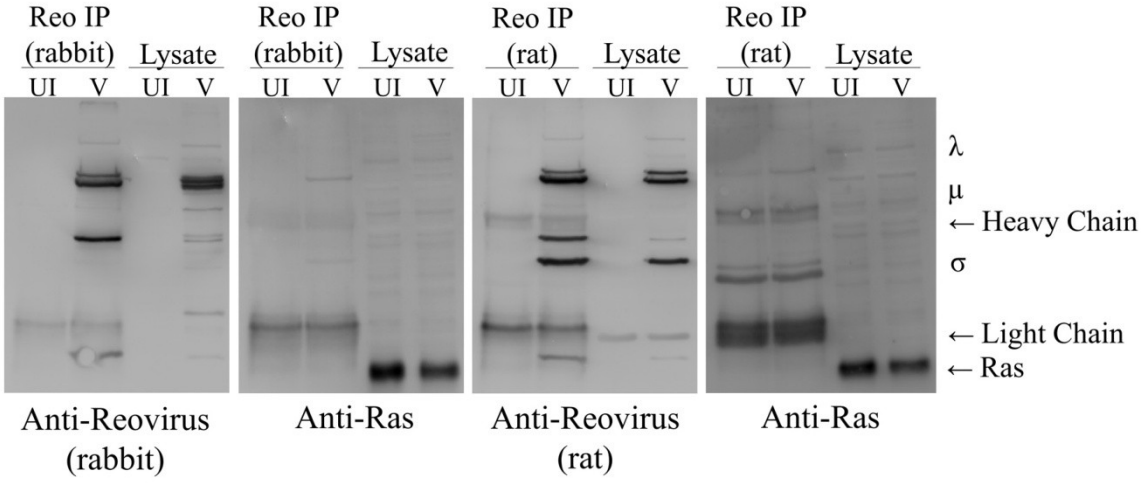
Reo IP (rabbit)
Lysate
UI V UI V
Reo IP (rabbit)
Lysate
UI V UI V
Reo IP (rat)
Lysate
UI V UI V
Reo IP (rat)
Lysate
UI V UI V
λ
μ
← Heavy Chain
σ
← Light Chain
← Ras
Anti-Reovirus (rabbit)
Anti-Ras
Anti-Reovirus (rat)
Anti-Ras

3.2. Depalmitoylated H-RasV12 Increases during Reovirus Infection

Ras is a small GTPase that functions as a molecular switch. When bound to GDP, Ras is inactive and unable to bind downstream effectors. RasGEFs exchange GDP to GTP to activate Ras and enable downstream signalling (Vigil et al., 2010). Single amino acid substitutions, typically at sites 12, 13, and 61, result in mutated Ras proteins that are unable to hydrolyze GTP intrinsically or through the action of RasGAPs, and consequently, remain constitutively activated (Bos, 1989). Therefore, the level of GTP-bound Ras is also a measure of activated Ras. Using a Ras activation assay, which pulls down GTP-bound Ras using the Raf-1 RBD, changes to the GTP-loading status of H-RasV12 were assessed in the context of reovirus infection. Total Ras levels, inclusive of all GDP and GTP-bound Ras isoforms, remained constant during infection; however, activated Ras levels were slightly upregulated in reovirus infected cells when compared to the uninfected control. The most notable change was not due to the levels of Ras activation, but to the large gel mobility shift that occurred between 6 and 12 hpi in lysates that were not treated with βME (Figure 3.4A). Due to the addition of lipid groups, H-RasV12 exists in many forms throughout the cell at any given time, including newly synthesized, farnesylated, and dually and monopalmitoylated (Arozarena et al., 2011). During SDS-PAGE, lipidated Ras runs more quickly through the gel than its non-lipidated form as the lipid groups increase SDS binding and the overall negative charge on the protein (Gutierrez et al., 1989; Hancock et al., 1989). Therefore, an upward gel mobility shift of H-RasV12, like the one observed between 6 and 12 hpi, implies the removal of lipid groups from the oncogenic protein. Ras also has a half-life of 24 h, which is approximately the time it takes for reovirus to complete its life cycle in NIH3T3

cells (Magee et al., 1987). Since reovirus infection did not alter the expression levels of total Ras, targeting Ras lipidation would provide a feasible means to manipulate the oncogenic protein. After undergoing farnesylation, Ras is permanently modified; thus, making the reversible modification of palmitoylation a more likely target for reovirus (Ahearn et al., 2012). If this was the case, then treatment of the pull down samples with the reducing agent, βME, should cleave the thioester linkage between H-RasV12 and its palmitoyl groups, and abolish the gel mobility shift (Stickney et al., 2001). It is worth noting that βME is unable to cleave the stable, thioether linkage that exists between Ras and its farnesyl group. βME treatment of the Ras pull downs eliminated the previously observed gel shift and resulted in the migration of Ras at its expected molecular weight of ~21 kD in both uninfected and reovirus-infected samples; suggesting that reovirus infection may manipulate Ras palmitoylation (Figure 3.4).

Palmitoylation is a difficult modification to detect (Linder and Deschenes, 2006). There are no known antibodies against palmitoyl groups and the classical approach involves metabolic labelling by radioactive palmitate with long exposure times. As such, recently developed acyl-biotin exchange chemistry was performed to quantify the amount of Ras palmitoylation following reovirus infection (Drisdel et al., 2006). Acyl-biotin exchange chemistry involves removing the palmitoyl group from Ras and replacing it with a detectable reagent: in this case, biotin-BMCC. H-RasV12xx was engineered to be palmitoylation deficient (C181S and C184S) and served as a control for this study. The lack of palmitoylation could be observed by the gel mobility shift in the H-RasV12xx and hydroxylamine-treated H-RasV12 samples (Figure 3.5A). Unexpectedly, hydroxylamine treatment of immunoprecipitations from H-RasV12 cells resulted in prominent bands that

were double the size of Ras in the anti-Ras western blot. This observation was also noted in N-Ras transformed cells, and subsequent treatment of the samples with βME eliminated the upper Ras band (data not shown). Biochemical analysis has suggested that soluble and farnesylated Ras can form dimers (Goodwin et al., 2005). At 12hpi, a small amount of biotin was detected in the H-RasV12xx control cells and the H-RasV12 cells treated with PBS. This was considered background levels of detection and represented cysteine residues within the Ras sequence that were insufficiently quenched by NEM and resultantly, available for biotin-BMCC binding. Longer NEM incubation times over-quenched the system and thus, the western blot represents the optimized conditions for this assay. In the H-RasV12 samples treated with hydroxylamine, palmitoylated proteins were represented by the presence of a strong biotin signal. When compared to the uninfected control, reovirus infection of H-RasV12 transformed cells decreased Ras palmitoylation levels by 29% at 12 hpi (Figure 3.5B).

Figure 3.4: Reovirus infection results in a gel mobility shift in GTP-bound Ras. H-RasV12 transformed cells were mock or reovirus infected at an MOI of 20 and collected at the indicated times post-infection. (A) Left and center panels: Cell lysates were incubated with Raf-1 RBD conjugated agarose beads to pull-down GTP-bound Ras. The resulting pull-down was treated with 2x Laemmli buffer (+/- β-mercaptoethanol) and subjected to SDS-PAGE and anti-Ras western blot probing. Right panel: Western blot of whole-cell lysates to determine the total amount of Ras present at each time-point. Arrows indicate the location of Ras. (B) As a control, western blots of whole-cell lysates were probed using anti-reovirus and anti-β-actin antibodies. Blots are representative of three independent experiments. λ, μ, and σ represent the location of reovirus proteins. UI: uninfected.

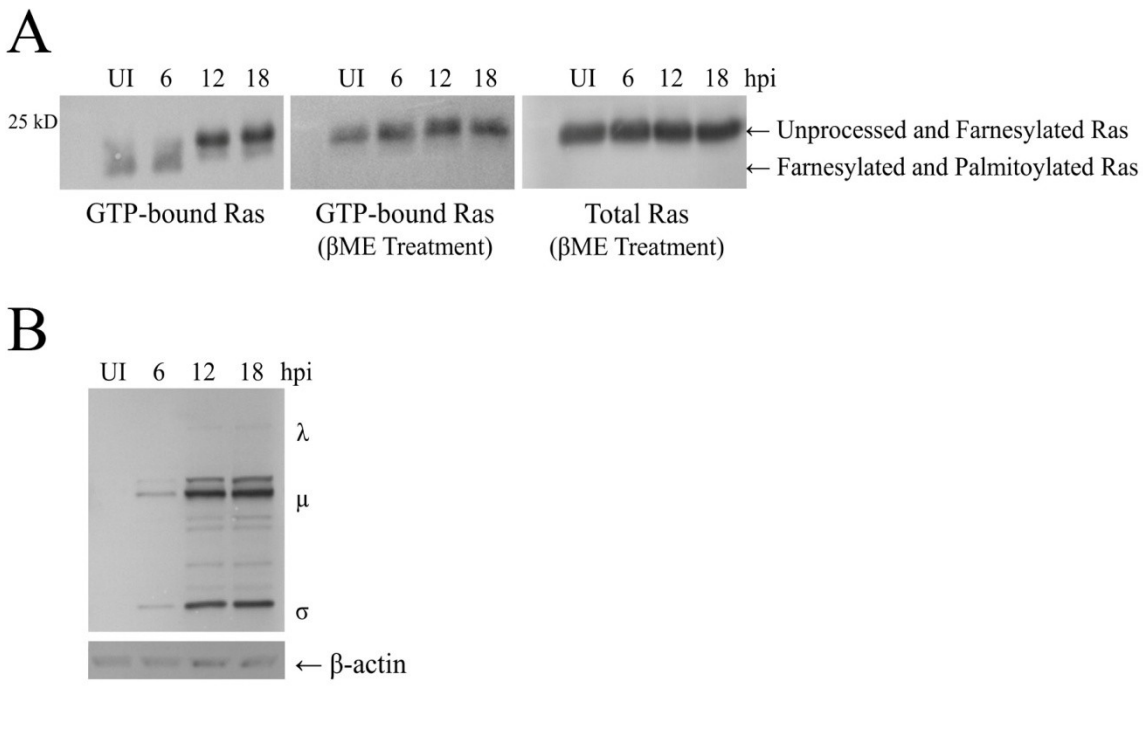
A
UI 6 12 18
UI 6 12 18
UI 6 12 18 hpi
25 kD
← Unprocessed and Farnesylated Ras
← Farnesylated and Palmitoylated Ras
GTP-bound Ras
GTP-bound Ras
(βME Treatment)
Total Ras
(βME Treatment)
B
UI 6 12 18 hpi
λ
μ
σ
← β-actin

Figure 3.5: Reovirus infection of H-RasV12 cells decreases Ras palmitoylation. H-RasV12 and H-RasV12xx transformed cells were mock or reovirus infected at an MOI of 100 and collected at 12 hpi. (A) Cell lysates were immunoprecipitated using anti-Ras antibodies and treated with either PBS (control) or hydroxylamine to remove palmitate groups from Ras. All samples underwent acyl-biotin exchange chemistry and the resulting western blots were probed with anti-Ras and streptavidin. UI: uninfected; V: reovirus infected; C: beads + anti-Ras (no cell lysate); H: hydroxylamine treatment. (B) Quantification of the acyl-biotin exchange assay. Western blot bands were analyzed by densitometry and a paired t-test was used to compare the data (± S.E.; n = 3). (C) As a control, western blots of whole-cell lysates were probed using anti-reovirus and anti-β-actin antibodies. λ, μ, and σ represent the location of reovirus proteins.

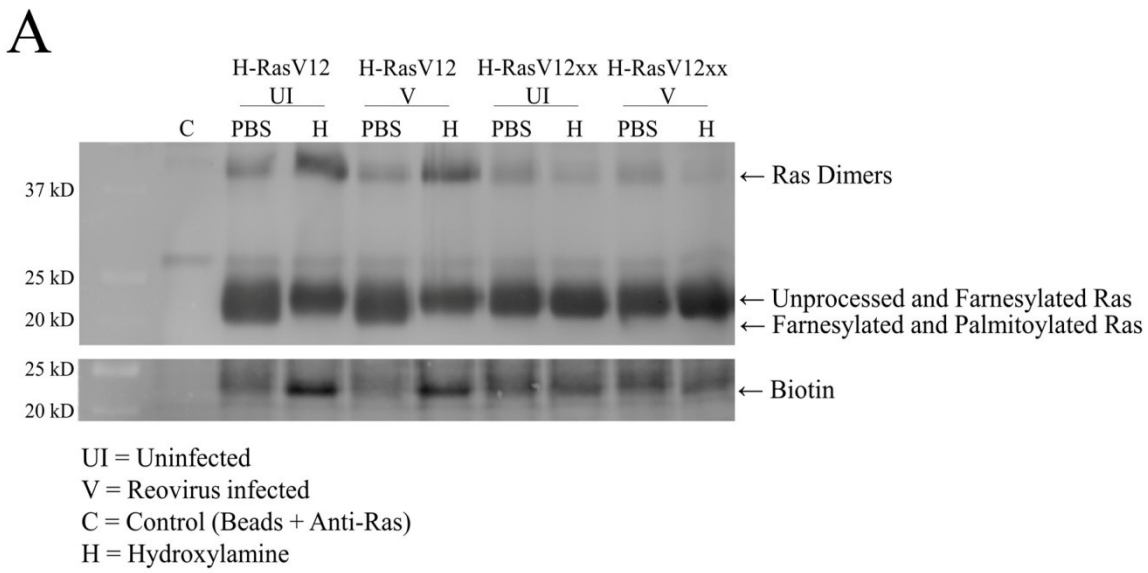
A
H-RasV12
UI
H-RasV12
V
H-RasV12xx
UI
H-RasV12xx
V
C
PBS
H
PBS
H
PBS
H
PBS
H
37 kD
25 kD
20 kD
25 kD
20 kD
← Ras Dimers
← Unprocessed and Farnesylated Ras
← Farnesylated and Palmitoylated Ras
← Biotin
UI = Uninfected
V = Reovirus infected
C = Control (Beads + Anti-Ras)
H = Hydroxylamine

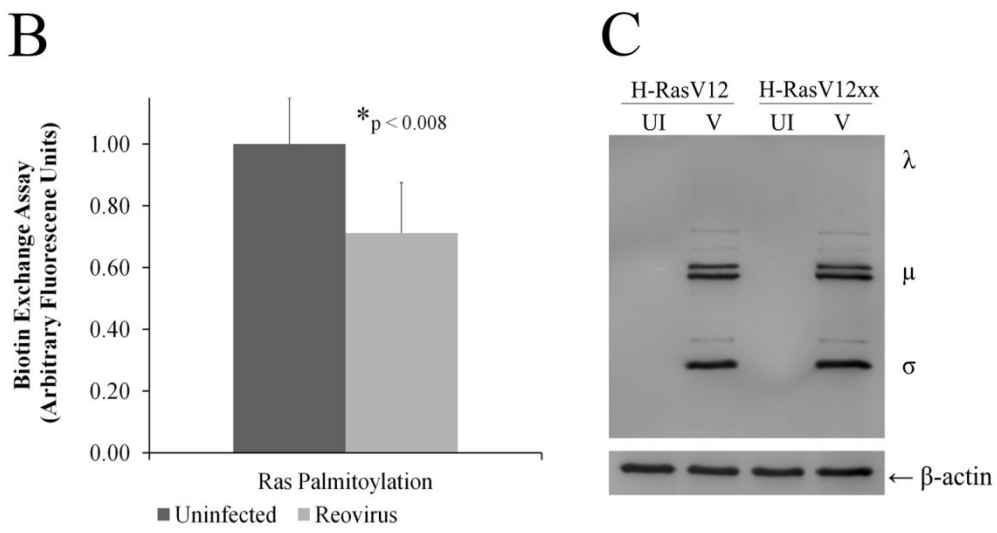
B
Biotin Exchange Assay
(Arbitrary Fluorescene Units)
1.00
0.80
0.60
0.40
0.20
0.00
*p < 0.008
Ras Palmitoylation
Uninfected
Reovirus
C
H-RasV12
H-RasV12xx
UI
V
UI
V
λ
μ
σ
← β-actin

3.3. Reovirus Infection Causes Golgi Fragmentation and the Accumulation of H-RasV12 in the TGN

Ras is palmitoylated at the Golgi body, and with reovirus infection reducing the levels of palmitoylated Ras, it prompted a closer investigation of the organelle itself. Using confocal microscopy, the flattened stacks of the Golgi complex, as well as the typical perinuclear crescent formation could clearly be seen in both uninfected non- and H-RasV12 transformed cells (Figure 3.6A-B; top panels). In reovirus infected cells, the perinuclear stacks were broken up into punctate structures; an indication of early Golgi fragmentation (Figure 3.6A-B; bottom panels). Golgi fragmentation is usually observed during mitosis, but it can also occur as an early apoptotic event or through cytoskeletal interference (Colanzi et al., 2003; Mukherjee et al., 2007; Nozawa et al., 2002). In support of the later, uninfected H-RasV12 cells were treated with nocodazole to disrupt microtubules and induce their depolymerization. Similar to reovirus infection, the Golgi complex formed punctate structures in the presence of the drug (Figure 3.6C). It is well known that reovirus utilizes cytoskeletal elements to setup viral inclusion bodies and that the structural protein, μ2, associates with microtubules (Parker et al., 2002; Sharpe et al., 1982). Since reovirus T3D inhibits cell proliferation of infected cells (Poggioli et al., 2000), it is likely the formation of perinuclear reovirus factories and the lytic nature of the virus that contribute to Golgi fragmentation.

Earlier in this chapter, it was shown that oncogenic Ras formed punctate structures following reovirus infection; however, the identity of these structures was unknown at the time. H-RasV12 is subjected to post-translational modifications that enable its interaction with endomembranes and the plasma membrane (Ahearn et al.,

2012). Oncogenic H-Ras is typically associated with the plasma membrane, but when its palmitate group is removed, it cycles back to the Golgi body for another round of palmitoylation. Knowing that reovirus infection decreased the palmitoylation levels of H-RasV12 and caused Golgi fragmentation, it was likely that the punctate structures were either the ER or the Golgi. Confocal immunofluorescence microscopy of reovirus infected H-Ras transformed cells revealed colocalization of Ras punctate structures with the Trans Golgi marker, TGN38 (Figure 3.7). Therefore, reovirus-induced fragmentation of the Golgi body leads to accumulation of H-RasV12 in this organelle.

Figure 3.6: Reovirus infection causes fragmentation of the Golgi body in non- and H-RasV12 transformed cells. (A) Non-transformed and (B) H-RasV12 transformed cells were infected with reovirus at an MOI of 40 and 20, respectively. The cells were fixed at 12 hpi and stained with antibodies against Golgin97 (red) and reovirus (blue) proteins. Imaging was performed at 630x magnification by confocal microscopy. White squares denote regions that were further enlarged under the "Zoom" heading. Scale bar: 20 μm. (C) Prior to fixation, uninfected H-RasV12 transformed cells were treated with nocodazole for 2 h. The cells were stained with anti-Golgin97 (red) and anti-Ras (green) antibodies, and visualized by confocal microscopy at 630x magnification. Scale bar: 10 μm. Images are representative of three independent experiments.

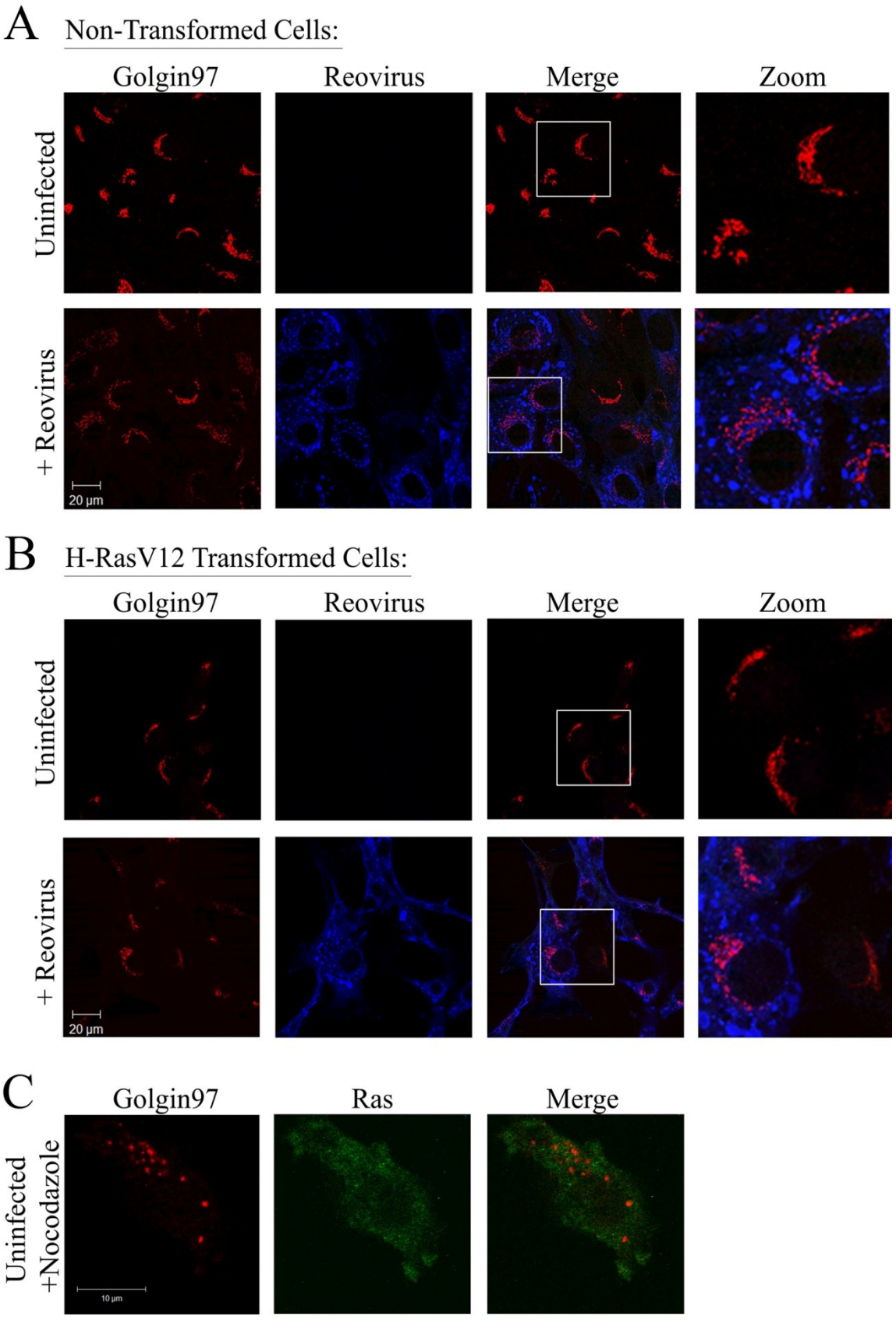
A
Non-Transformed Cells:
Golgin97
Reovirus
Merge
Zoom
Uninfected
+ Reovirus
20 µm
B
H-RasV12 Transformed Cells:
Golgin97
Reovirus
Merge
Zoom
Uninfected
+ Reovirus
20 µm
C
Golgin97
Ras
Merge
Uninfected
+Nocodazole
10 µm

Figure 3.7: H-RasV12 accumulates in the Trans Golgi Network (TGN) during reovirus infection. (A) H-RasV12 transformed cells were infected with reovirus at an MOI of 20. The cells were fixed at 12 hpi and stained with anti-Ras (green), anti-reovirus (blue), and anti-TGN38 (red) antibodies. Imaging was done by confocal microscopy at 630x magnification. White squares highlight regions that are enlarged under the "Zoom" heading. Scale bar: 20 μm. (B) A further enlargement of reovirus infected cells. Scale bar: 20 μm. Images are representative of three independent experiments.

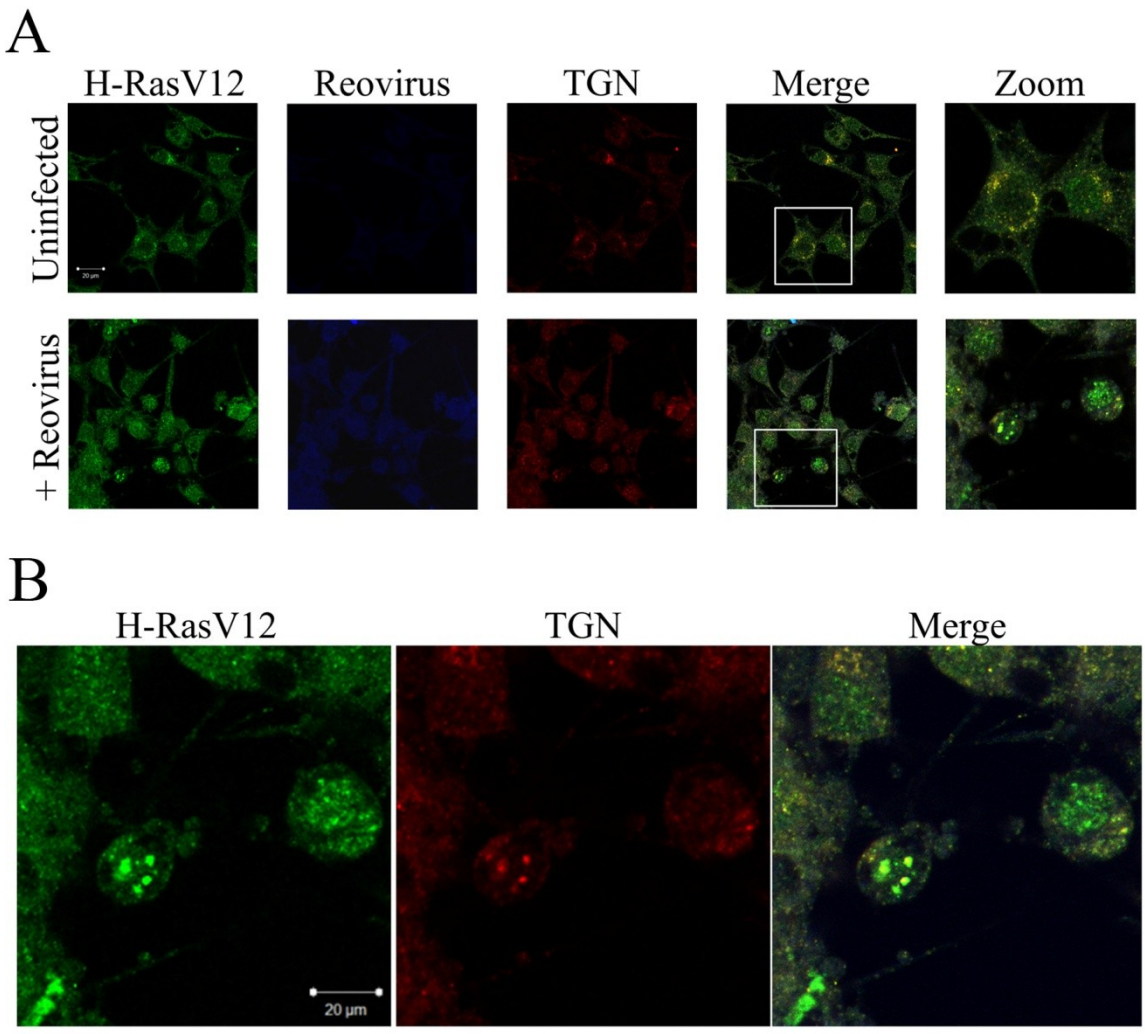
A
H-RasV12
Reovirus
TGN
Merge
Zoom
Uninfected
+ Reovirus
B
H-RasV12
TGN
Merge
20 µm

3.4 The Palmitoylation Inhibitor 2BP Causes Further Accumulation of H-RasV12 in the Golgi body and Promotes Reovirus Spread

With reovirus infection causing H-RasV12 to accumulate in the Golgi body and decreasing Ras palmitoylation levels, it was speculated that the use of a palmitoylation inhibitor could provide synergistic effects to reovirus oncolysis. Despite being non-specific, 2BP is commonly used as a Ras palmitoylation inhibitor and is believed to target the Ras PAT, DHHC9-GCP16 (Resh, 2006). 2BP is predicted to act as a palmitate analog and compete with palmitic acid to irreversibly bind target cysteine residues or incorporate into the binding pocket of PATs. It is also known to interfere with fatty acid β-oxidation and triacylglycerol biosynthesis. While it is more effective at preventing the palmitoylation of monopalmitoylated N-Ras, 2BP can reduce the levels of palmitoylation in oncogenic H-Ras by ~20% (Roy et al., 2005; Webb et al., 2000). Using confocal microscopy, 2BP treatment of reovirus infected H-RasV12 cells resulted in twice the amount of Ras puncta formation, which once again showed colocalization with the Golgi body (Figure 3.8A-C). Uninfected cells with and without 2BP treatment also showed Ras-TGN colocalization, however the distinct punctate formation was not observed. Furthermore, reovirus infected cells treated with 2BP were stained with the ER marker, calnexin, and despite the formation of numerous Ras puncta, ER colocalization was not observed (Figure 3.8D). It is worth mentioning that immunofluorescence was originally supposed to be performed using HA-tagged Ras constructs to distinguish between endogenous and retrovirally-introduced Ras. However, after fusing single or double HA tags onto the N-terminus of all Ras constructs, it was found that the addition of the tag(s) reduced cell transformation and was considered unacceptable for use in reovirus studies

(data not shown). Despite the technical impediment, the above still demonstrates that oncogenic Ras accumulates in the Golgi body following reovirus infection; a movement which can be enhanced in the presence of the palmitoylation inhibitor, 2BP.

To assess the effect of 2BP on reovirus oncolysis, a plaque assay was performed. Non-transformed and H-RasV12 transformed cells were infected with reovirus and treated with increasing concentrations of 2BP or DMSO control (Figure 3.9). Consistent with previous data, reovirus spread was enhanced in Ras-transformed cells (Marcato et al., 2007). In comparison to Ras-transformed cells, non-transformed cells are known to produce a robust IFN response, and consequently, generate smaller reovirus plaques (Shmulevitz et al., 2010). More noticeably was the effect that 2BP had on reovirus oncolysis. In the presence of 2BP, reovirus plaque size markedly increased in a concentration dependent manner in H-RasV12 transformed cells. In contrast, no enhancement was observed in the non-transformed cells. Taken collectively, the data suggests that 2BP causes further accumulation of H-RasV12 in the Golgi body of reovirus infected cells and that use of the inhibitor has a positive effect on reovirus oncolysis.

Figure 3.8: 2BP enhances the accumulation of Ras in the TGN during reovirus infection. (A) H-RasV12 transformed cells were infected with reovirus at an MOI of 20 and treated with 2BP (50 μM). Uninfected cells were also treated with 2BP. The cells were fixed at 12 hpi and stained with anti-Ras (green), anti-reovirus (blue), and anti-TGN38 (red) antibodies. Imaging was done by confocal microscopy at 400x magnification. White squares highlight regions that are enlarged under the "Zoom" heading. Scale bar: 20 μm. (B) A further enlargement of reovirus infected cells with 2BP treatment. Scale bar: 20 μm. (C) The number of Ras puncta resulting from reovirus infection +/- 2BP treatment was quantified. A paired t-test was used to compare the data (± S.E.; n = 3). (D) H-RasV12 transformed cells were infected with reovirus at an MOI of 20 and treated with 2BP (50 μM). The cells were fixed at 12 hpi and stained with anti-Ras (green), anti-reovirus (blue), and anti-calnexin (red) antibodies. Imaging was done by confocal microscopy at 400x magnification. The white square highlights a region that is further enlarged under the "Zoom" heading. Scale bar: 20 μm. Images are representative of three independent experiments.

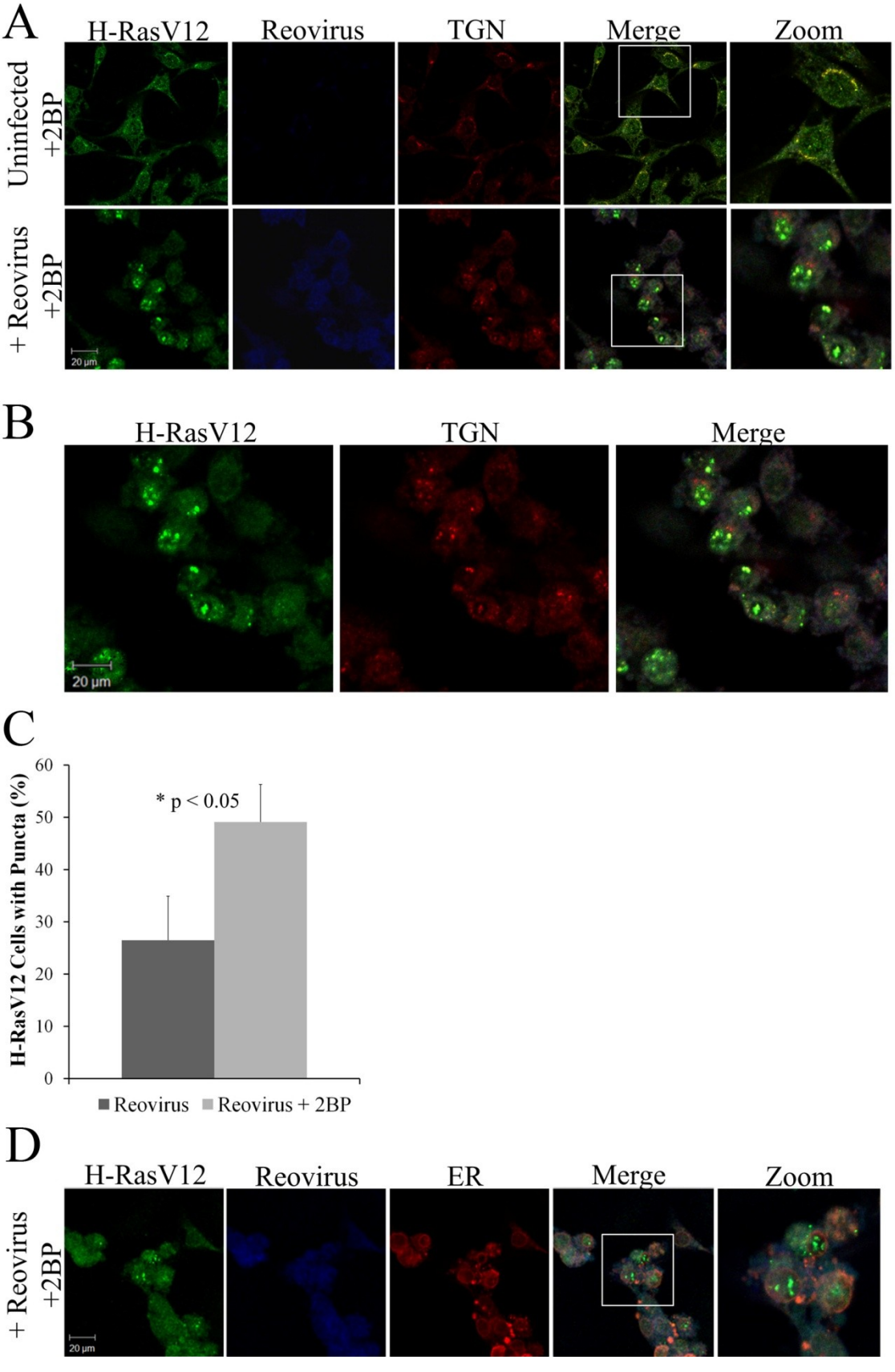
A
H-RasV12
Reovirus
TGN
Merge
Zoom
Uninfected +2BP
+ Reovirus +2BP
20 µm
B
H-RasV12
TGN
Merge
20 µm
C
H-RasV12 Cells with Puncta (%)
* p < 0.05
60
50
40
30
20
10
0
Reovirus
Reovirus + 2BP
D
H-RasV12
Reovirus
ER
Merge
Zoom
+ Reovirus +2BP
20 µm

Figure 3.9: 2BP enhances reovirus spread in H-RasV12 transformed cells. A reovirus plaque assay was performed on non- and H-RasV12 transformed cells. Immediately following infection, increasing concentrations of DMSO or 2BP (25 to 75 μM) were added. Immunocytochemistry was performed 5 days later to visualize reovirus plaques. Images are representative of three independent experiments.

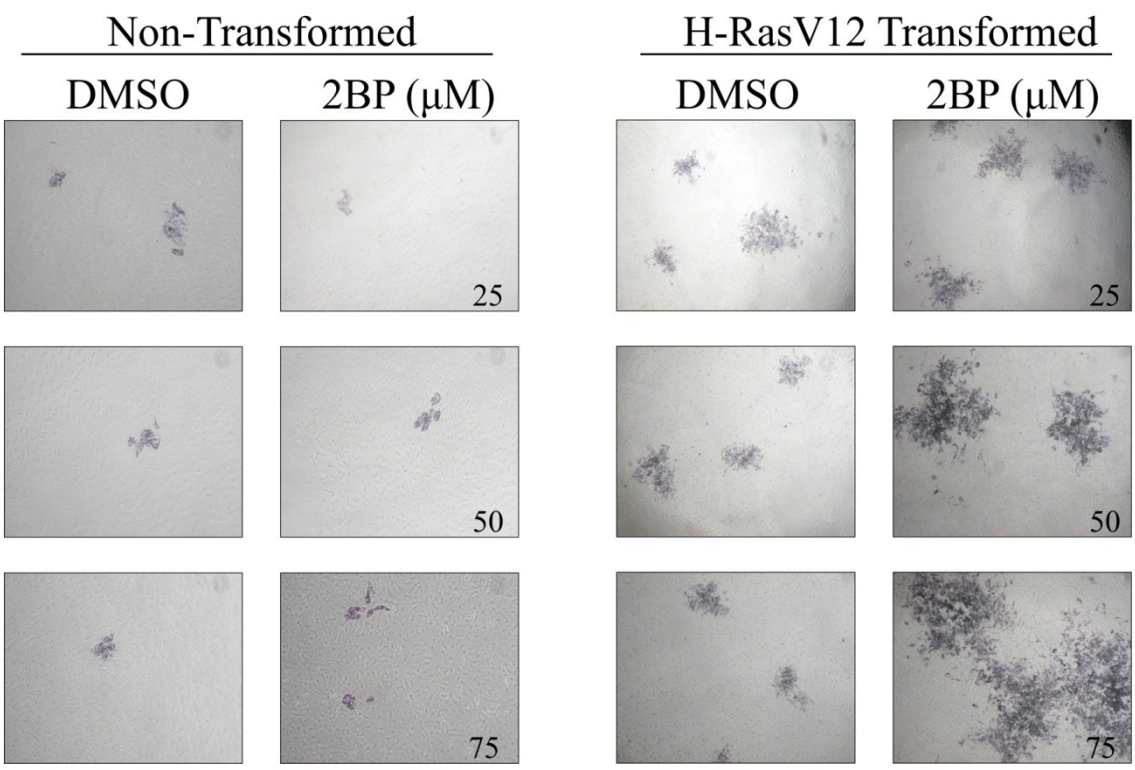

Reovirus Infected Cells = Dark Grey

3.5. 2BP Promotes Reovirus Release based on the Palmitoylation Status of Oncogenic Ras

The Ras HVR sequence dictates which post-translational modifications the isoforms will receive. The most notable variance is in the degree by which each isoform is palmitoylated (Hancock et al., 1990; Roy et al., 2005). K-Ras4B does not require palmitoylation for stable membrane binding, while H- and N-Ras necessitate dual and monopalmitoylation, respectively. Characterization of these isoforms in the model system indicated that NIH3T3 cells transformed by retrovirus containing oncogenic H-, N-, or K-Ras had elevated levels of activated Ras in comparison to the non-transformed control (Figure 3.10B). The cells displayed a higher capacity for H-RasV12 expression than oncogenic N- or K-Ras, however all cells were clearly transformed (Figure 3.10A and C). As mentioned above, 2BP is considered a general inhibitor of palmitoylation (Coleman et al., 1992; Webb et al., 2000). While it is effective at preventing Ras palmitoylation, it does not selectively inhibit specific proteins. In light of 2BP augmenting reovirus oncolysis, it was important to discern whether the inhibitor was acting on Ras palmitoylation, and furthermore, which stage(s) of the reovirus life cycle was being enhanced by its effects. To test this, cells transformed by H-RasV12, N-Ras61K, or K-RasV12 were infected with reovirus, treated with 2BP, and collected for analysis. Reovirus titers indicated that 2BP had no effect on the total amount of infectious virus being produced. In contrast, reovirus release titers suggested that 2BP increased the amount of virus being released by approximately 2 to 2.5 fold, and that the increase correlated with the palmitoylation status of the oncogenic Ras present (Figure 3.11A). The largest increase in reovirus release was observed in N-Ras61K cells, as it is

monopalmitoylated and highly susceptible to palmitoylation inhibitors like 2BP. This was followed by a smaller increase in cells transformed by dually palmitoylated H-RasV12. No change was observed in cells transformed by K-Ras4B, which utilizes a polybasic domain over palmitoylation for membrane binding. When considering other steps in the reovirus life cycle, 2BP did not affect the number of cells infected by the virus or the total amount of viral proteins being produced (Figure 3.11B and C). In addition, reovirus plaque assays performed on H-, N-, and K-Ras transformed cells reinforced the notion that the palmitoylation status of the oncogenic Ras influences the effect of 2BP treatment on reovirus release (Figure 3.12). N-Ras61K cells showed the largest increase in reovirus plaque size when in the presence of 2BP. 2BP also increased reovirus plaque size in infected H-RasV12 cells, and caused a slight increase in K-RasV12 transformed cells. The plaque size increase in K-RasV12 cells was unexpected. Since cell death was examined at 24 hpi and reovirus plaque size was assessed after 5 days, then perhaps the discrepancy exists within the time-frame of analysis. Another possible explanation lies with the non-specificity of 2BP. The inhibitor could be suppressing endogenous, palmitoylated Ras proteins or proteins with a longer palmitate half-life during the 5 days it takes for reovirus plaque formation. Therefore, despite the non-specificity of 2BP, the inhibitor clearly targets Ras efficiently. 2BP is likely acting independently of reovirus to promote its oncolysis. Reovirus-induced fragmentation of the Golgi body causes H-RasV12 accumulation in the TGN and decreases Ras palmitoylation, while 2BP inhibits Ras palmitoylation at the Golgi. Collectively, it leads to a proteomic back log and further accumulation of the oncogenic protein in the Golgi body as it awaits palmitoylation and vesicular transport to the plasma membrane.

Figure 3.10: Activated Ras levels of H-, N-, and K-Ras transformed cells. (A) Lysates from H-, N-, and K-Ras transformed cells underwent western blot analysis to detect total Ras levels. (B) Cell lysates from H-, N-, and K-Ras transformed cells were incubated with Raf-1 RBD conjugated agarose beads to pull-down GTP-bound Ras. The resulting pull-down was subjected to SDS-PAGE and anti-Ras western blotting. A proportional amount of whole-cell lysate was loaded to compare the amount of activated Ras to its total. Since H-RasV12 transformed cells contained a large amount of Ras, 3x less sample was loaded to prevent over-exposure upon western blot development. T: total Ras; A: activated GTP-bound Ras. β-actin was used as a control. (C) Images of non- and Ras-transformed cells.

A

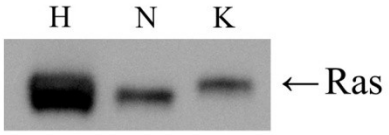

B

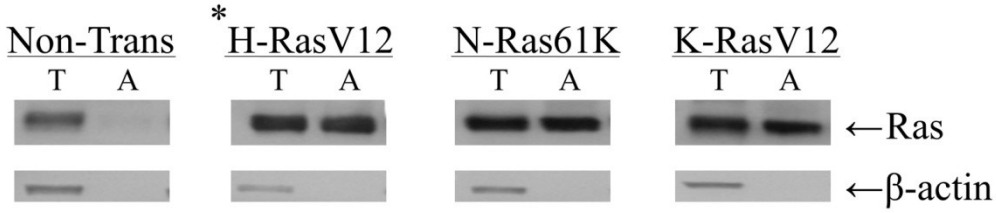

T = Total Ras
A = GTP-bound Ras
* 3x less H-RasV12 sample loaded as to not saturate the blot

C

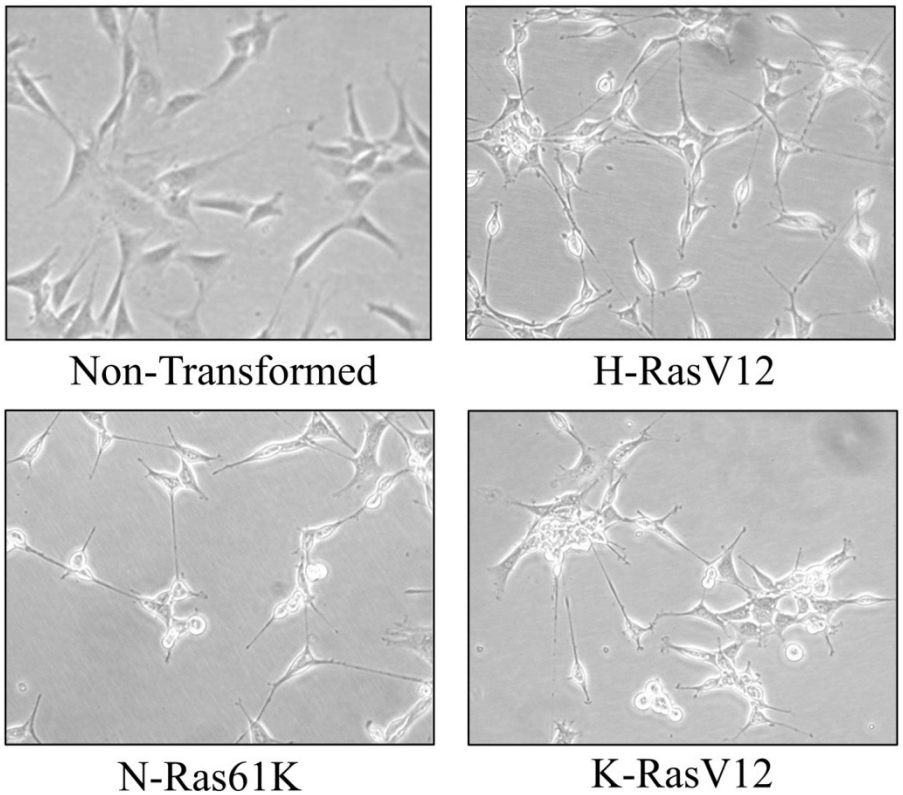

Figure 3.11: The increase in reovirus release by 2BP correlates with the degree of Ras palmitoylation. (A) Reovirus total and release samples from infected H-, N-, and K-Ras transformed cells in the presence of 2BP (50 μM) or DMSO were collected at 24 hpi for plaque titration. The plaque assay was performed on L929 cells and 5 days post-infection, the cells were stained with crystal violet for plaque quantification. A paired t-test was performed to compare the effects of 2BP on reovirus titer (± S.E.; n = 3). (B) Immunocytochemistry of reovirus infected H-, N-, and K-Ras transformed cells in the presence of 2BP (50 μM) or DMSO control at 12 hpi (n = 3). (C) Western blot analysis of reovirus protein synthesis over 6, 12, and 18 hpi in H-, N-, and K-Ras transformed cells in the presence of 2BP (50 μM) or DMSO (n = 3). β-actin served as a control for the western blot. All cells were infected at an MOI of 20. λ, μ, and σ represent the location of reovirus proteins. UI: uninfected.

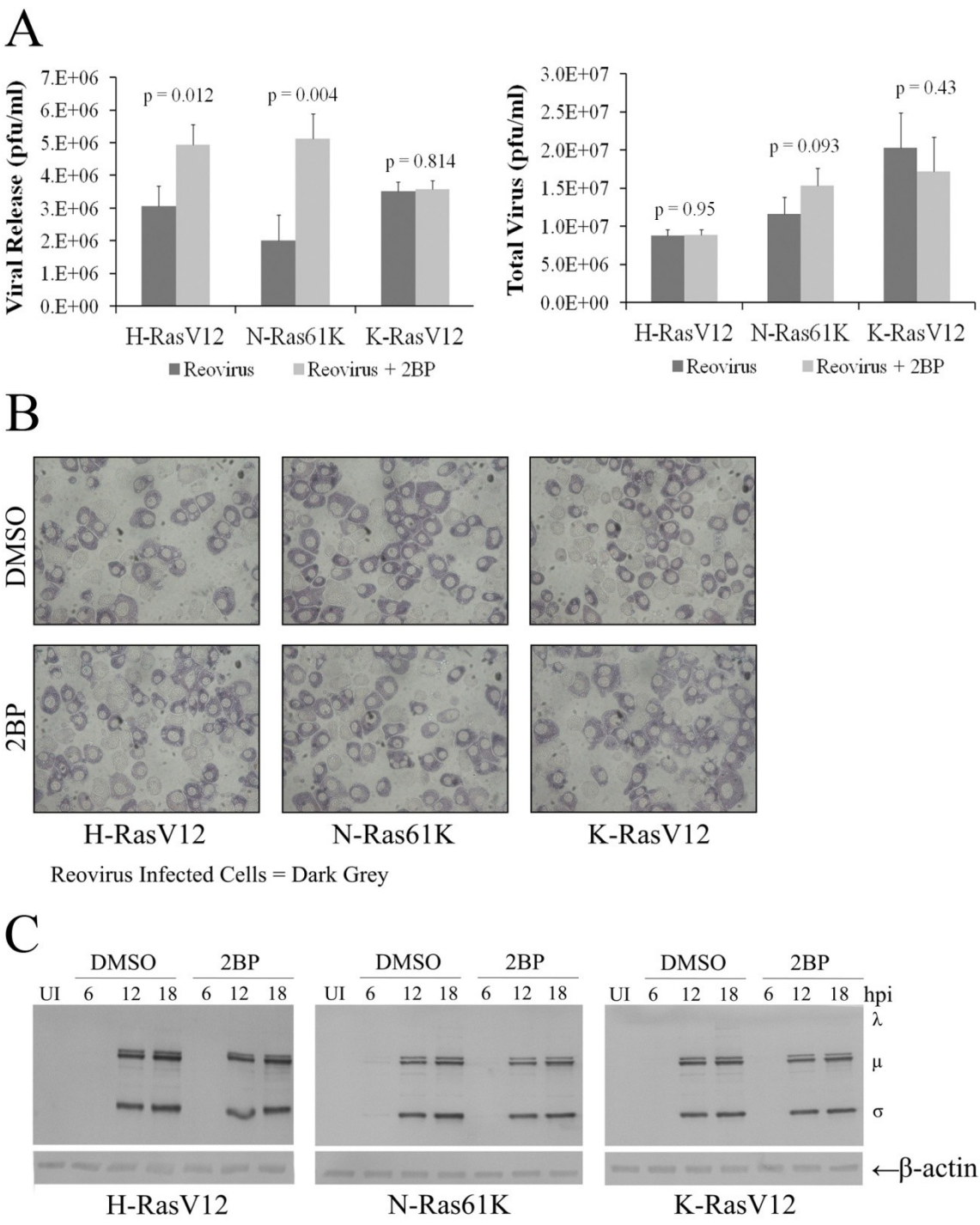
A
Viral Release (pfu/ml)
7.E+06
6.E+06
5.E+06
4.E+06
3.E+06
2.E+06
1.E+06
0.E+00
p = 0.012
p = 0.004
p = 0.814
H-RasV12
N-Ras61K
K-RasV12
Reovirus
Reovirus + 2BP
Total Virus (pfu/ml)
3.0E+07
2.5E+07
2.0E+07
1.5E+07
1.0E+07
5.0E+06
0.0E+00
p = 0.95
p = 0.093
p = 0.43
H-RasV12
N-Ras61K
K-RasV12
Reovirus
Reovirus + 2BP
B
DMSO
2BP
H-RasV12
N-Ras61K
K-RasV12
Reovirus Infected Cells = Dark Grey
C
DMSO
2BP
UI 6 12 18 6 12 18
hpi
λ
μ
σ
←β-actin
H-RasV12
N-Ras61K
K-RasV12

Figure 3.12: 2BP increases reovirus spread based on the palmitoylation status of cycling Ras. (A) A reovirus plaque assay was performed on non- and Ras transformed cells. Immediately following infection, DMSO or 2BP (50 μM) was added, and immunocytochemistry was performed 5 days later to visualize reovirus plaques. Scale bar: 2 mm. (B) The diameter of individual plaques was used to obtain reovirus plaque size +/- 2BP treatment. A nested ANOVA with Tukey test was performed to compare the data (± S.E.; n = 3).

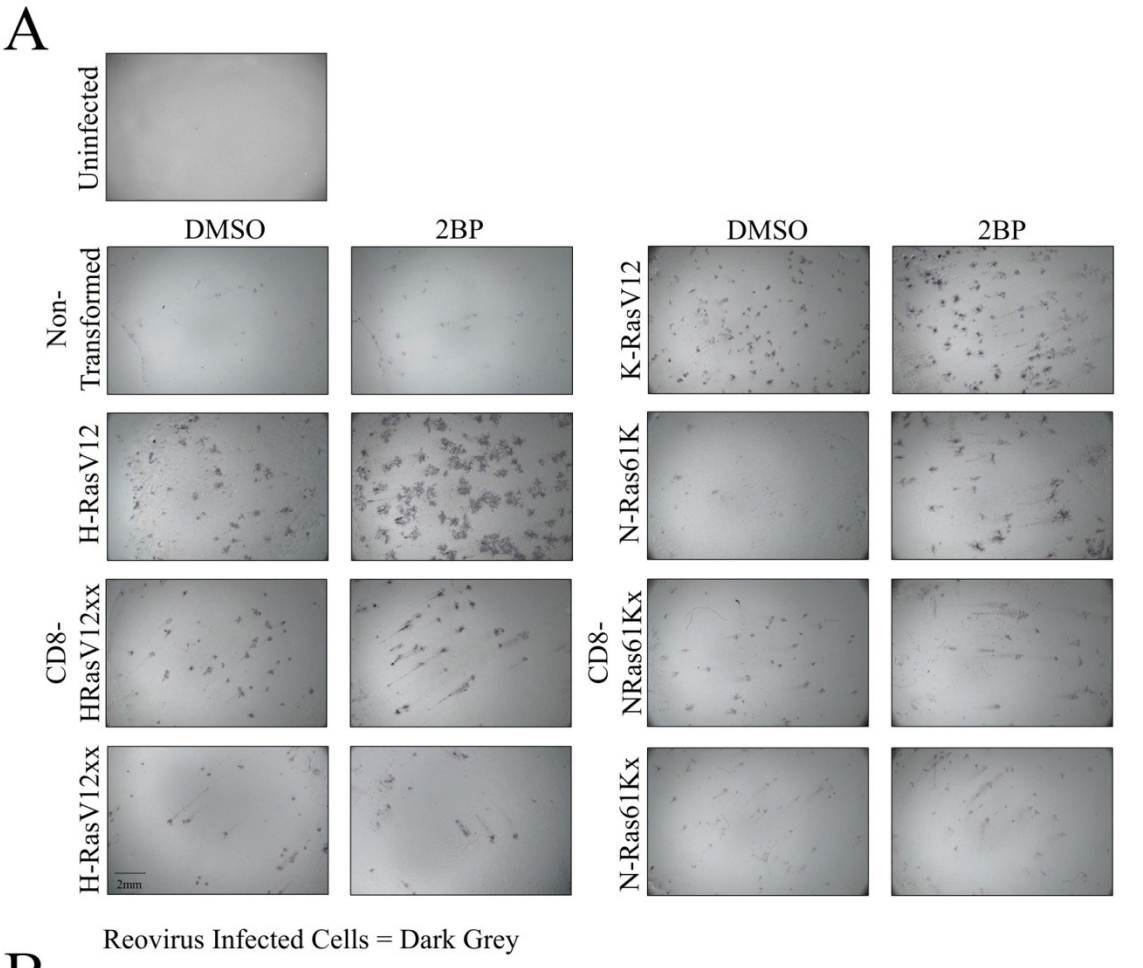
A
Uninfected
DMSO
2BP
DMSO
2BP
Non-Transformed
K-RasV12
H-RasV12
N-Ras61K
CD8-HRasV12xx
CD8-NRas61Kx
H-RasV12xx
N-Ras61Kx
2mm
Reovirus Infected Cells = Dark Grey
B
Reovirus Average Plaque Size (mm)
0.7
0.6
0.5
0.4
0.3
0.2
0.1
0
p = 0.168
p < 0.001
p = 0.196
p = 0.679
p < 0.001
p < 0.001
p = 0.842
p = 0.227
Non-Transformed
H-RasV12
CD8-HRasV12xx
H-RasV12xx
K-RasV12
N-Ras61K
CD8-NRas61Kx
N-Ras61Kx
Reovirus
Reovirus + 2BP

3.6. Cycling H-RasV12 is a Requirement of Efficient Reovirus Oncolysis

To investigate the importance of Ras localization during reovirus oncolysis, constructs were generated to tether oncogenic H- and N-Ras to the plasma membrane, as well as render them palmitoylation deficient. Palmitoylation deficient constructs, denoted as H-RasV12xx and N-Ras61Kx, were created by mutating cysteine to serine residues at known sites of palmitoylation (C181S and C184S for H-RasV12xx; C181S for N-Ras61Kx). Tethering was achieved by the addition of the transmembrane domain of the CD8α receptor to the N-terminus of Ras. The CD8α receptor is known to reside in the bulk/disordered microdomain of the plasma membrane (Matallanas et al., 2006). These constructs were designated as CD8-HRasV12xx and CD8-NRas61Kx. A schematic of the various Ras constructs and sites of mutagenesis can be found in Figure 3.13A. Worth mentioning is the transforming potential of these constructs. Ras tethered to the plasma membrane resulted in highly transformed cells; whereas, palmitoylation deficient Ras produced cells similar to the non-transformed control (Figure 3.13B). Further characterization of the H-RasV12 variants revealed similar levels of total and activated Ras, as well as the presence of the expected partial HA tag in the tethered Ras construct (Figure 3.14A-B). This was also the case for the N-Ras transformed cell lines (data not shown). Confocal immunofluorescence microscopy confirmed differences in localization between the H-RasV12 variants (Figure 3.14C). Tethered H-RasV12 colocalized with the transferrin receptor; a marker for the disordered microdomain of the plasma membrane where activated H-Ras is known to interact with downstream effectors (Figure 3.14D). On the other hand, palmitoylation deficient H-RasV12xx colocalized with the ER marker,

calnexin (Figure 3.14E). This construct is known to have reduced plasma membrane affinity and to shuttle between the ER/Golgi and cytoplasmic pools (Chiu et al., 2002).

With the constructs well established, H-RasV12xx and CD8-HRasV12xx cell lines were examined in the context of reovirus infection. This was to determine whether the movement of Ras from the plasma membrane to the Golgi body was a requirement of efficient reovirus oncolysis. As such, H-RasV12 cell lines were equally infected with reovirus and collected for cell death and viral titer analysis at 24 hpi (Figure 3.15C). Reovirus-induced cell death was highest in H-RasV12 cells, while cells transformed by plasma membrane tethered and/or palmitoylation deficient H-RasV12 showed basal levels of cell death comparable to the non-transformed control (Figure 3.15A). Data derived from reovirus release titers confirmed the above. Though the total amount of infectious virus produced was similar between cell lines, only cells transformed by H-RasV12 exhibited high levels of reovirus release (Figure 3.15B).

Earlier in this chapter, it was shown that reovirus caused distinct Golgi fragmentation and TGN colocalization of H-RasV12. To determine if Ras formed puncta in reovirus infected CD8-HRasV12xx and H-RasV12xx cells, confocal immunofluorescence microscopy was once again utilized. Reovirus triggered Golgi fragmentation in both cell lines, but no change was detected in the localization of Ras from tethered and/or palmitoylation deficient H-RasV12 cells (Figure 3.16 and Figure 3.17). Furthermore, as 2BP treatment caused an increase in reovirus-induced cell death and virus release in H-RasV12 transformed cells, the effect of 2BP was also assessed in tethered CD8-HRasV12xx cells. 2BP did not influence reovirus-induced cell death or virus release in CD8-HRasV12xx cells (Figure 3.18). As expected, 2BP had no effect on

reovirus plaque size in non-transformed cells, or in cells expressing plasma membrane tethered and/or palmitoylation deficient H-RasV12 or N-Ras61K (Figure 3.12). It is worth noting that oncogenic Ras suppresses IFN-β production to promote reovirus spread (Shmulevitz et al., 2010). To determine if the various Ras constructs also suppressed interferon and if 2BP promoted reovirus spread by further altering IFN-β production, qRT-PCR was performed. Unsurprisingly, non-transformed cells drastically upregulated IFN-β mRNA in the presence of reovirus, while cell lines stably transformed by any oncogenic Ras expressed low levels (Figure 3.19A-B). Additionally, 2BP had no effect on the expression of IFN-β mRNA (Figure 3.19B).

It was recently discovered that the inhibitor, FK506, alters the normal distribution of Ras (Ahearn et al., 2011). FKBP12 is involved in priming Ras for depalmitoylation by APT-1, and inhibition of FKBP12 by FK506 enriches the amount of H-Ras on the plasma membrane, while decreasing Ras levels at the Golgi. With reovirus infection causing basal levels of cell death in plasma membrane tethered CD8-HRasV12xx cells, it was postulated that use of FK506 would produce similar results. To test this, H-RasV12 cell lines were equally infected with reovirus, treated with FK506, and collected for cell death quantification at 24 hpi and plaque size analysis at 5 days post-infection (Figure 3.20C). FK506 had no effect on reovirus-induced cell death or plaque size in non-transformed, CD8-HRasV12xx, or H-RasV12xx cells (Figure 3.20A-B). In contrast, FK506 decreased reovirus-induced cell death and plaque size in cycling H-RasV12 cells to levels and sizes comparable to its plasma membrane tethered form. Therefore, restricting Ras to the plasma membrane during reovirus infection reduces the ability of the virus to induce

apoptosis and progeny release. In other words, efficient reovirus oncolysis requires oncogenic H-Ras to be released from the plasma membrane and accumulate in the Golgi.

Reinforcing the importance of Ras localization during reovirus oncolysis was use of the farnesylation inhibitor, FTI-277. Western blot analysis revealed the effectiveness of the inhibitor on H- and N-Ras transformed cells by the presence of a large gel mobility shift indicative of unprocessed Ras (Figure 3.21A). Using low concentrations of FTI-277 (10 μM), H- and N-Ras transformed cells were equally infected with reovirus and collected for cell death and plaque size analysis. FTI-277 had no effect on reovirus-induced cell death at 24 hpi, but did decrease reovirus plaque size in H- and N-Ras transformed cells at 5 days post-infection (Figure 3.21B-D).

Figure 3.13: A representation of Ras constructs and cell lines. (A) Schematic of the various Ras constructs. X's indicate the location of site-directed mutations that resulted in cysteine to serine exchanges within the Ras amino acid sequence. Tm: CD8 transmembrane domain; F: farnesylation site; P: palmitoylation site. (B) Images of the various Ras cell lines generated through retrovirus infection and antibiotic selection.

A

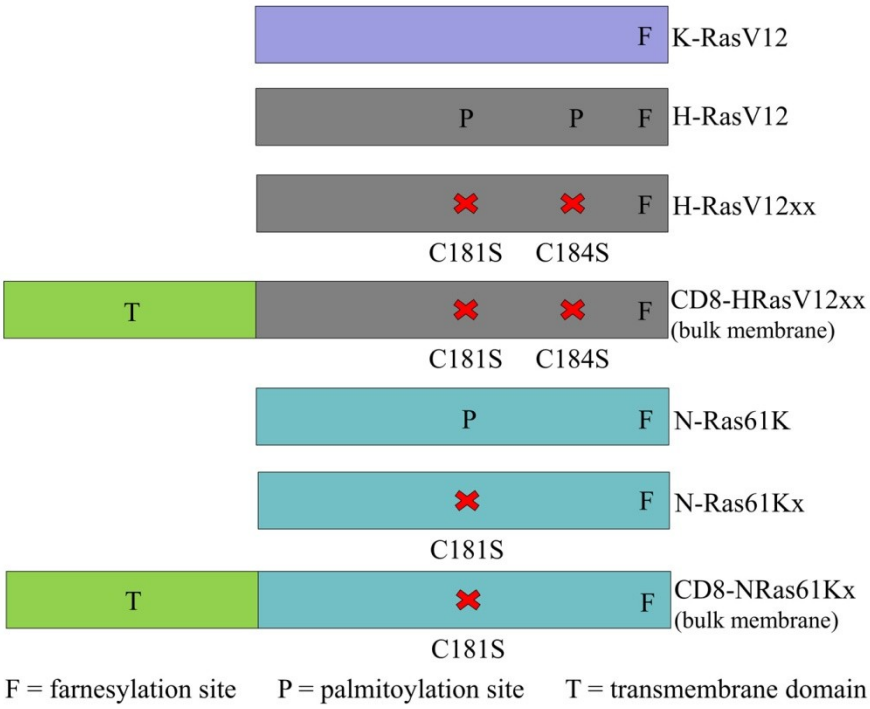
F
K-RasV12
P
P
F
H-RasV12
F
H-RasV12xx
C181S
C184S
T
F
CD8-HRasV12xx
(bulk membrane)
C181S
C184S
P
F
N-Ras61K
F
N-Ras61Kx
C181S
T
F
CD8-NRas61Kx
(bulk membrane)
C181S
F = farnesylation site
P = palmitoylation site
T = transmembrane domain

B

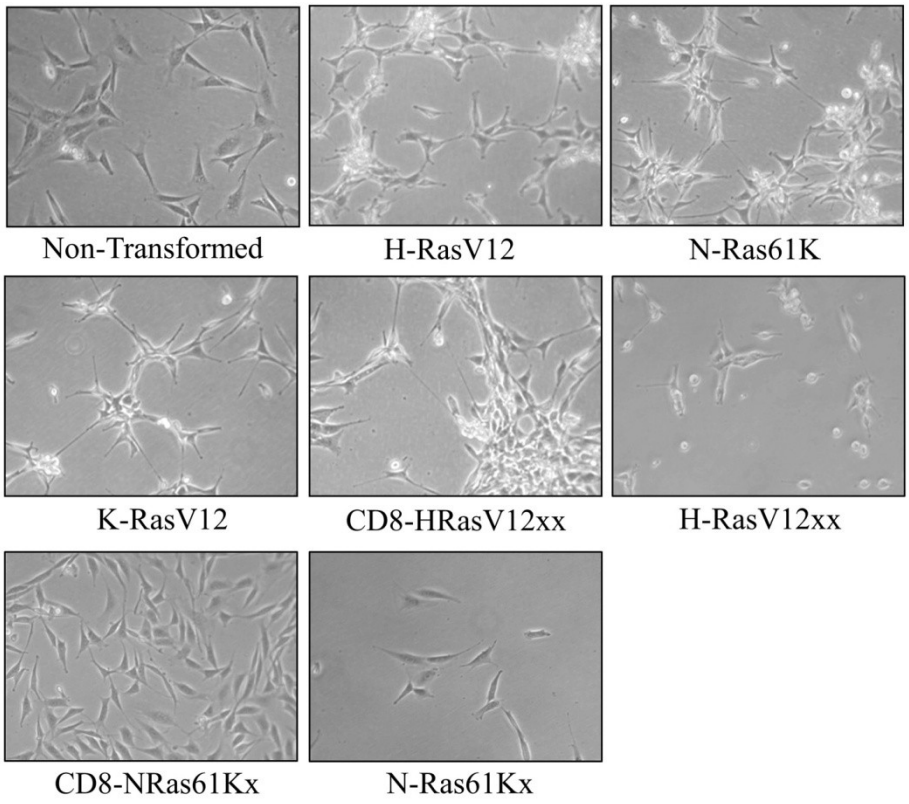
Non-Transformed
H-RasV12
N-Ras61K
K-RasV12
CD8-HRasV12xx
H-RasV12xx
CD8-NRas61Kx
N-Ras61Kx

Figure 3.14: Characterization of the activated state and locale of H-RasV12 cell lines. (A) Lysates from non-transformed and H-RasV12 cells lines were incubated with Raf-1 RBD conjugated agarose beads to pull-down GTP-bound Ras. The resulting pull-down was subjected to SDS-PAGE and anti-Ras western blotting. A proportional amount of whole-cell lysate was loaded to compare the amount of activated Ras to its total. β-actin was used as a control. T: total Ras; A: activated GTP-bound Ras. (B) Lysates from non-transformed and CD8-HRasV12xx cells were subjected to SDS-PAGE and subsequent western blot probing by anti-Ras and anti-HA antibodies. β-actin served as a control. Tm: Ras containing the CD8 transmembrane domain. (C) Non-transformed and H-RasV12 cell lines were fixed and stained with anti-Ras (green). Imaging was done by confocal microscopy at 400x magnification. Scale bar: 20 μm. (D) CD8-HRasV12xx transformed cells were fixed and stained with anti-Ras (green) and anti-transferrin receptor (red) antibodies. Imaging was done by confocal microscopy at 1000x magnification. Scale bar: 10 μm. (E) H-RasV12xx cells were fixed and stained with anti-Ras (green) and anti-calnexin (red) antibodies. Imaging was done by confocal microscopy at 400x magnification. Scale bar: 20 μm.

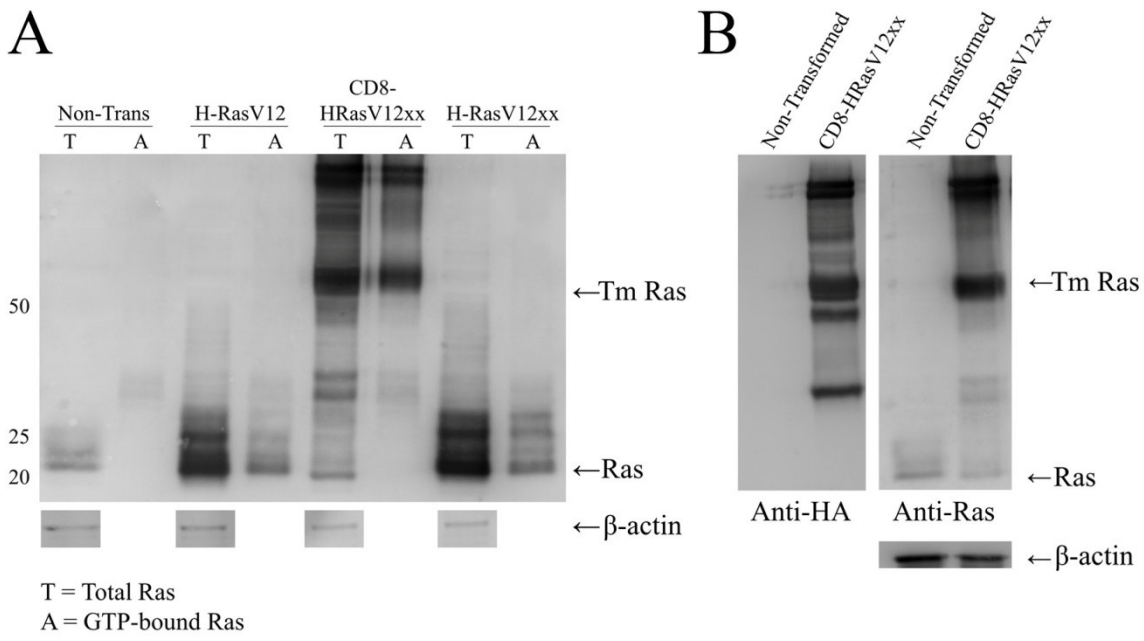
A
Non-Trans
H-RasV12
CD8-HRasV12xx
H-RasV12xx
T
A
50
25
20
←Tm Ras
←Ras
←β-actin
T = Total Ras
A = GTP-bound Ras
B
Non-Transformed
CD8-HRasV12xx
Anti-HA
Anti-Ras
←Tm Ras
←Ras
←β-actin

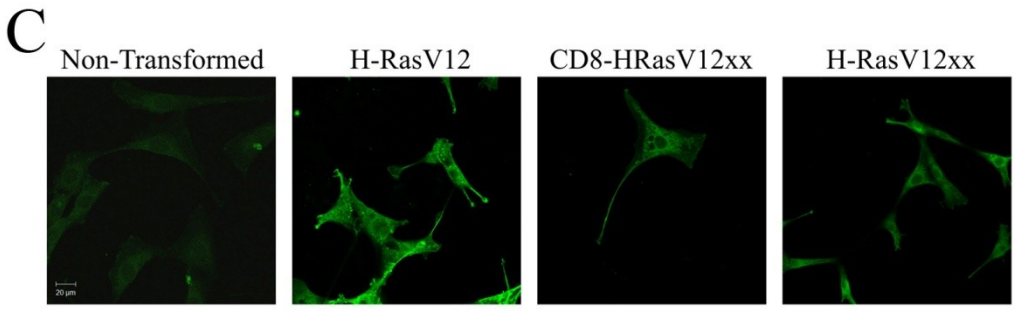
C
Non-Transformed
H-RasV12
CD8-HRasV12xx
H-RasV12xx

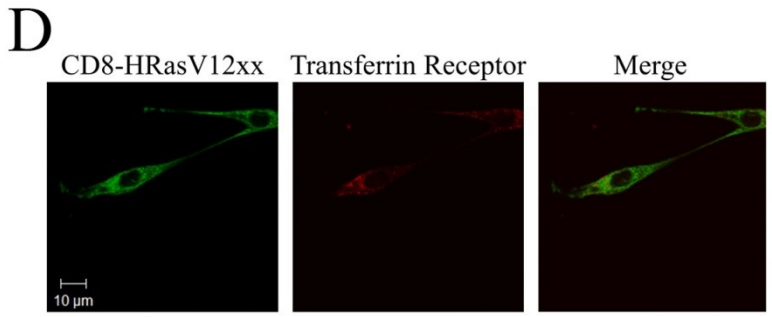
D
CD8-HRasV12xx
Transferrin Receptor
Merge
10 µm

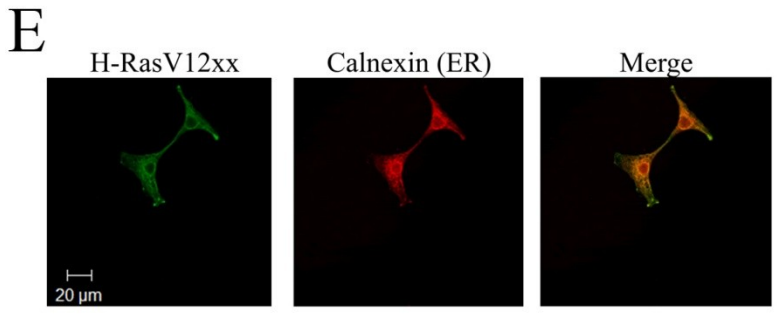
E
H-RasV12xx
Calnexin (ER)
Merge
20 µm

Figure 3.15: Reovirus-induced cell death and virus release is dependent on the ability of H-RasV12 to move from the plasma membrane during infection. Non-transformed and H-RasV12 cell lines were infected with reovirus at a particular MOI to achieve similar levels of percent infected (MOI of 20 for H-RasV12 cells, MOI of 40 for non-transformed and H-RasV12xx cells, and MOI of 80 for CD8-HRasV12xx cells). (A) At 24 hpi, the cells were photographed (right) and collected for cell death analysis (left) by trypan blue exclusion staining. An ANOVA with Tukey test was performed to compare the levels of reovirus-induced death between cell lines (± S.E.; n = 3). (B) Reovirus total and release samples from infected non-transformed and H-RasV12 cell lines were collected at 24 hpi for plaque titration. The plaque assay was performed on L929 cells and 5 days post-infection, the cells were stained with crystal violet for plaque quantification. An ANOVA with Tukey test was performed to compare the reovirus titer between cell lines (± S.E.; n = 3). (C) At 12 hpi, the cells were fixed for FACS analysis. The cells were stained with anti-reovirus antibodies to determine the percentage of cells infected by the virus. An ANOVA with Tukey test was performed to compare the number of reovirus infected cells between cell lines (± S.E.; n = 3). *: significantly different from other cell lines.

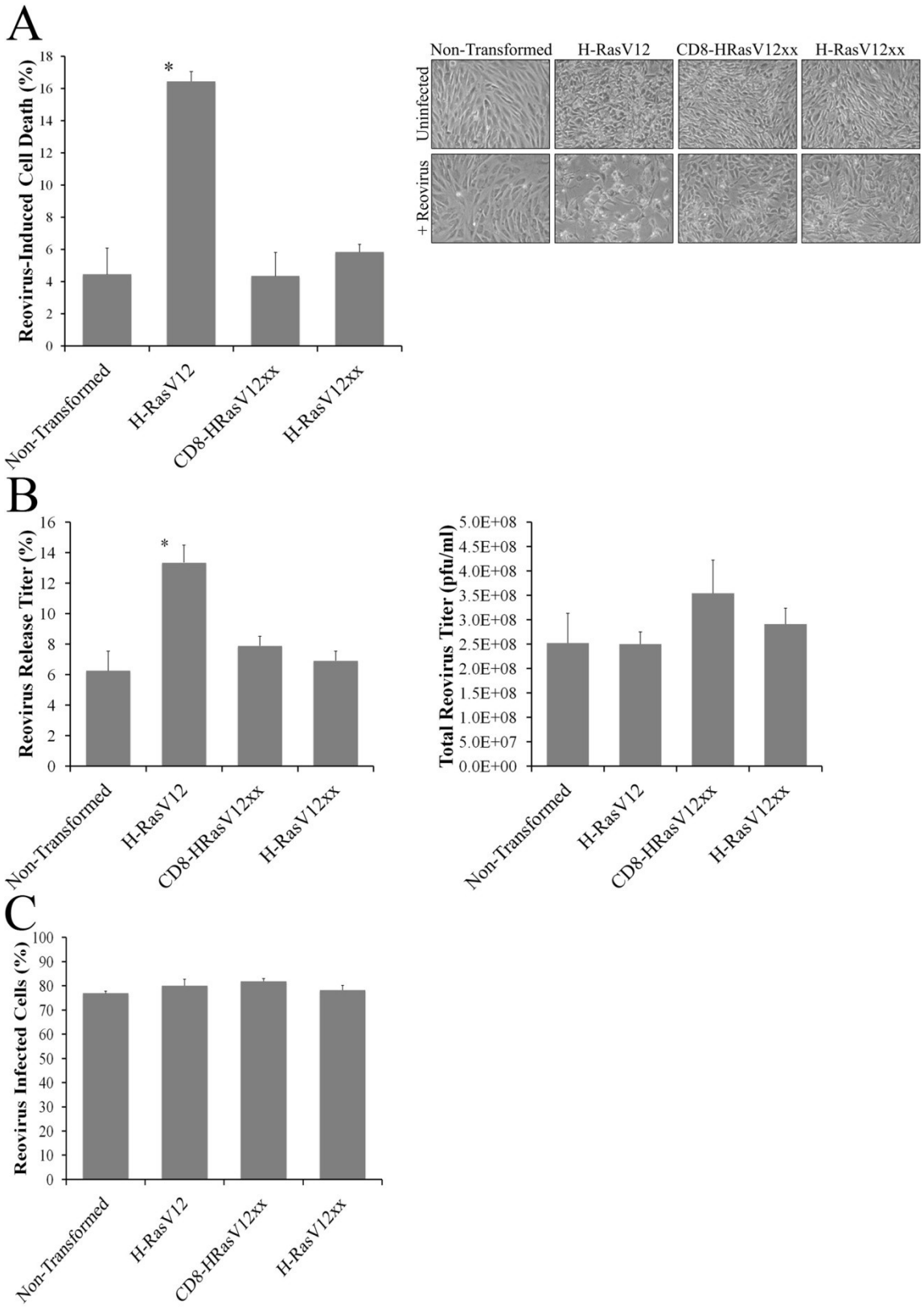
A
Reovirus-Induced Cell Death (%)
18
16
14
12
10
8
6
4
2
0
*
Non-Transformed
H-RasV12
CD8-HRasV12xx
H-RasV12xx
Non-Transformed
H-RasV12
CD8-HRasV12xx
H-RasV12xx
Uninfected
+ Reovirus
B
Reovirus Release Titer (%)
16
14
12
10
8
6
4
2
0
*
Non-Transformed
H-RasV12
CD8-HRasV12xx
H-RasV12xx
Total Reovirus Titer (pfu/ml)
5.0E+08
4.5E+08
4.0E+08
3.5E+08
3.0E+08
2.5E+08
2.0E+08
1.5E+08
1.0E+08
5.0E+07
0.0E+00
Non-Transformed
H-RasV12
CD8-HRasV12xx
H-RasV12xx
C
Reovirus Infected Cells (%)
100
90
80
70
60
50
40
30
20
10
0
Non-Transformed
H-RasV12
CD8-HRasV12xx
H-RasV12xx

Figure 3.16: Reovirus infection causes fragmentation of the Golgi body in plasma membrane tethered and palmitoylation deficient H-RasV12 cell lines. (A) CD8-HRasV12xx and (B) H-RasV12xx cell lines were infected with reovirus at an MOI of 80 and 40, respectively. The cells were fixed at 12 hpi and stained using antibodies against Golgin97 (red) and reovirus (blue) proteins. Imaging was performed at 630x magnification by confocal microscopy. White squares denote regions that were further enlarged under the "Zoom" heading. Scale bar: 20 μm. Images are representative of three independent experiments.

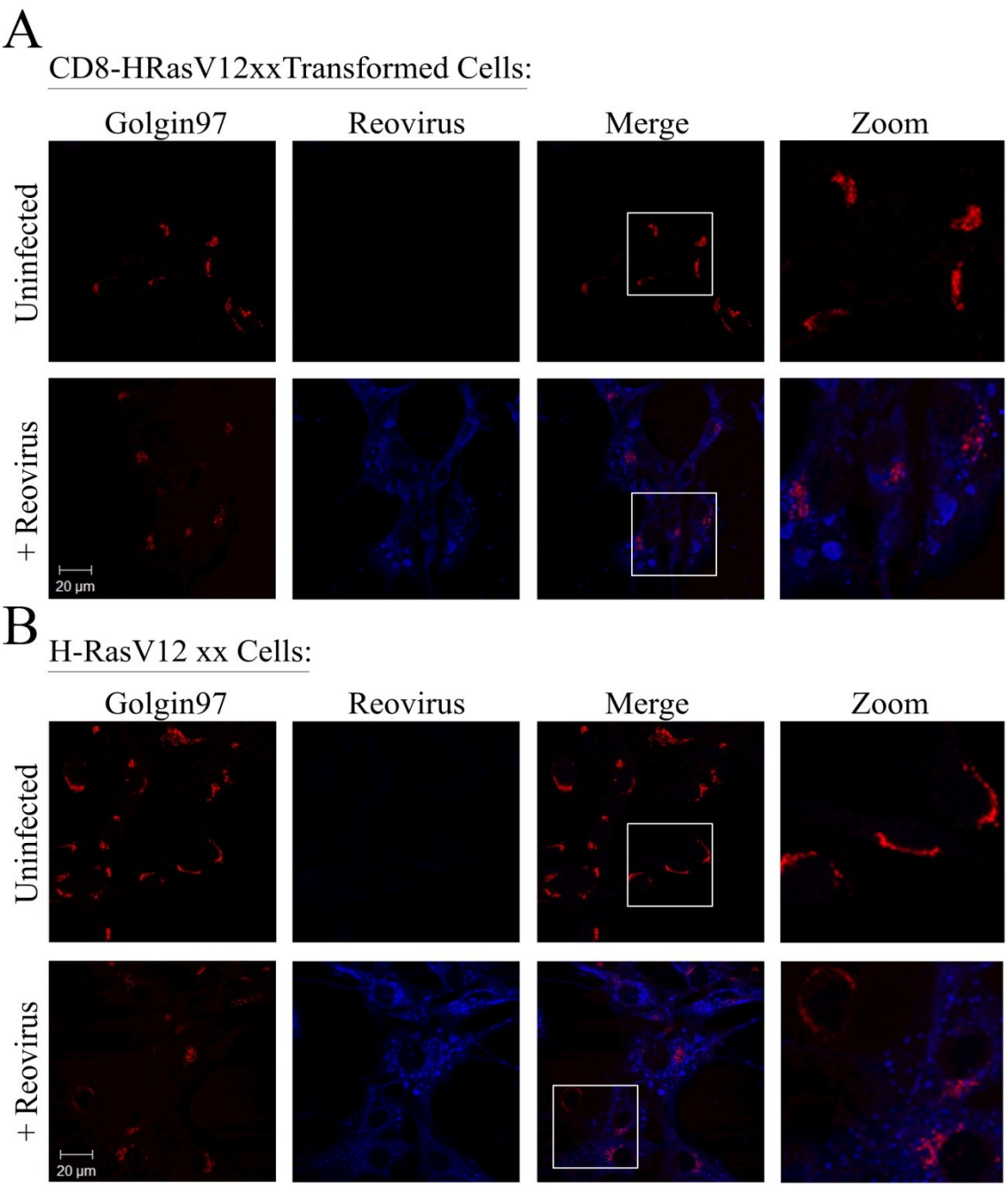
A
CD8-HRasV12xxTransformed Cells:
Golgin97
Reovirus
Merge
Zoom
Uninfected
+ Reovirus
20 µm
B
H-RasV12 xx Cells:
Golgin97
Reovirus
Merge
Zoom
Uninfected
+ Reovirus
20 µm

Figure 3.17: Tethered and/or palmitoylation deficient H-RasV12 does not relocate to the TGN following reovirus infection. (A) CD8-HRasV12xx or (B) H-RasV12xx cell lines were mock or reovirus infected at an MOI of 100. The cells were fixed at 12 hpi and stained with anti-Ras (green), anti-reovirus (blue), and anti-TGN38 (red) antibodies. Imaging was done by confocal microscopy at 400x magnification. Insets enlarge a single cell from within the field of view. Scale bar: 20 μm. Images are representative of three independent experiments.

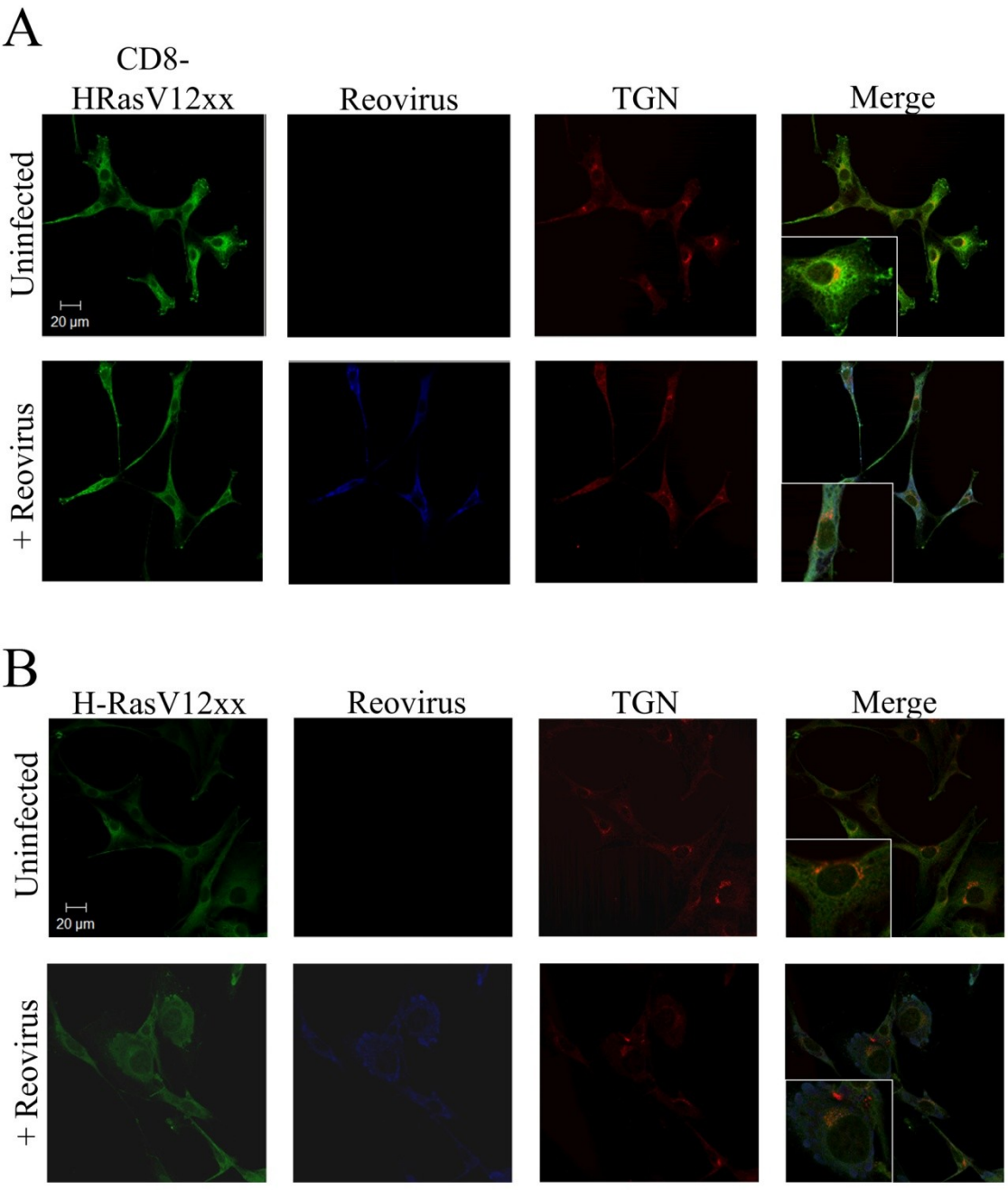
A
CD8-
HRasV12xx
Reovirus
TGN
Merge
Uninfected
20 µm
+ Reovirus
B
H-RasV12xx
Reovirus
TGN
Merge
Uninfected
20 µm
+ Reovirus

Figure 3.18: 2BP does not affect reovirus-induced cell death and virus release in tethered H-RasV12 cells. (A) H-RasV12 transformed cells were infected with reovirus at an MOI of 20 and treated with 2BP (50 μM) or DMSO. At 24 hpi, the cells were photographed (right) and stained with Annexin V-PE and 7-AAD to determine the level of cell apoptosis and death by FACS analysis (bottom panels). The change in cell death by 2BP was represented as a fold increase (left) and a one sample t-test (hypothesis > 1) was employed to compare the data (± S.E.; n = 3). (B) CD8-HRasV12xx transformed cells were infected with reovirus at an MOI of 80 and treated with 2BP (50 μM) or DMSO. At 24 hpi, the cells were photographed (right) and stained with trypan blue to determine the percentage of cell death (left). A two sample t-test was employed to compare the effects of 2BP on cell death (± S.E.; n = 3). (C) Reovirus total and release samples from infected CD8-HRasV12xx transformed cells were collected at 24 hpi for plaque titration. The plaque assay was performed on L929 cells and 5 days post-infection, the cells were stained with crystal violet for plaque quantification. A two sample t-test was employed to compare the effects of 2BP on reovirus release (± S.E.; n = 3).

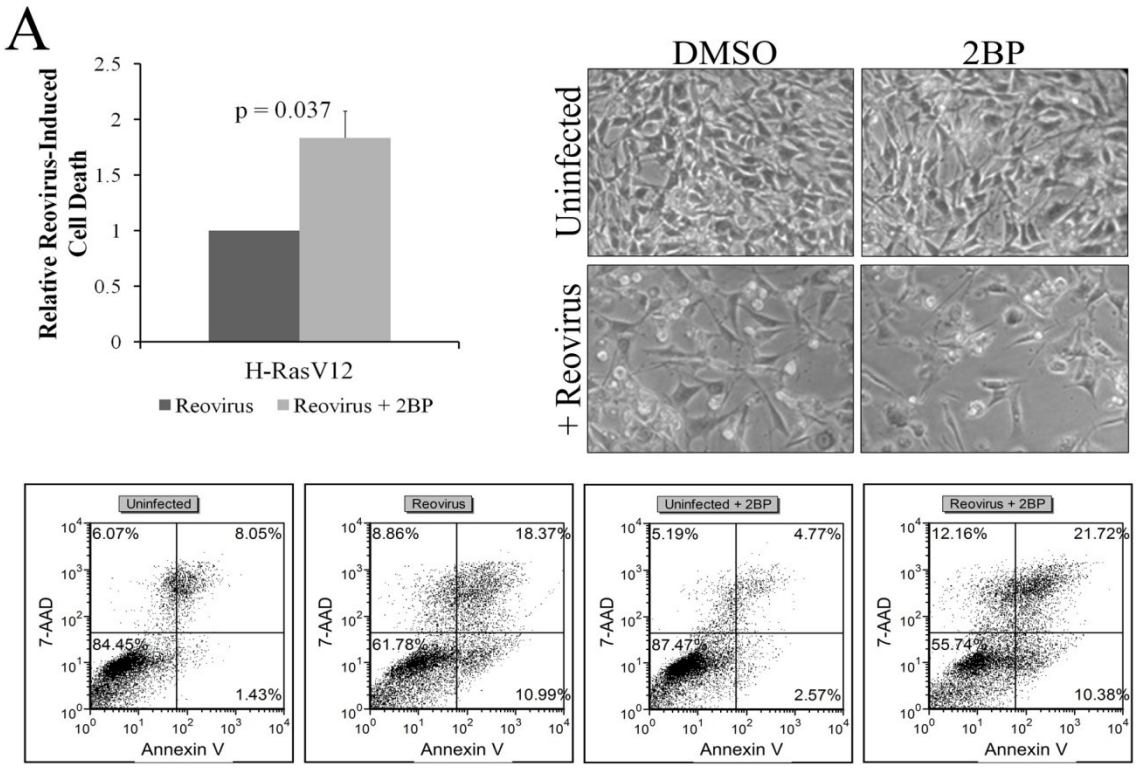
A
Relative Reovirus-Induced Cell Death
2.5
2
1.5
1
0.5
0
p = 0.037
H-RasV12
Reovirus
Reovirus + 2BP
DMSO
2BP
Uninfected
+ Reovirus
Uninfected
6.07%
8.05%
84.45%
1.43%
Reovirus
8.86%
18.37%
61.78%
10.99%
Uninfected + 2BP
5.19%
4.77%
87.47%
2.57%
Reovirus + 2BP
12.16%
21.72%
55.74%
10.38%
7-AAD
Annexin V

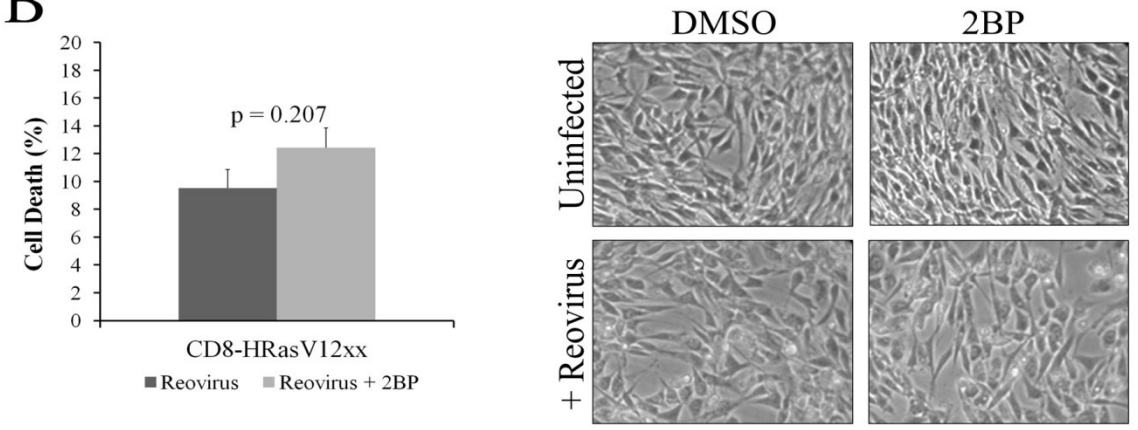
B
Cell Death (%)
20
18
16
14
12
10
8
6
4
2
0
p = 0.207
CD8-HRasV12xx
Reovirus
Reovirus + 2BP
DMSO
2BP
Uninfected
+ Reovirus

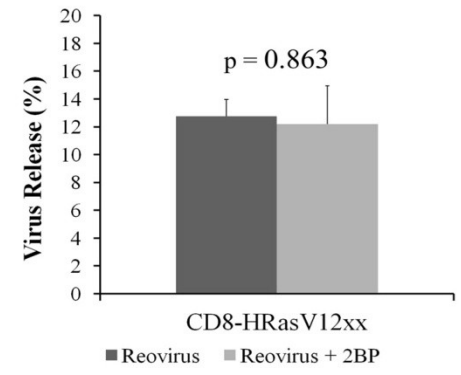
C
Virus Release (%)
20
18
16
14
12
10
8
6
4
2
0
p = 0.863
CD8-HRasV12xx
Reovirus
Reovirus + 2BP

Figure 3.19: IFN-β mRNA levels remain low in reovirus infected Ras-transformed cells treated with 2BP or vehicle. (A) qRT-PCR analysis of IFN-β in uninfected or reovirus infected non- and Ras-transformed cells at 12 hpi. (B) qRT-PCR analysis of IFN-β in uninfected or reovirus infected non-transformed and N-Ras61K cell lines +/- 2BP at 12 hpi. An ANOVA with Tukey test was performed to compare the IFN-β mRNA levels in the presence of 2BP (n = 3). Note: the logarithmic y-axis in both graphs.

A

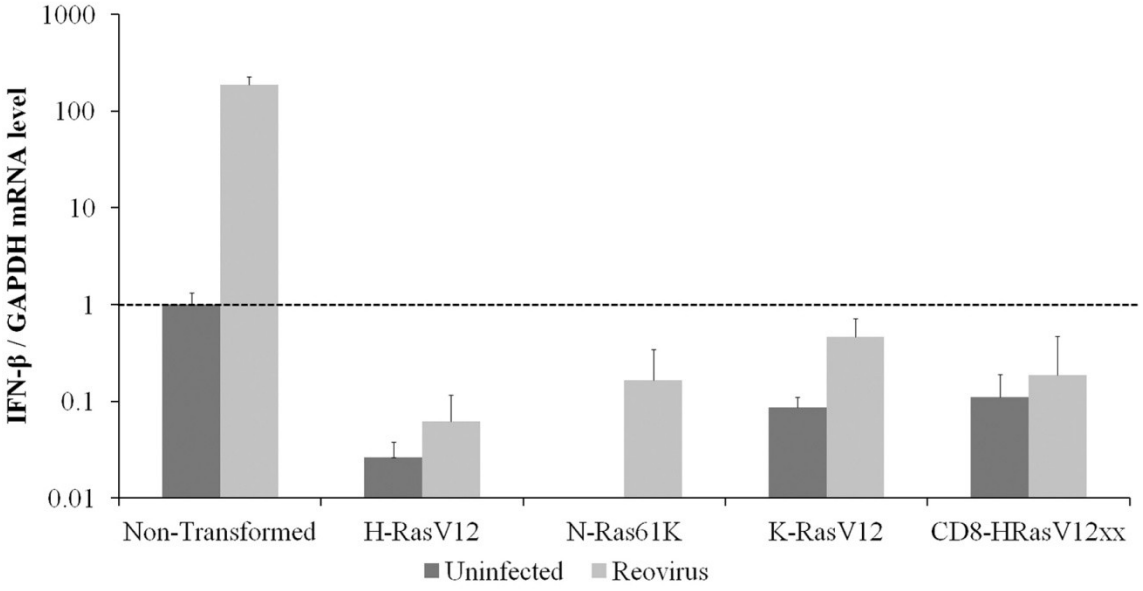
1000
100
10
1
0.1
0.01
IFN-β / GAPDH mRNA level
Non-Transformed
H-RasV12
N-Ras61K
K-RasV12
CD8-HRasV12xx
Uninfected
Reovirus

B

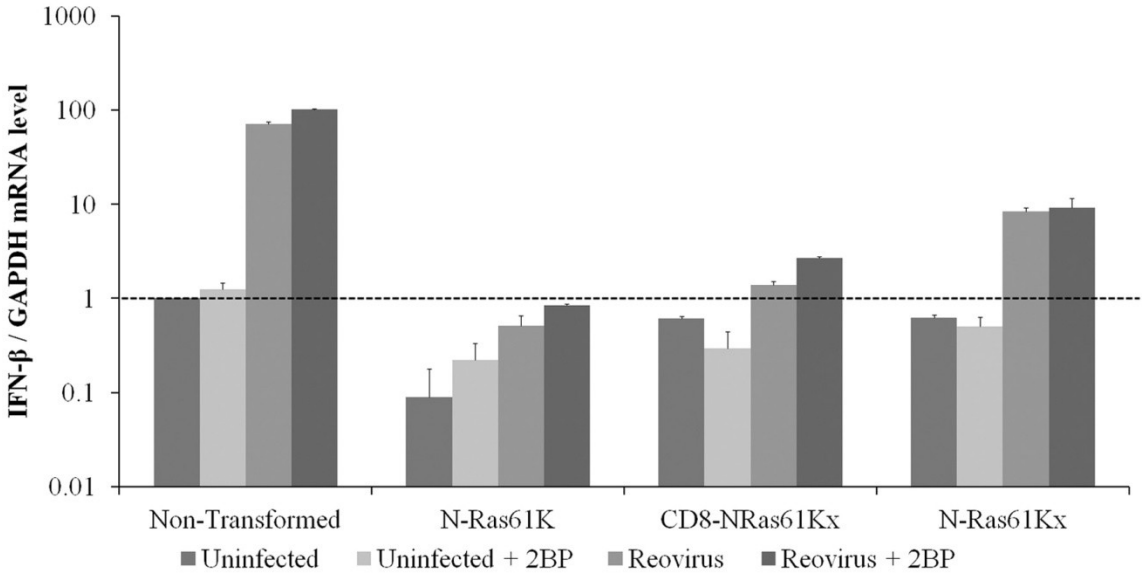
1000
100
10
1
0.1
0.01
IFN-β / GAPDH mRNA level
Non-Transformed
N-Ras61K
CD8-NRas61Kx
N-Ras61Kx
Uninfected
Uninfected + 2BP
Reovirus
Reovirus + 2BP

Figure 3.20: Inhibition of FKBP12 by FK506 decreases reovirus-induced cell death in H-RasV12 transformed cells. (A) Mock and reovirus infected non-transformed and H-RasV12 cell lines were treated with FK506 (10 μM) or DMSO. To achieve similar levels of percent infected, all cells were infected at a particular MOI (MOI of 20 for H-RasV12 cells, MOI of 40 for non-transformed and H-RasV12xx cells, and MOI of 80 for CD8-HRasV12xx cells). At 24 hpi, photographs of cell death were taken (right), and the cells were collected for cell death analysis by trypan blue exclusion staining. A two sample t-test was performed to compare the levels of reovirus-induced death +/- FK506 treatment (left; ± S.E.; n = 2). (B) A reovirus plaque assay was performed on non-transformed and H-RasV12 cell lines. Immediately following infection, DMSO or FK506 (10 μM) was added, and immunocytochemistry was performed 5 days later to visualize reovirus plaques (right). Scale bar: 2 mm. A nested ANOVA with Tukey test was performed to compare reovirus plaque size +/- FK506 treatment (left; ± S.E.; n = 3). (C) Mock and reovirus infected non-transformed and H-RasV12 cell lines +/- FK506 (10 μM) were fixed at 12 hpi for FACS analysis. The cells were stained with anti-reovirus antibodies to determine the percentage of cells infected by the virus. A two sample t-test was performed to compare the number of reovirus infected cells +/- FK506 treatment (± S.E.; n = 2).

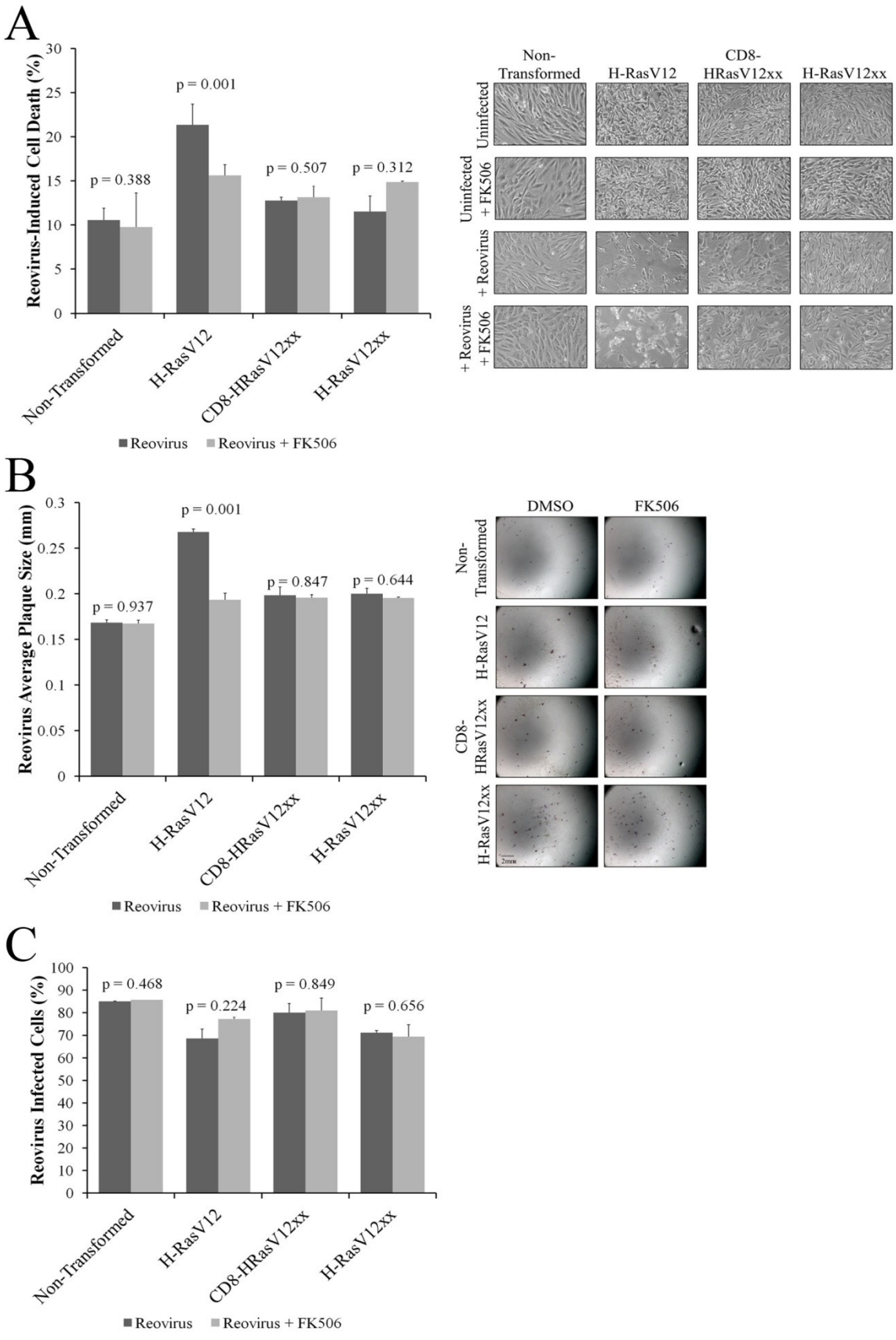
A
Reovirus-Induced Cell Death (%)
30
25
20
15
10
5
0
p = 0.388
p = 0.001
p = 0.507
p = 0.312
Non-Transformed
H-RasV12
CD8-HRasV12xx
H-RasV12xx
Reovirus
Reovirus + FK506
Non-Transformed
H-RasV12
CD8-HRasV12xx
H-RasV12xx
Uninfected
Uninfected + FK506
+ Reovirus
+ Reovirus + FK506
B
Reovirus Average Plaque Size (mm)
0.3
0.25
0.2
0.15
0.1
0.05
0
p = 0.937
p = 0.001
p = 0.847
p = 0.644
Non-Transformed
H-RasV12
CD8-HRasV12xx
H-RasV12xx
Reovirus
Reovirus + FK506
DMSO
FK506
Non-Transformed
H-RasV12
CD8-HRasV12xx
H-RasV12xx
2mm
C
Reovirus Infected Cells (%)
100
90
80
70
60
50
40
30
20
10
0
p = 0.468
p = 0.224
p = 0.849
p = 0.656
Non-Transformed
H-RasV12
CD8-HRasV12xx
H-RasV12xx
Reovirus
Reovirus + FK506

Figure 3.21: Inhibiting Ras farnesylation decreases reovirus spread. (A) Non-transformed, H-RasV12, and N-Ras61K cells were treated with FTI-277 (5 or 10 μM) for 24 h. The cells were lysed, immunoprecipitated with anti-Ras, and subjected to SDS-PAGE and western blotting. β-actin served as a loading control. NT: no treatment (DMSO only). (B) Non-transformed, H-RasV12, and N-Ras61K cells were infected with reovirus (MOI of 20 for H-RasV12 and N-Ras61K cells, and MOI of 40 for non-transformed cells) and treated with FTI-277 (10 μM) or DMSO. At 24 hpi, the cells were collected for cell death analysis by trypan blue exclusion staining. A two-way ANOVA was performed to compare the levels of reovirus-induced death +/- FTI-277 treatment (± S.E.; n = 3). (C) Non-transformed, H-RasV12, and N-Ras61K cells were infected with reovirus (MOI of 20 for H-RasV12 and N-Ras61K cells, and MOI of 40 for non-transformed cells) and treated with FTI-277 (10 μM) or DMSO. The cells were fixed at 12 hpi for FACS analysis and stained with anti-reovirus antibodies to determine the percentage of cells infected by the virus. A two sample t-test was performed to compare the number of reovirus infected cells +/- FTI-277 treatment (± S.E.; n = 3). (D) A reovirus plaque assay was performed on non-transformed, H-RasV12, and N-Ras61K cells. Immediately following infection, DMSO or FTI-277 (10 μM) was added, and immunocytochemistry was performed 5 days later to visualize reovirus plaques (right). Scale bar: 2 mm. A nested ANOVA with Tukey test was performed to compare reovirus plaque size +/- FTI-277 treatment (left; ± S.E.; n = 3).

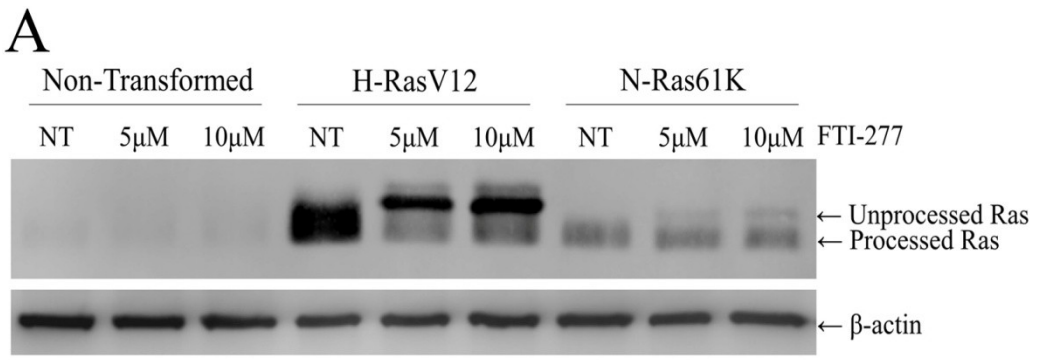

NT = No Treatment

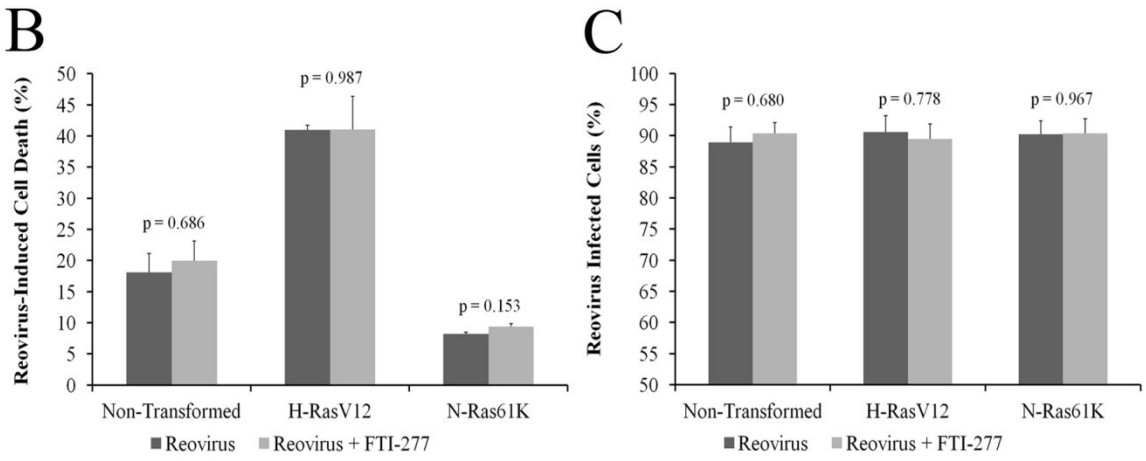

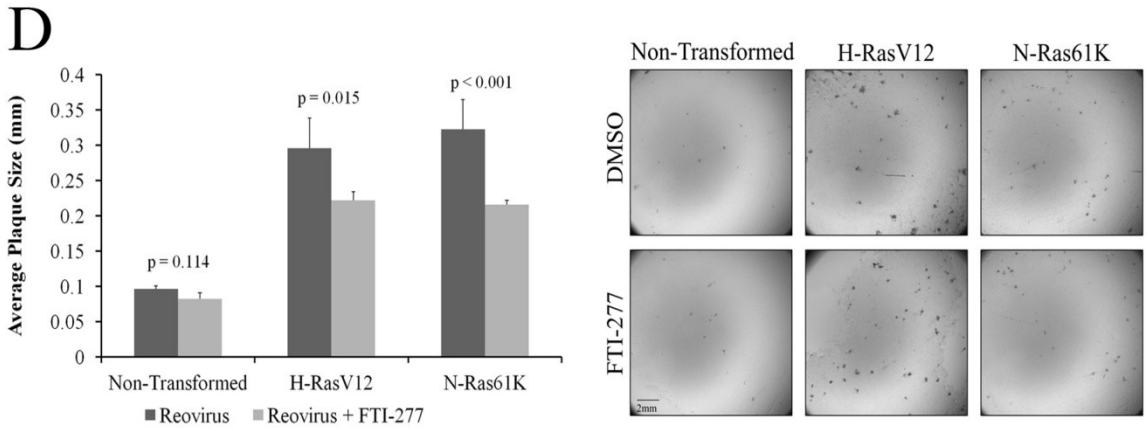

3.7. Reovirus-Induced Cell Death Requires JNK Activation by Cycling H-RasV12

Ras is a dynamic protein that exhibits compartmentalized signalling (Mor and Philips, 2006). In addition to signalling from the plasma membrane, activated Ras interacts with downstream effectors at the ER, mitochondria, endosomes, and Golgi body. The outcome of Ras signalling is the initiation of various downstream pathways that are involved in a wide range of cellular processes, including cell migration, growth, differentiation, and death. With reovirus-induced cell death fluctuating in the presence of spatially distinct H-RasV12 isoforms, it was important to discern any differences in the ability of the targeted constructs to activate well-known Ras downstream effector pathways. In the absence of reovirus, CD8-HRasV12xx (plasma membrane tethered) and H-RasV12xx (palmitoylation deficient) cells were more effective at activating Akt than Erk1/2. In fact, the level of phosphorylated Erk1/2 was comparable to the non-transformed cells, while activated Akt levels resembled the H-RasV12 transformed cells (Figure 3.22A and Figure 3.23). Activated p38 levels were also comparable to the non-transformed control cells (Figure 3.23). JNK activation is linked to Ras-mediated transformation (Kennedy and Davis, 2002), and as expected, phosphorylated JNK was elevated in all three H-RasV12 cell lines, but somewhat reduced in the tethered and/or palmitoylation deficient Ras cells (Figure 3.24A). These results were similar to those obtained by Matallanas et al. (2006) in their study of site-specific Ras activation in NIH3T3 cells.

With downstream signalling levels established in uninfected cells, activation of the effectors was then reassessed in the context of reovirus infection. Following infection,

activated Erk1/2 and Akt levels rose slightly in all cell lines, however differences were not significant with the current sample size (Figure 3.22A and Figure 3.23). Furthermore, reovirus activated p38 in both the non- and Ras-transformed cells to similar levels of activation (Figure 3.23). These results were in support of previously published data that examined downstream signalling in reovirus infected non- and H-RasV12 transformed cells (Shmulevitz et al., 2010). Interestingly, it was the difference in JNK activation, which plays a key role in inducing cell apoptosis, that was most notable between cell lines (Figure 3.24A). Increased JNK activation was found in all reovirus infected cells. A slight increase was noted in the non-transformed, CD8-HRasV12xx transformed, and H-RasV12xx cells, while a much more significant increase occurred in cells expressing H-RasV12. Since the Ras cell lines varied in their ability to activate JNK following infection, a JNK inhibitor was used to determine if the pathway was involved in reovirus-induced cell death and if it could explain the contrasting death and reovirus release data from the spatially distinct H-RasV12 cell lines. JNK inhibitor II, which is also known as SP600125, reversibly inhibits JNK by competing with ATP to prevent JNK phosphorylation. JNK inhibition significantly decreased reovirus-induced cell death in H-RasV12 and H-RasV12xx cell lines, but had no effect on non-transformed or CD8-HRasV12xx cell lines (Figure 3.24B). This supported the above western blot data, as cells which significantly activated JNK following reovirus infection, or cells expressing Ras that could associate with the Golgi body were the ones susceptible to the JNK inhibitor. Additionally, JNK inhibition had no effect on the number of cells infected by the virus, and as a control, a western blot was used to demonstrate that phosphorylated JNK levels did actually decline in the presence of the inhibitor (Figure 3.24C-D). To

determine if the use of another inhibitor would demonstrate a similar effect, a MEK1/2 inhibitor was employed (Figure 3.22D). MEK1/2 is responsible for activating Erk1/2, which was slightly upregulated in reovirus infected cells. The MEK1/2 inhibitor had little effect on reovirus-induced cell death or on the number of cells infected by the virus (Figure 3.22B-C). Therefore, the data suggests that the ability of reovirus to induce cell death is dependent on JNK activation and that the activation of JNK is dependent on Ras localization during reovirus infection.

Figure 3.22: MEK 1/2 inhibition has no affect on reovirus-induced cell death. Non-transformed and H-RasV12 cell lines were infected with reovirus. To achieve similar levels of percent infected, cells were infected at an MOI of 20 for H-RasV12 cells, an MOI of 40 for non-transformed and H-RasV12xx cells, and an MOI of 80 for CD8-HRasV12xx cells. (A) Cell lysates were collected at 8 hpi, and subjected to SDS-PAGE and western blotting to assess total and phosphorylated levels of Erk 1/2 (left). Reovirus and β-actin served as controls. Relative levels of Erk 1/2 phosphorylation are indicated in the bar graph (right; ± S.E.). ANOVA analysis showed no significant effect of treatment ($n = 3$; $p = 0.076$). UI: uninfected; V: reovirus infected. (B) Mock and reovirus infected non-transformed and H-RasV12 cell lines were treated with the MEK 1/2 inhibitor, U0126 (40 μM), or DMSO at 2 hpi. At 24 hpi, photographs of cell death were taken (right), and the cells were collected for trypan blue exclusion staining. A two sample t-test was performed to compare the levels of reovirus-induced death with MEK 1/2 inhibition (left; ± S.E.; $n = 2$). (C) Mock and reovirus infected non-transformed and H-RasV12 cell lines were treated with U0126 (40 μM) or DMSO at 2 hpi. At 12 hpi, the cells were fixed and stained with anti-reovirus antibodies for FACS analysis. A two sample t-test was performed to compare the number of reovirus infected cells +/- MEK 1/2 inhibition (± S.E.; $n = 2$). (D) Western blot of non-transformed and H-RasV12 cell lines +/- MEK 1/2 inhibition. β-actin served as a loading control.

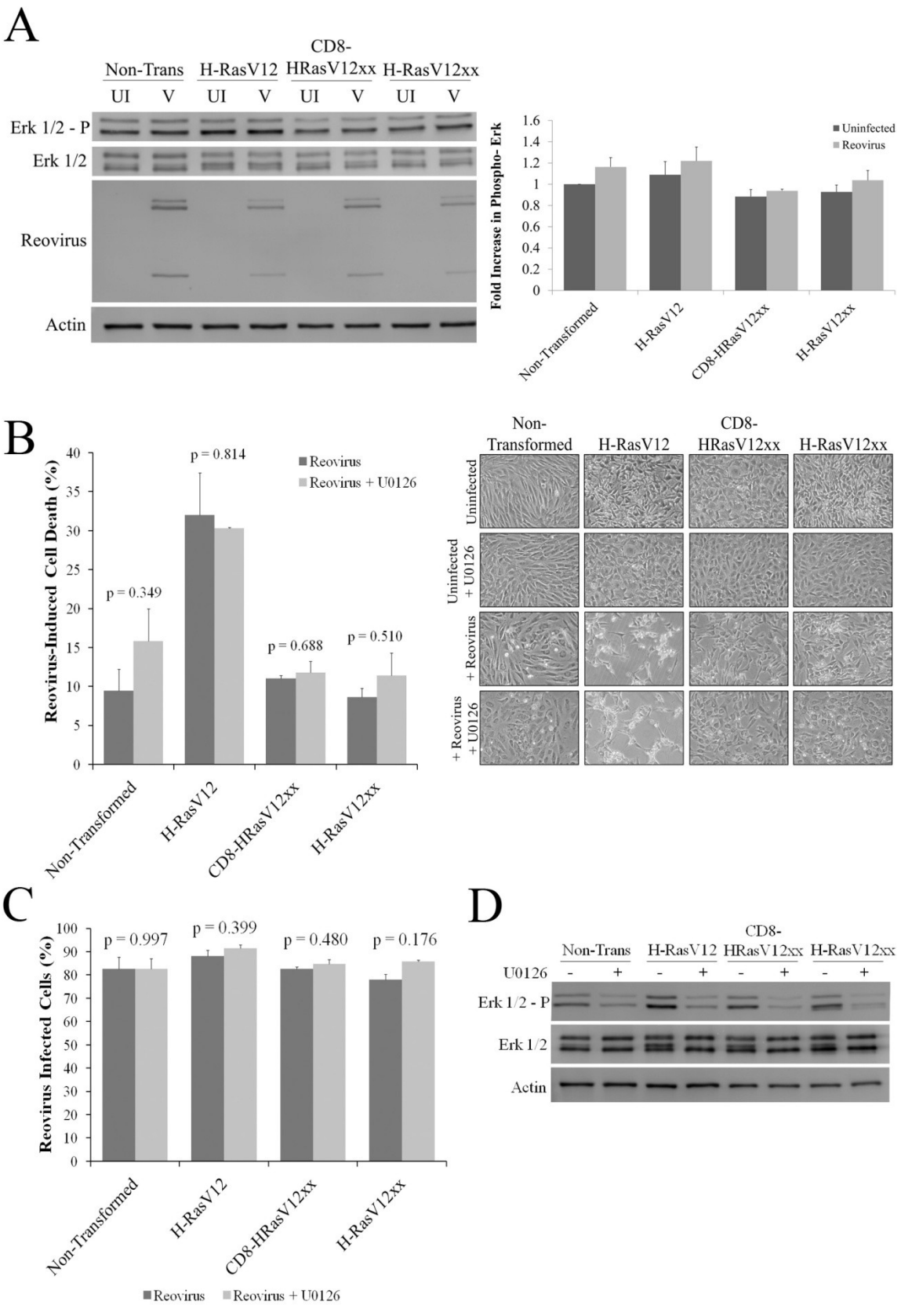
A
Non-Trans
H-RasV12
CD8-HRasV12xx
H-RasV12xx
UI
V
Erk 1/2 - P
Erk 1/2
Reovirus
Actin
Fold Increase in Phospho- Erk
Uninfected
Reovirus
Non-Transformed
H-RasV12
CD8-HRasV12xx
H-RasV12xx
B
Reovirus-Induced Cell Death (%)
Reovirus
Reovirus + U0126
p = 0.349
p = 0.814
p = 0.688
p = 0.510
Non-Transformed
H-RasV12
CD8-HRasV12xx
H-RasV12xx
Uninfected
Uninfected + U0126
+ Reovirus
+ Reovirus + U0126
C
Reovirus Infected Cells (%)
p = 0.997
p = 0.399
p = 0.480
p = 0.176
Non-Transformed
H-RasV12
CD8-HRasV12xx
H-RasV12xx
Reovirus
Reovirus + U0126
D
Non-Trans
H-RasV12
CD8-HRasV12xx
H-RasV12xx
U0126
Erk 1/2 - P
Erk 1/2
Actin

Figure 3.23: Phosphorylated p38 increases with reovirus infection. Non-transformed and H-RasV12 cell lines were infected with reovirus. To achieve similar levels of percent infected, cells were infected at an MOI of 20 for H-RasV12 cells, an MOI of 40 for non-transformed and H-RasV12xx cells, and an MOI of 80 for CD8-HRasV12xx cells. Cell lysates were collected at 8 hpi, and subjected to SDS-PAGE and western blotting to assess total and phosphorylated levels of Akt and p38. β-actin served as a loading control. Relative levels of Akt and p38 phosphorylation are indicated below the blot. ANOVA analysis showed no significant effect of treatment on Akt phosphorylation ($n = 3$; ± S.E.; $p = 0.109$), but was significant for p38 phosphorylation ($n = 3$; ± S.E.; $p < 0.001$). P-values from significant Tukey comparisons are in the bar graph. UI: uninfected; V: reovirus infected.

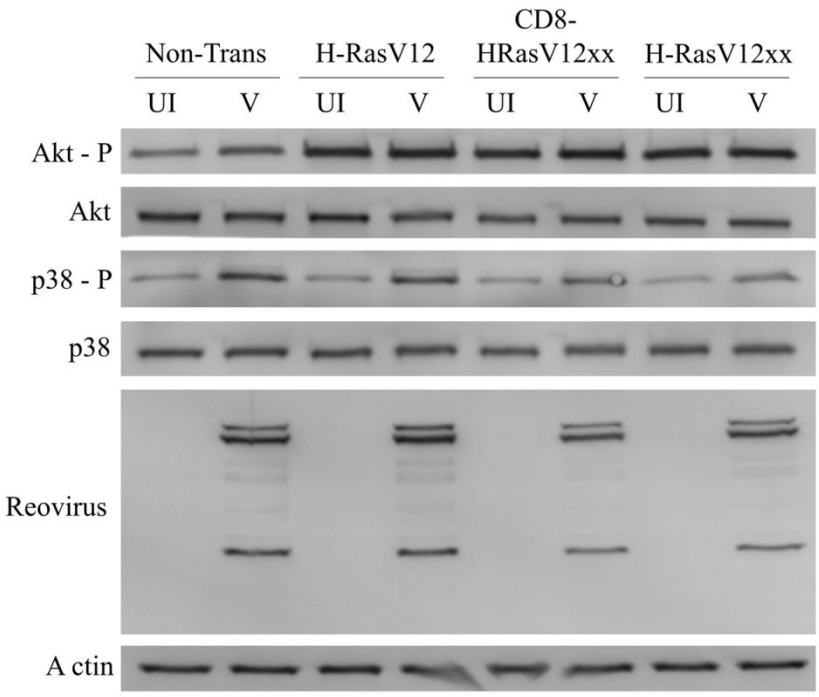
Non-Trans
H-RasV12
CD8-HRasV12xx
H-RasV12xx
UI
V
Akt - P
Akt
p38 - P
p38
Reovirus
A ctin

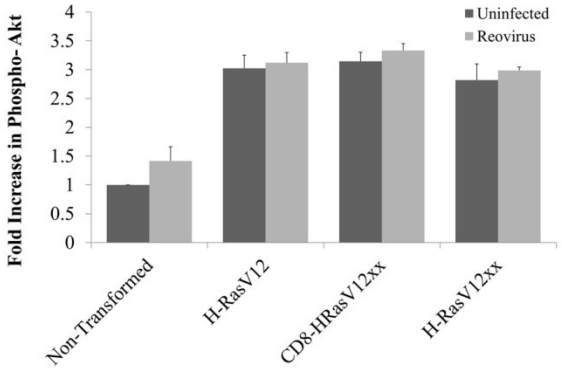
Fold Increase in Phospho- Akt
Uninfected
Reovirus
Non-Transformed
H-RasV12
CD8-HRasV12xx
H-RasV12xx

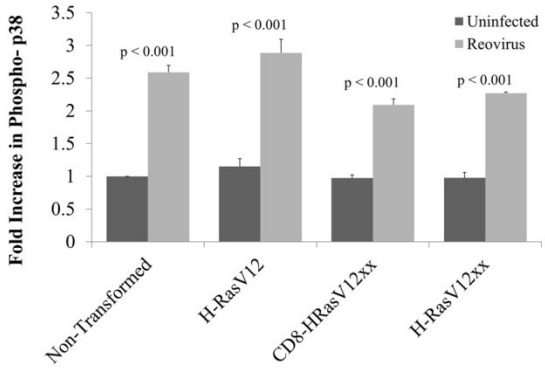
Fold Increase in Phospho- p38
p < 0.001
Uninfected
Reovirus
Non-Transformed
H-RasV12
CD8-HRasV12xx
H-RasV12xx

Figure 3.24: JNK is activated following reovirus infection. Non-transformed and H-RasV12 cell lines were infected with reovirus. To achieve similar levels of percent infected, cells were infected at an MOI of 20 for H-RasV12 cells, an MOI of 40 for non-transformed and H-RasV12xx cells, and an MOI of 80 for CD8-HRasV12xx cells. (A) Cell lysates were collected at 8 hpi, and subjected to SDS-PAGE and western blotting to assess total and phosphorylated levels of JNK (left). Reovirus and β-actin served as controls. Relative levels of JNK phosphorylation are indicated in the bar graph (right; ± S.E.). ANOVA analysis showed a significant effect of treatment ($n = 3$; $p < 0.001$). P-values from significant Tukey comparisons are in the bar graph. UI: uninfected; V: reovirus infected. (B) Mock and reovirus infected non-transformed and H-RasV12 cell lines were treated with JNK inhibitor II (50 μM) or DMSO at 2 hpi. At 24 hpi, photographs of cell death were taken (right), and the cells were collected for cell death analysis by trypan blue exclusion staining. A two sample t-test was performed to compare the levels of reovirus-induced death with JNK inhibition (left; ± S.E.; $n = 2$; $n = 5$ for H-RasV12xx). (C) Mock and reovirus infected non-transformed and H-RasV12 cell lines were treated with JNK inhibitor II (50 μM) or DMSO at 2 hpi. At 12 hpi, the cells were fixed and stained with anti-reovirus antibodies for FACS analysis. A two sample t-test was performed to compare the number of reovirus infected cells +/- JNK inhibition (± S.E.; $n = 2$). (D) Western blot of phosphorylated JNK levels from H-RasV12 transformed cells treated with or without JNK inhibitor II for 24 h. β-actin served as a loading control.

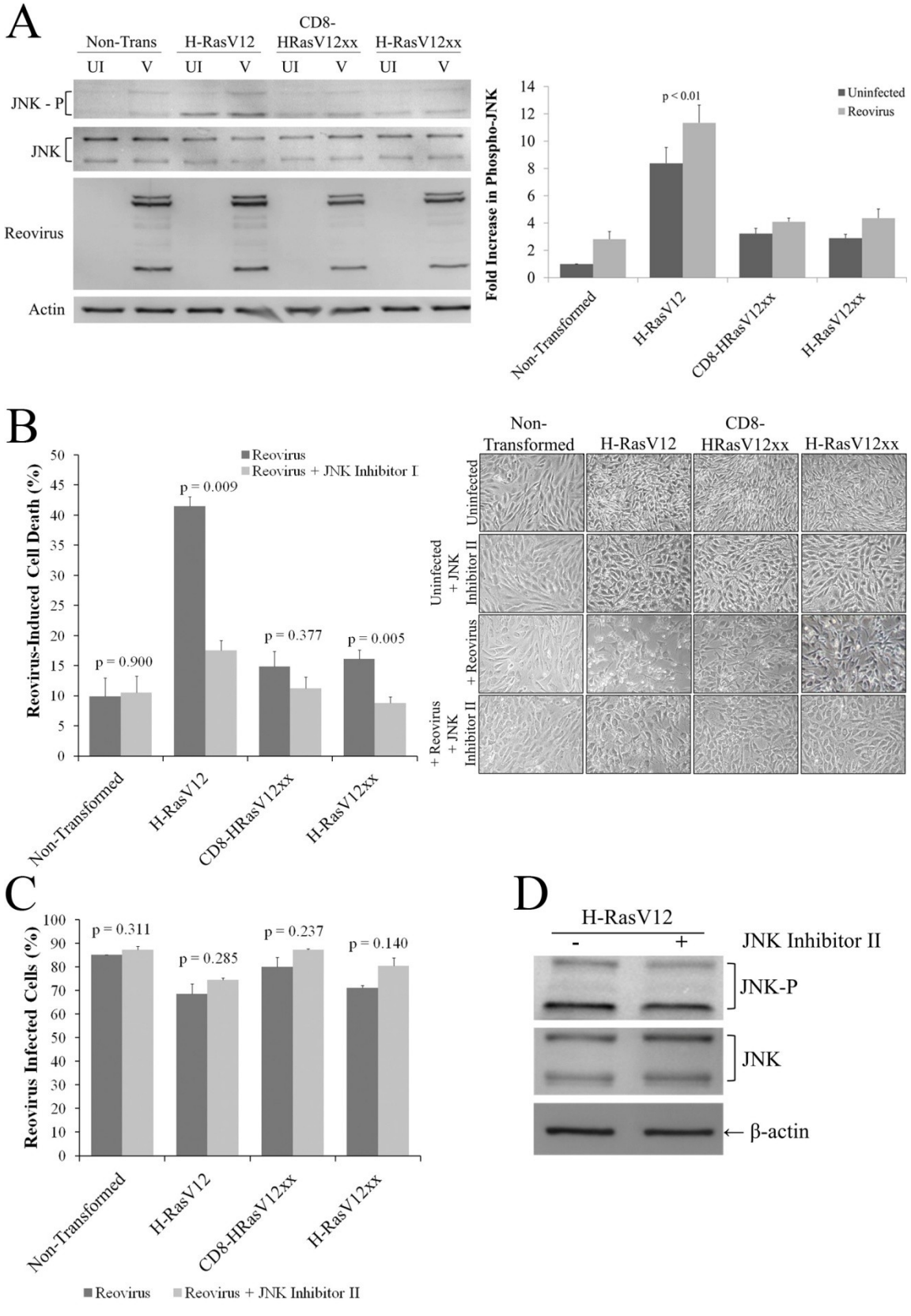
A
Non-Trans
H-RasV12
CD8-HRasV12xx
H-RasV12xx
UI
V
JNK - P
JNK
Reovirus
Actin
Fold Increase in Phospho-JNK
p < 0.01
Uninfected
Reovirus
Non-Transformed
H-RasV12
CD8-HRasV12xx
H-RasV12xx
B
Reovirus-Induced Cell Death (%)
Reovirus
Reovirus + JNK Inhibitor I
p = 0.900
p = 0.009
p = 0.377
p = 0.005
Non-Transformed
H-RasV12
CD8-HRasV12xx
H-RasV12xx
Uninfected
Uninfected + JNK Inhibitor II
+ Reovirus
+ Reovirus + JNK Inhibitor II
C
Reovirus Infected Cells (%)
p = 0.311
p = 0.285
p = 0.237
p = 0.140
Reovirus
Reovirus + JNK Inhibitor II
D
H-RasV12
-
+
JNK Inhibitor II
JNK-P
JNK
β-actin

3.8. 2BP Promotes Reovirus-Induced Cell Death through Activation of the Ras/MEKK1/MKK4/JNK Pathway

It is evident that the accumulation of H-RasV12 in the Golgi body, and its subsequent activation of JNK, plays a key role in the death of reovirus infected cells. Previous studies have indicated that Ras is capable of signalling from the Golgi body, but there are conflicting opinions as to which downstream effectors are activated from this organelle (Chiu et al., 2002; Matallanas et al., 2006). Nonetheless, activation of JNK has been linked to Golgi-tethered Ras. With the palmitoylation inhibitor, 2BP, causing further accumulation of H-RasV12 in the Golgi body and increasing reovirus-induced cell death and virus release, the next experiment determined if 2BP treatment activated similar downstream signalling pathways. One of the Ras downstream effectors linked to JNK activation is MEKK1 (Russell et al., 1995). Activation of MEKK1 initiates a kinase cascade that leads to the phosphorylation of MKK4 and subsequent phosphorylation of JNK. As such, non-transformed and H-RasV12 cell lines were treated with 2BP to assess the activation of MKK4 and JNK in the context of reovirus infection. In comparison to uninfected cells, reovirus infection caused an increase in both MKK4 and JNK phosphorylation (Figure 3.25). This work already demonstrated that JNK activation occurs with reovirus infection, and since MKK4 is upstream of JNK, this data was expected. Interestingly, when uninfected H-RasV12 transformed cells were treated with 2BP, the levels of MKK4 and JNK activation were enhanced. Furthermore, when these cells were infected with reovirus, the levels increased even further. Non-transformed cells treated with 2BP showed elevated levels of phosphorylated MKK4, but this increase did not translate to further activation of its downstream effector, JNK. When considering the

tethered and/or palmitoylation deficient cell lines, 2BP had little to no effect on uninfected or reovirus-infected CD8-HRasV12xx and H-RasV12xx cell lines.

In light of 2BP promoting JNK activation in H-RasV12 transformed cells, reovirus-induced cell death was assessed in the context of JNK inhibition and 2BP treatment. Foremost, use of either inhibitor did not affect the number of cells infected by the virus (Figure 3.26B). As expected, JNK inhibition reduced virus-related cell death in H-RasV12 transformed cells, while 2BP enhanced it (Figure 3.26A). Treatment of H-RasV12 cells with both the JNK inhibitor and 2BP decreased reovirus-induced cell death significantly, but not to levels of the JNK inhibitor alone. In addition, CD8-HRasV12xx transformed cells were used as a negative control, as individual or combination treatments with 2BP and/or JNK inhibitor II did not alter the basal levels of reovirus-induced cell death. As a control, a western blot was also used to show decreasing levels of activated JNK when in the presence of the JNK inhibitor (Figure 3.26C). It is well known that reovirus infection triggers caspase-dependent cell death and that activated JNK can stimulate the release of cytochrome C and Smac/Diablo from the mitochondria to initiate the caspase cascade (Clarke et al., 2004; Kominsky et al., 2002a, 2002b). Increased apoptosis is linked to reovirus release and contributes to efficient spread of the virus to neighbouring cells (Marcato et al., 2007). Consequently, inhibiting caspase activity drastically reduces virus-related cell death and release. As determined by FACS analysis, treatment of reovirus-infected cells with the caspase inhibitor, ZVAD, inhibited cell death in H-RasV12 transformed cells (Figure 3.27). Combination treatment of H-RasV12 cells with 2BP and ZVAD also caused a significant decline in reovirus-induced

cell death; indicating that the ability of 2BP to promote cell death in the presence of reovirus is also dependent on caspase activation.

Taken collectively, this body of work suggests that reovirus infection causes fragmentation of the Golgi body; likely through its association with microtubules during viral factory formation (Figure 3.28). As a result, oncogenic H-Ras accumulates in the Golgi body as it cycles back for re-palmitoylation and initiates cellular apoptosis through activation of the MEKK1/MKK4/JNK signalling pathways. Tethering of Ras to the plasma membrane reduces virus-related cell death to levels comparable to that of the non-transformed control. Alternatively, use of the palmitoylation inhibitor, 2BP, further promotes the association of Ras with the Golgi body and causes additional activation of the MEKK1/MKK4/JNK signalling pathway to initiate higher levels of reovirus-induced cell death.

Figure 3.25: 2BP promotes reovirus-induced cell death through the MEKK1/MKK4/JNK pathway. Non-transformed and H-RasV12 cell lines were infected with reovirus and treated with 2BP (50 μM). To achieve similar levels of infection, cells were infected at an MOI of 20 for H-RasV12 cells, an MOI of 40 for non-transformed and H-RasV12xx cells, and an MOI of 80 for CD8-HRasV12xx cells. Cell lysates were collected at 8 hpi, and subjected to SDS-PAGE and western blotting to assess total and phosphorylated levels of MKK4 and JNK. Reovirus and β-actin served as controls. Relative levels of MKK4 and JNK phosphorylation are indicated below the blot in respective bar graphs (n = 3; ± S.E.; ANOVA -*statistically significant effect of reovirus; **statistically significant effect of reovirus and 2BP). Uninfected samples (no 2BP) were set to a value of 1 and served as a baseline comparison for each cell line. UI: uninfected; V: reovirus infected.

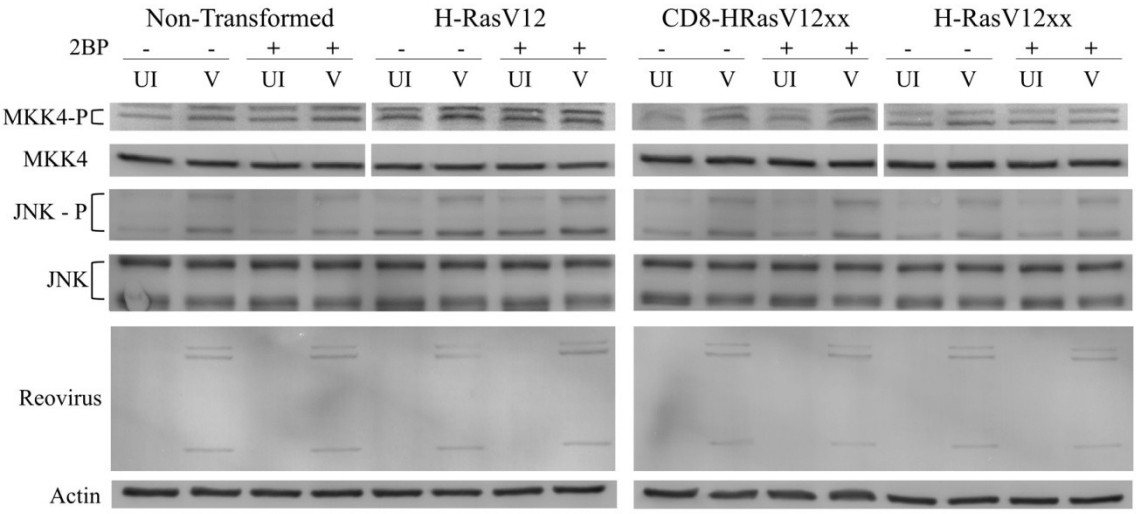
Non-Transformed
H-RasV12
CD8-HRasV12xx
H-RasV12xx
2BP
UI
V
MKK4-P
MKK4
JNK - P
JNK
Reovirus
Actin

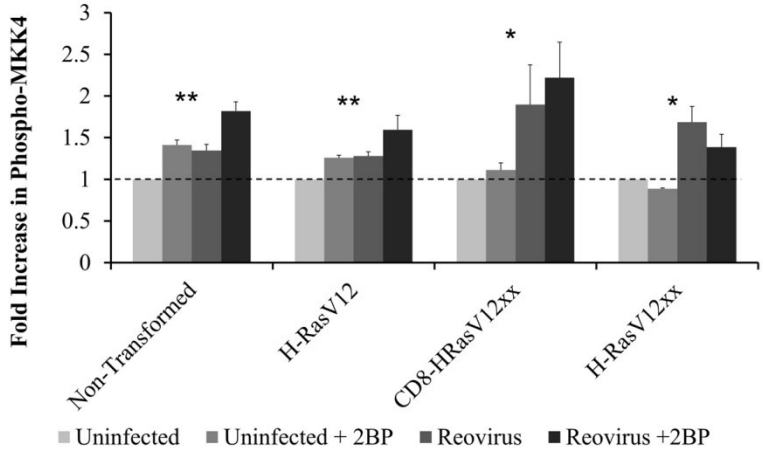
Fold Increase in Phospho-MKK4
Non-Transformed
H-RasV12
CD8-HRasV12xx
H-RasV12xx
Uninfected
Uninfected + 2BP
Reovirus
Reovirus +2BP

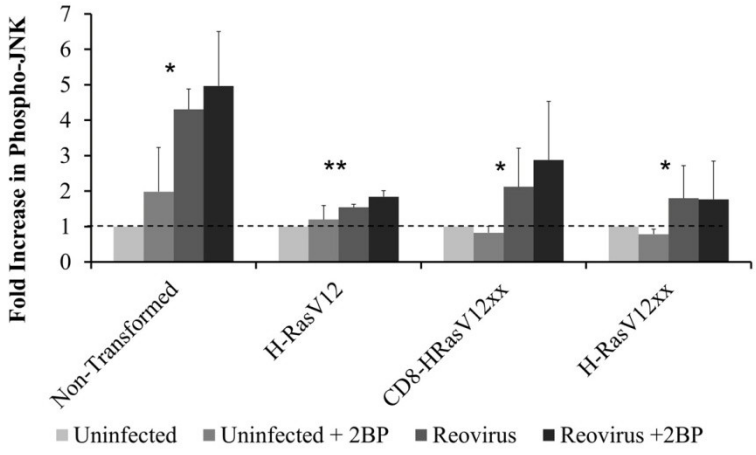
Fold Increase in Phospho-JNK
Non-Transformed
H-RasV12
CD8-HRasV12xx
H-RasV12xx
Uninfected
Uninfected + 2BP
Reovirus
Reovirus +2BP

Figure 3.26: JNK inhibition negates the effect of 2BP on reovirus-induced cell death. H-RasV12 and CD8-HRasV12xx transformed cells were infected with reovirus at an MOI of 20 and 80, respectively, and treated with 2BP (1 μM) and/or JNK inhibitor II (100 μM). (A) At 24 hpi, photographs of cell death were taken, and the cells were collected for trypan blue exclusion staining. An ANOVA with Tukey test was performed to compare the levels of reovirus-induced death in the presence of 2BP and/or JNK inhibitor II (left; ± S.E.; n = 3; *significantly different). (B) At 12 hpi, the cells were fixed and stained with anti-reovirus antibodies for FACS analysis. An ANOVA with Tukey test was performed to compare the percent of reovirus infected cells in the presence of the various inhibitors (± S.E.; n = 2). (C) Western blot of phosphorylated JNK levels from H-RasV12 and CD8-HRasV12xx transformed cells treated with or without JNK inhibitor II. β-actin served as a loading control.

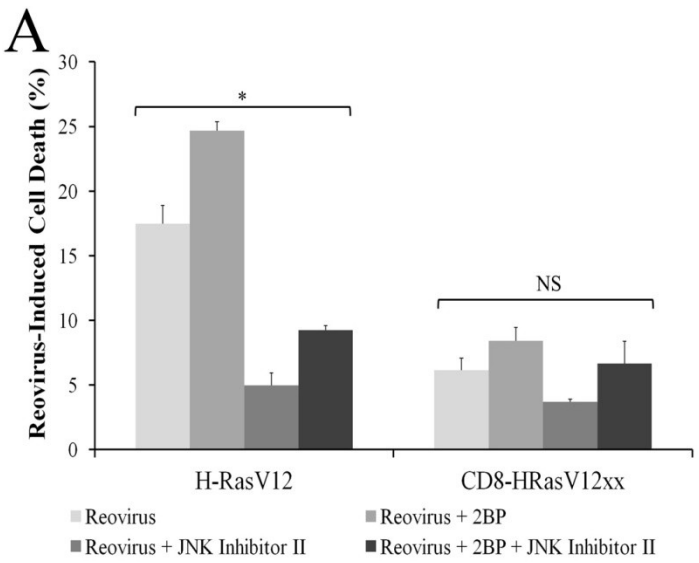
A
Reovirus-Induced Cell Death (%)
30
25
20
15
10
5
0
*
NS
H-RasV12
CD8-HRasV12xx
Reovirus
Reovirus + 2BP
Reovirus + JNK Inhibitor II
Reovirus + 2BP + JNK Inhibitor II

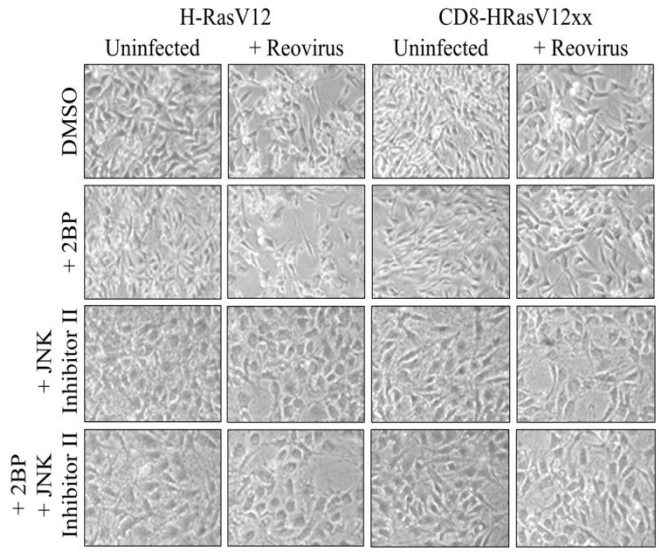
H-RasV12
CD8-HRasV12xx
Uninfected
+ Reovirus
Uninfected
+ Reovirus
DMSO
+ 2BP
+ JNK Inhibitor II
+ 2BP + JNK Inhibitor II

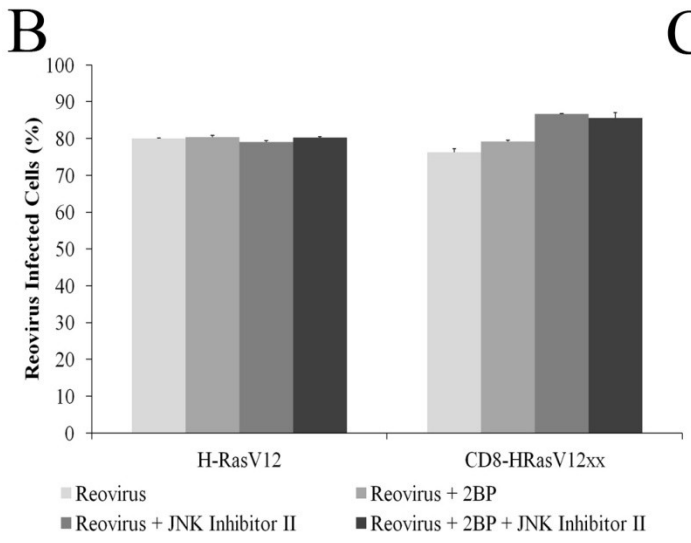
B
Reovirus Infected Cells (%)
100
90
80
70
60
50
40
30
20
10
0
H-RasV12
CD8-HRasV12xx
Reovirus
Reovirus + 2BP
Reovirus + JNK Inhibitor II
Reovirus + 2BP + JNK Inhibitor II

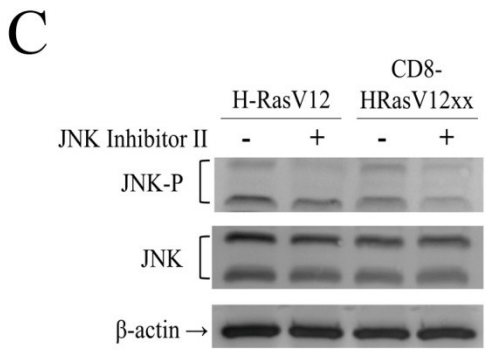
C
H-RasV12
CD8-HRasV12xx
JNK Inhibitor II
-
+
-
+
JNK-P
JNK
β-actin →

Figure 3.27: 2BP increases reovirus-induced cell death through caspase-dependent apoptosis. H-RasV12 transformed cells were infected with reovirus at an MOI of 20 and treated with 2BP (50 μM) and/or ZVAD (50 μM). At 24 hpi, the cells were stained with Annexin V-PE and 7-AAD to determine the level of cell apoptosis and death by FACS analysis (bottom panels). An ANOVA with Tukey test was performed to compare the levels of reovirus-induced death in the presence of 2BP and/or ZVAD (± S.E.; n = 3).

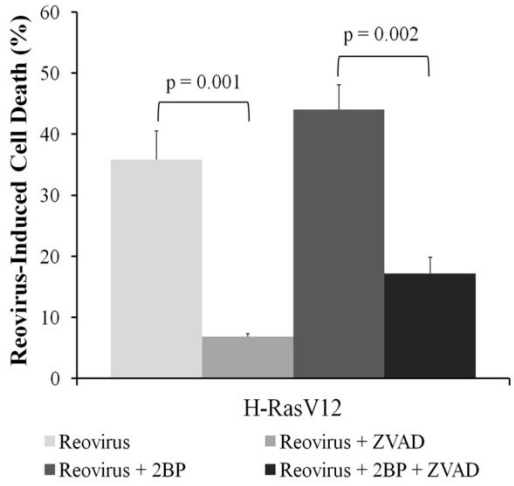
Reovirus-Induced Cell Death (%)
60
50
40
30
20
10
0
p = 0.001
p = 0.002
H-RasV12
Reovirus
Reovirus + ZVAD
Reovirus + 2BP
Reovirus + 2BP + ZVAD

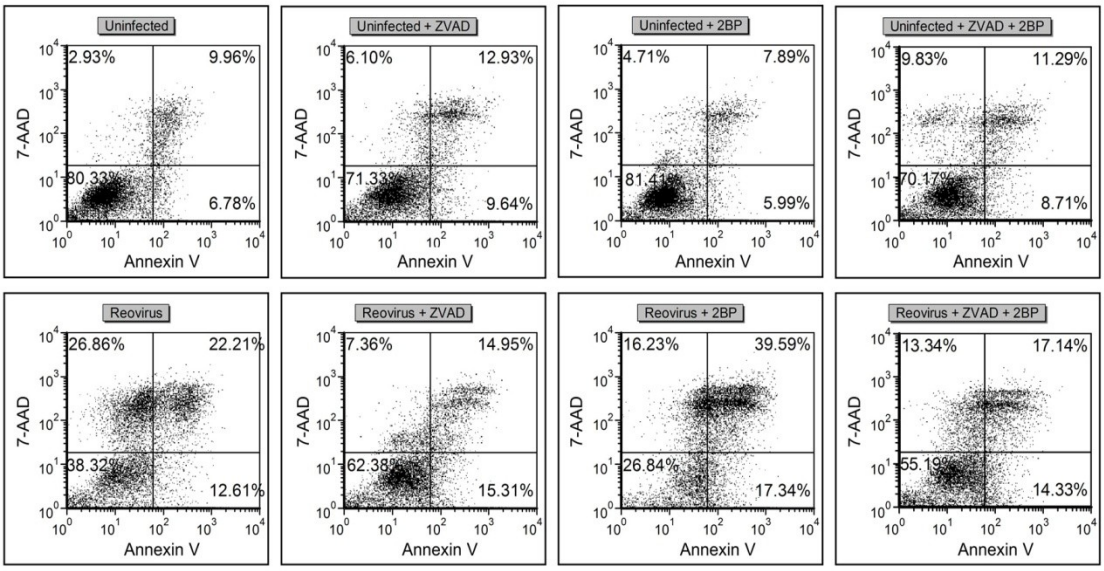
Uninfected
2.93%
9.96%
80.33%
6.78%
Uninfected + ZVAD
6.10%
12.93%
71.33%
9.64%
Uninfected + 2BP
4.71%
7.89%
81.41%
5.99%
Uninfected + ZVAD + 2BP
9.83%
11.29%
70.17%
8.71%
Reovirus
26.86%
22.21%
38.32%
12.61%
Reovirus + ZVAD
7.36%
14.95%
62.38%
15.31%
Reovirus + 2BP
16.23%
39.59%
26.84%
17.34%
Reovirus + ZVAD + 2BP
13.34%
17.14%
55.19%
14.33%
7-AAD
Annexin V

Figure 3.28: Proposed model. Reovirus interacts with microtubules to setup cytoplasmic viral inclusion bodies. This leads to Golgi fragmentation and a disruption of cellular vesicular transport. As a result, H-RasV12 is retained in the Golgi body. In turn, Ras activates its downstream effector, MEKK1, which initiates cell death through activation of MKK4 and JNK. Use of the palmitoylation inhibitor, 2BP, results in further accumulation of Ras in the Golgi and even greater levels of reovirus-induced cell death. Tethering of Ras to the plasma membrane generates the opposite effect; producing basal levels of cell death that are comparable to infected non-transformed cells.

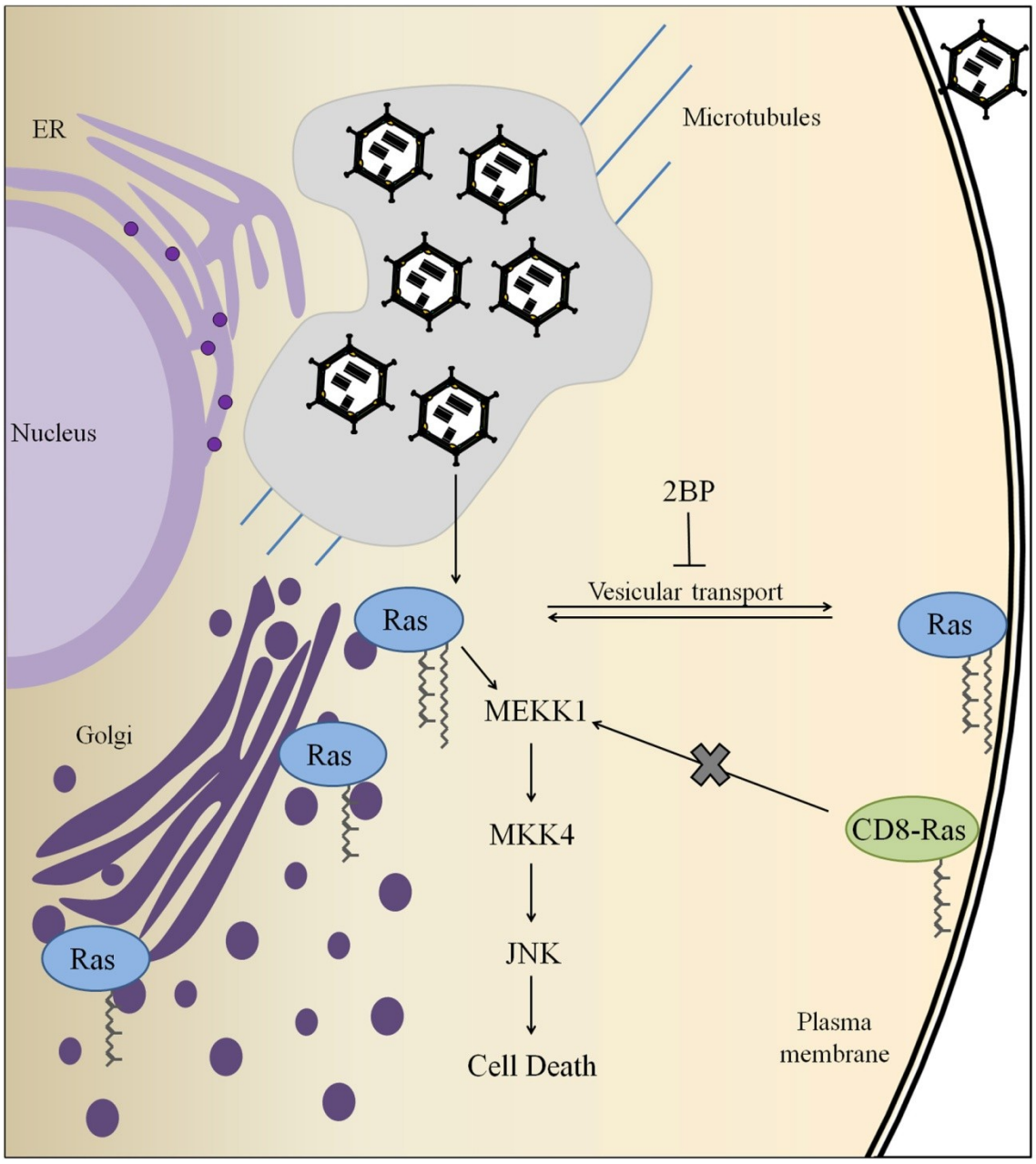
ER
Microtubules
Nucleus
2BP
Vesicular transport
Ras
Ras
MEKK1
Golgi
Ras
MKK4
CD8-Ras
Ras
JNK
Plasma
membrane
Cell Death

CHAPTER 4: DISCUSSION

Constitutive Ras activity and its associated downstream pathways play a significant role in human oncogenesis (Calvo et al., 2010). In response to constitutive Ras activation, the cellular environment is forced to change, and if possible, maintain a new level of homeostasis. This altered state provides an opportunity for adaptive pathogens to target these cells and use them as a platform for propagation. It is well established that the pathogenicity of reovirus is relatively benign in normal cells, and that it preferentially targets Ras-transformed cells (Coffey et al., 1998; Strong et al., 1998). So far, studies have identified aspects of the reovirus life cycle that are enhanced in cells harboring activated Ras (Marcato et al., 2007; Shmulevitz et al., 2010). Conversely, this work illustrates how reovirus alters the activity of oncogenic Ras itself.

4.1. Prenyl- and Acylation of Viral Proteins: Targeting Ras through its Modification Enzymes

In order to manipulate Ras activity, I originally speculated that reovirus would target Ras directly or sequester one of its modification enzymes. Co-immunoprecipitations revealed no direct involvement between reovirus and Ras at 12 hpi (Figure 3.3); still leaving the possibility of a transient interaction or an association at a different time point during the reovirus life cycle. Other RNA viruses are known to utilize Ras modification enzymes, specifically the farnesyltransferase, in their pathogenesis. For instance, the accessory protein, $p13^{II}$, of human T-cell leukemia virus type 1 is known to bind the farnesyltransferase and localize to the inner mitochondrial membrane. Once there, it alters the membrane potential; thereby, increasing its

permeability to potassium, inducing reactive oxygen species production, and potentially favouring apoptosis (Lefebvre et al., 2002; Silic-Benussi et al., 2010). Alternatively, hepatitis D virus, which requires a pre-existing hepatitis B virus infection for its pathogenesis, is known to have its large antigen prenylated by the Ras farnesyltransferase (Otto and Casey, 1996). This modification to the large antigen serves a dual purpose. It enables interaction of the large antigen with hepatitis B virus envelope proteins that are essential to virus assembly and release, and also localizes the large antigen to the nucleus to suppress viral replication during early stages of infection (Lin et al., 1999).

The reovirus life cycle is approximately 24 h in NIH3T3 cells, which is also consistent with the half-life of Ras (Magee et al., 1987). Since farnesylation is a permanent modification, the likelihood of reovirus manipulating Ras through disruption of farnesylation seemed unlikely within this time frame. Farnesylation inhibitors proved to be ineffective during the first round of infection, whereas plaque size analysis after 5 days revealed a reduction in reovirus spread when in the presence of the inhibitor (Figure 3.21). On the other hand, palmitoylation is a more likely candidate. It is a reversible modification with a relatively short half-life, and its presence on Ras, or lack thereof, is known to cause relocalization. Many viral proteins are known to be palmitoylated (Blanc et al., 2013; Veit, 2012). Viruses do not encode their own palmitoyl acyltransferase and require the activity of host DHHC enzymes for this post-translational modification to occur. Viral proteins which undergo palmitoylation are typically categorized into transmembrane or peripheral membrane proteins. Viral transmembrane proteins interact with host cell membranes, such as those that occur during viral entry, pore formation, and assembly. For example, the envelope glycoprotein, hemagglutinin (HA), from the

influenza virus is known to be palmitoylated. Palmitoylation of HA is believed to play a role during entry of certain serotypes by facilitating the fusion of the influenza membrane with that of the host endosomal membrane, and enabling release of the viral nucleocapsid into the cytoplasm (Wagner et al., 2005). Additionally, influenza acquires its envelope as it exits infected cells and palmitoylation of HA may aid in viral assembly and budding by targeting the protein to lipid raft microdomains in the plasma membrane (Takeda et al., 2003). In contrast to transmembrane proteins, peripheral membrane proteins lack a hydrophobic domain and require lipid modifications for membrane anchoring and targeting. For instance, the core protein of the hepatitis C virus, which makes up the viral nucleocapsid, is modified by palmitoylation (Majeau et al., 2009). Palmitoylation ensures proper association of the core protein with membranes of the smooth ER and neighbouring lipid droplets; a process critical to hepatitis C virus assembly.

As discussed above, numerous viral proteins are known to undergo palmitoylation (Veit, 2012); however, the process of identifying sites of palmitoylation and determining if acylation actually occurs is a difficult task. Unlike farnesylation, which has an identifiable CAAX motif, there is no strict consensus sequence for palmitoylation. Patterns have been identified to aid in palmitoylation site recognition, but in the case of viral pathogenesis, one may be looking for a protein that is only detectable in small amounts, palmitoylated at a certain time point during infection, and may not constitute a viral structural component. In support of the latter, the non-structural protein, p10, from avian and Nelson Bay reoviruses is a fusion-associated small transmembrane protein whose ability to be palmitoylated is essential for cell fusion, syncytium formation, and virus release (Shmulevitz et al., 2003). Knowing that other members of the

Orthoreovirus genus utilized palmitoylation in their pathogenesis, I speculated that mammalian reovirus T3D could also undergo this post-translational modification and perhaps, sequester the Ras palmitoyl acyltransferase. After all, it was already established that the reovirus outer capsid protein, μ1N, was myristoylated at an N-terminal glycine residue, and under certain circumstances, myristoylation can serve as a precursor to palmitoylation (Nibert et al., 1991; Veit, 2012). While I was able to detect μ1N myristoylation, I was unable to get [^{3}H]-palmitic acid radiolabelling to work (data not shown). Therefore, the possibility still exists that μ1 or another reovirus protein could be palmitoylated, and perhaps, a different technique should be employed. On that note, there are 25 human DHHC family members; any one of which is capable of palmitoylating a viral protein (Mitchell et al., 2006). Viral palmitoylation does not necessarily imply that the Ras palmitoyl acyltransferase, DHHC9-GCP16, is involved. That being said, use of the palmitoylation inhibitor, 2BP, which is known to target the Ras palmitoyl acyltransferase (Resh, 2006), produced a favourable outcome when coupled with reovirus infection. While it is possible that a reovirus protein could undergo palmitoylation and produce a similar result, a more likely scenario is that 2BP is acting independently of reovirus infection. Surprisingly, the way that reovirus manipulates Ras activity is not through direct interaction or sequestering of Ras modification enzymes, but through the process of Golgi fragmentation.

4.2. Golgi Fragmentation

This work demonstrates that reovirus infection causes fragmentation of the Golgi body. As a result, oncogenic H-Ras accumulates in the Golgi body as it awaits re-

palmitoylation and initiates cellular apoptosis through activation of the MEKK1/MKK4/JNK signalling pathway. Tethering of Ras to the plasma membrane reduces virus-related cell death to levels comparable to that of the non-transformed control. Alternatively, use of the palmitoylation inhibitor, 2BP, further promotes the association of Ras with the Golgi body and causes additional activation of the MEKK1/MKK4/JNK signalling pathway to initiate higher levels of reovirus-induced cell death.

As previously mentioned, fragmentation of the Golgi body is a normal cellular response to mitosis, apoptosis, or cytoskeletal interference (Colanzi et al., 2003; Mukherjee et al., 2007; Nozawa et al., 2002). The Golgi body, which consists of interconnected stacks of cisternae, functions in the sorting, processing, and transport of lipids and proteins (Wang and Seemann, 2011). During fragmentation, the tubular bridges between the stacks disassemble. This process is followed by unstacking and shortening of the cisternae into small clusters and fragments. As expected, vesicular transport is severely compromised or completely inhibited during this time (Rabouille et al., 1995; Storrie and Yang, 1998). In the case of mitosis, or removal of the stressor causing cytoskeletal interference, the Golgi body can reassemble to form a functioning organelle, however, apoptotic disassembly of the Golgi body is an irreversible process (Yadav and Linstedt, 2011).

When considering reovirus-induced fragmentation of the Golgi body, it is well established that reovirus T3D inhibits cell proliferation of infected cells (Poggioli et al., 2000). With mitosis excluded, reovirus likely contributes to Golgi fragmentation by forming viral inclusion bodies in the perinuclear region of the cell, and subsequently,

inducing apoptosis. After all, reovirus interacts with cytoskeletal elements during viral factory formation, and its structural protein, μ2, is known to associate with microtubules (Parker et al., 2002; Sharpe et al., 1982). With the palmitoylation inhibitor, 2BP, causing further accumulation of oncogenic Ras in the Golgi body, I would speculate that reovirus induces varying degrees of Golgi fragmentation during the course of its life cycle in NIH3T3 cells. Golgi fragmentation is known to fluctuate from subtle reorganization of the Golgi membranes during cell differentiation and migration to complete fragmentation during mitosis and apoptosis (Yadav and Linstedt, 2011). As such, initial interaction of the viral proteins with the cytoskeleton during factory formation likely contributes to partial Golgi fragmentation. At this point, Ras would still be able to reach the plasma membrane, but it would do so at a reduced rate. The semi-fragmented Golgi body would create a back-log of proteins awaiting palmitoylation and vesicular transport. 2BP treatment is believed to target the Golgi-resident Ras palmitoyl acyltransferase and reduce palmitoylation levels of oncogenic H-Ras by ~20% (Webb et al., 2000); thereby, adding to the pre-existing accumulation of oncogenic Ras during reovirus infection. At later stages of infection, reovirus induces apoptosis; consequently, resulting in further fragmentation of the Golgi body and complete inhibition of vesicular transport.

Based on the above, additional experiments may determine the extent of reovirus-induced Golgi disassembly by examining the individual components of the organelle and observing how they change over the course of infection. To identify which reovirus protein(s) is responsible for inducing fragmentation, expression plasmids encoding for each of the reovirus proteins can be transfected individually, or in combination, into target cells. Furthermore, it would be interesting to add 2BP to reovirus infection at time

points later than 2 hpi. I believe reovirus pathogenesis to be highly regulated and time-dependent. I suspect that 2BP would only enhance reovirus oncolysis when applied to early stages of infection, and not at later time points when apoptosis is induced and Golgi fragmentation is complete.

This is the first study to demonstrate that reovirus causes fragmentation of the Golgi body; however, other viruses have also been linked to disassembly of this organelle. Positive-strand RNA viruses are known to interact with cellular membranes for replication of their genome (Miller and Krijnse-Locker, 2008). For instance, poliovirus and foot-and-mouth disease virus, both of which are members of the Picornaviridae family, cause Golgi body fragmentation during their life cycle (Beske et al., 2007; Zhou et al., 2013). As numerous proteins require the secretory pathway and vesicular transport for efficient processing and localization, it is a novel finding that reovirus oncolysis is so dependent on the specific accumulation of oncogenic Ras in the Golgi. Vaccinia virus, myxomavirus, coxsackievirus B3, and herpes simplex virus (HSV) are other oncolytic viruses that are associated with signalling both up- and downstream of Ras activity (Ilkow et al., 2014). Of these, coxsackievirus and HSV are both known to induce Golgi fragmentation (Alconada et al., 1999; Avitabile et al., 1995; Cornell et al., 2006). Coxsackievirus B3 is also a single-stranded, positive-sense RNA virus from the Picornaviridae family. It disrupts the Golgi body by using its non-structural proteins, 2B, 2BC, and 3A, to inhibit protein trafficking and prevent components of the immune system (i.e. MHC-I, cytokines, and cytokine receptors) from reaching the cell surface (Cornell et al., 2006). Coxsackievirus B3 is linked to Ras activity through its involvement in the PI3K/Akt signalling pathway. The virus activates this pathway for efficient viral

RNA expression (Esfandiarei et al., 2004). On the other hand, HSV is a large double-stranded DNA virus that alters microtubule organization to cause Golgi fragmentation (Alconada et al., 1999; Avitabile et al., 1995). HSV also activates the PI3K/Akt signalling pathway (Cheshenko et al., 2013; Hsu et al., 2010). Similar to the pathways upregulated by reovirus infection, the ICP27 protein of HSV-1 enhances p38 and JNK activation (Hargett et al., 2005). In addition, wild-type HSV-2 is able to activate the Ras/MEK/ERK pathway using the kinase encoded by its *ICP10* gene. Removing the N-terminus of this kinase impairs virus growth in normal cells, but enables the virus to selectively target and lyse tumor cells expressing activated Ras (Filippakis et al., 2010; Fu et al., 2006). With the above viruses implicated in both Ras activity and Golgi fragmentation, it would be interesting to determine if Ras accumulation occurs as part of their pathogenesis, and if it also plays a role in their ability to induce apoptosis of target cells.

4.3. Ras Compartmentalization and Signalling

As previously mentioned, numerous proteins utilize the secretory pathway for proper processing and localization. After identifying that reovirus infection induces accumulation of oncogenic Ras in the Golgi body, I wanted to discern if the movement of Ras, and its resulting activity, was a requirement for reovirus oncolysis. Oncogenic H-RasV12 primarily localizes to the plasma membrane and only cycles back to the Golgi body for re-palmitoylation (Lommerse et al., 2005). Within the plasma membrane, GDP-bound H-Ras is associated with lipid rafts, while activated H-Ras complexes with galectin-1 to form nanoclusters in the bulk plasma membrane (Rotblat et al., 2004, 2010).

Therefore, when considering how to restrict the movement of Ras during reovirus infection, it was important to choose a tether that would mimic its "natural" state. As such, I obtained the previously established CD8-HRasV12xx construct and sub-cloned it into pBABE-puro (Matallanas et al., 2006). CD8-HRasV12xx is known to reside in the bulk plasma membrane, where the active form of H-Ras normally associates. The CD8 transmembrane domain is approximately the same size as Ras, and my previous experience working with HA-tagged oncogenic Ras resulted in cells that exhibited reduced, or absent, transforming potential. Thankfully, under my experimental conditions, the CD8-HRasV12xx construct generated highly transformed cells and activated expected downstream signalling pathways (Figure 3.13). To eliminate any doubt from the addition of a tether, I also utilized the FKBP12 inhibitor, FK506, on non-tethered H-RasV12 cells. As stated earlier, FK506 treatment results in an accumulation of Ras on the plasma membrane, while decreasing Ras levels at the Golgi body (Ahearn et al., 2011); essentially creating a temporary, pseudo-tether of oncogenic Ras. Using this strategy, I was able to restrict oncogenic Ras to the plasma membrane during the narrow time frame of the reovirus life cycle. As expected, FK506 treatment decreased reovirus-induced cell death, which mimicked the results obtained from the plasma membrane tethered CD8-HRasV12xx cells (Figure 3.15 and Figure 3.20).

With the above demonstrating that Ras confined to the plasma membrane at later stages of infection was detrimental to reovirus oncolysis, I speculated on the usefulness of generating a Golgi-restricted Ras cell line. Golgi-tethered constructs are produced through the addition of a mutated KDEL receptor to the N-terminus of Ras (Caloca et al., 2003; Cole et al., 1996). Matallanas et al. (2006) established that Golgi-tethered Ras was

capable of Ral and JNK activation, but did not transform murine fibroblasts. On the other hand, Chiu et al. (2002) showed that Ras tethered to the Golgi complex caused transformation of rodent fibroblasts, and efficiently activated PI3K/Akt and Erk signalling pathways, but not JNK. Unfortunately, the latter study utilized a functional KDEL receptor as its tether; meaning Ras was not specifically restricted to the Golgi body and was capable of shuttling between the ER and Golgi. While Golgi-tethered Ras is beneficial to cell signalling analysis, it does not represent a probable scenario for reovirus infection. Rather than allowing Ras to accumulate in the Golgi as infection progressed, Golgi-tethered Ras would run the risk of generating non-transformed cells and localizing Ras to the Golgi prior to infection; thereby throwing off the balance and timing of the reovirus life cycle. To reinforce this point, 2BP treatment of Ras-transformed cells prior to reovirus infection resulted in lower percentages of cells being infected by the virus (data not shown). The same reasoning applies to knockdown of the Ras palmitoyl acyltransferase, which effectively mimics the H-RasV12xx cell line. To recall, Ras in this non-transformed cell line exists in a dynamic equilibrium between the cytoplasm and ER, and when challenged with reovirus, produced basal levels of virus-related cell death (Figure 3.14 and Figure 3.15). Therefore, when considering other tactics, I feel that the use of CD8-HRasV12xx cells and FK506 treatment were well justified in demonstrating that Ras relocalization from the plasma membrane to the Golgi body is required for efficient reovirus oncolysis.

It is one thing to establish that oncogenic Ras relocalization to the Golgi body is important for reovirus oncolysis. It is another to determine how this relocalization alters the activity of Ras; specifically its signalling to downstream effectors. I originally

contemplated that reovirus would modify Ras signalling to initiate pro-apoptotic signalling pathways required for viral progeny release. Interestingly, this hypothesis ended up being supported through investigation of a lesser known Ras effector, MEKK1. MEKK1 is a kinase that directly interacts with Ras, and similar to other MEK kinase family members, is known to localize to Golgi-associated structures (Fanger et al., 1997; Russell et al., 1995). Once activated, MEKK1 phosphorylates MKK4, which sequentially activates p38/JNK signalling pathways to promote cell apoptosis. Apoptosis-driven MEKK1 activation can occur in response to cytoskeletal interruption, the presence of dsRNA, or binding of TRAIL to its associated death receptor; all of which are involved in reovirus oncolysis (Clarke et al., 2000; Parker et al., 2002; Sharpe et al., 1982; Sun et al., 2011; Tricker et al., 2011; Xia et al., 2000). Furthermore, previous work implicated MEKK1 and JNK activity in reovirus-induced cell death (Clarke et al., 2004); however the exact mechanism remained undetermined until now. My work revealed that cycling Ras, and not its plasma membrane tethered form, was efficient at MKK4 and JNK activation following reovirus infection; an effect which could be further enhanced through the addition of 2BP (Figure 3.24, Figure 3.25, and Figure 3.26). Therefore, all experimental evidence supports the notion that Golgi-associated Ras drives MEKK1 activation, which is critical to reovirus-induced apoptosis of target cancer cells.

4.4. Potential Implications to Oncolytic Virotherapy

Efficient virotherapy is based on the successful delivery of virus to target cells, as well as the dissemination of viral progeny to both neighbouring and distant cancer cells. With Ras being a major constituent in human oncogenesis, this work reinforces the

potential benefits of introducing reovirus into cancer cells specifically expressing constitutively active H-Ras, N-Ras, or K-Ras4A. These isoforms require Golgi-associated enzymes for proper processing and localization, and as a result of reovirus-induced Golgi fragmentation, would be susceptible to accumulation in this organelle. In addition to activating mutations in Ras itself, cancer cells expressing mutated EGFR or members of the Src family of tyrosine kinases can lead to downstream activation of Ras and serve as potential reovirus targets. Furthermore, cancers driven by palmitoylated members of the Src family, such as Lyn, Yes, and Lck are also known to associate with the Golgi body and could possibly accumulate during reovirus infection (Summy and Gallick, 2003). The most frequently detected Ras mutation in human cancers is observed in K-Ras4B. Despite K-Ras4B being palmitoylation null, reovirus may still effectively lyse these cells through their dependency on endogenous, wild-type Ras (Grabocka et al., 2014). In K-Ras4B driven cancers, reovirus-induced Golgi fragmentation would sequester endogenous Ras; likely leading to signal disruption, sensitization of these cells to chemotherapeutic agents, and cell death.

Most would agree that the future of oncolytic virotherapy will occur in the form of combination strategies. Many of the chemotherapeutic agents currently utilized in reovirus clinical trials are known to stabilize microtubules and fragment the Golgi body (Heinemann et al., 2011; Oncolytics Biotech Inc, 2014). Thus far, these trials are well tolerated and generate an effective local response; suggesting that combining reovirus with drugs capable of cytoskeletal interference or Golgi fragmentation would likely produce a synergistic outcome. A recent study, which targeted K-Ras driven pancreatic cancer cells, combined reovirus with pharmacological agents that caused ER-stress

(Carew et al., 2013). While the overall effect was synergistic, the drugs they choose to use (i.e. brefeldin A, tunicamycin, and bortezomib) are also known to induce Golgi fragmentation or inhibit protein palmitoylation (Harada et al., 2003; Resh, 2006; Siddhanta et al., 2003); thereby, supporting my proposed model of reovirus-induced apoptosis. Similar to the action of 2BP, the above drugs are also relatively non-specific, and since bortezomib is being considered for a phase I clinical trial with reovirus, then perhaps, the safety and efficacy of 2BP should be investigated in this manner as well.

As opposed to focusing on Golgi fragmentation, another opportunity for combination therapy is utilizing reovirus with Ras inhibitors. Targeting Ras for cancer therapy has proven difficult, and current avenues stem from interfering with Ras-associated chaperones and modification enzymes (Baines et al., 2011). Specifically, it would be interesting to combine reovirus with Salirasib®, which competes with Ras for galectin binding, and causes Ras to dislodge from the plasma membrane and alter its downstream signalling. In either case, this work reinforces the need for Ras-specific inhibitors, and in particular, those which retain Ras at the Golgi or alter its palmitoylation status. Reovirus is already an effective anti-cancer agent and with this study establishing its mechanism of oncolysis, specific inhibitors can be designed or introduced to further promote its oncolysis and increase its efficacy as a cancer therapeutic.

REFERENCES

Ahearn, I.M., Tsai, F.D., Court, H., Zhou, M., Jennings, B.C., Ahmed, M., Fehrenbacher, N., Linder, M.E., and Philips, M.R. (2011). FKBP12 binds to acylated H-Ras and promotes depalmitoylation. Mol. Cell *41*, 173–185.

Ahearn, I.M., Haigis, K., Bar-Sagi, D., and Philips, M.R. (2012). Regulating the regulator: post-translational modification of RAS. Nat. Rev. Mol. Cell Biol. *13*, 39–51.

Ahmadian, M.R., Zor, T., Vogt, D., Kabsch, W., Selinger, Z., Wittinghofer, A., and Scheffzek, K. (1999). Guanosine triphosphatase stimulation of oncogenic Ras mutants. Proc. Natl. Acad. Sci. *96*, 7065–7070.

Akslen, L.A., Angelini, S., Straume, O., Bachmann, I.M., Molven, A., Hemminki, K., and Kumar, R. (2005). BRAF and NRAS mutations are frequent in nodular melanoma but are not associated with tumor cell proliferation or patient survival. J. Invest. Dermatol. *125*, 312–317.

Alconada, A., Bauer, U., Sodeik, B., and Hoflack, B. (1999). Intracellular traffic of herpes simplex virus glycoprotein gE: characterization of the sorting signals required for its trans-Golgi network localization. J. Virol. *73*, 377–387.

Alvarez-Moya, B., López-Alcalá, C., Drosten, M., Bachs, O., and Agell, N. (2010). K-Ras4B phosphorylation at Ser181 is inhibited by calmodulin and modulates K-Ras activity and function. Oncogene *29*, 5911–5922.

Appels, N.M.G.M., Beijnen, J.H., and Schellens, J.H.M. (2005). Development of farnesyl transferase inhibitors: a review. Oncologist *10*, 565–578.

Arozarena, I., Matallanas, D., Berciano, M.T., Sanz-Moreno, V., Calvo, F., Munoz, M.T., Egea, G., Lafarga, M., and Crespo, P. (2004). Activation of H-Ras in the endoplasmic reticulum by the RasGRF family guanine nucleotide exchange factors. Mol. Cell. Biol. *24*, 1516–1530.

Arozarena, I., Calvo, F., and Crespo, P. (2011). Ras, an actor on many stages: posttranslational modifications, localization, and site-specified events. Genes Cancer *2*, 182–194.

Attoui, H., Biagini, P., Stirling, J., Mertens, P.P., Cantaloube, J.F., Meyer, A., de Micco, P., and de Lamballerie, X. (2001). Sequence characterization of Ndelle virus genome segments 1, 5, 7, 8, and 10: evidence for reassignment to the genus orthoreovirus, family reoviridae. Biochem. Biophys. Res. Commun. *287*, 583–588.

Avitabile, E., Di Gaeta, S., Torrisi, M.R., Ward, P.L., Roizman, B., and Campadelli-Fiume, G. (1995). Redistribution of microtubules and Golgi apparatus in herpes simplex virus-infected cells and their role in viral exocytosis. J. Virol. *69*, 7472–7482.

Babiss, L.E., Luftig, R.B., Weatherbee, J.A., Weihing, R.R., Ray, U.R., and Fields, B.N. (1979). Reovirus serotypes 1 and 3 differ in their in vitro association with microtubules. J. Virol. *30*, 863–874.

Baines, A., Xu, D., and Der, C. (2011). Inhibition of Ras for cancer treatment: the search continues. Future Med. Chem. *3*, 1787–1808.

Baker, T.L., Zheng, H., Walker, J., Coloff, J.L., and Buss, J.E. (2003). Distinct rates of palmitate turnover on membrane-bound cellular and oncogenic H-ras. J. Biol. Chem. *278*, 19292–19300.

Ballester, R., Furth, M.E., and Rosen, O.M. (1987). Phorbol ester- and protein kinase C-mediated phosphorylation of the cellular Kirsten ras gene product. J. Biol. Chem. *262*, 2688–2695.

Barceló, C., Paco, N., Beckett, A.J., Alvarez-Moya, B., Garrido, E., Gelabert, M., Tebar, F., Jaumot, M., Prior, I., and Agell, N. (2013). Oncogenic K-ras segregates at spatially distinct plasma membrane signaling platforms according to its phosphorylation status. J. Cell Sci. *126*, 4553–4559.

Barnier, J. V., Papin, C., Eychene, A., Lecoq, O., and Calothy, G. (1995). The mouse B-raf gene encodes multiple protein isoforms with tissue-specific expression. J. Biol. Chem. *270*, 23381–23389.

Barton, E., Forrest, J., Connolly, J., Chappell, J., Liu, Y., Schnell, F.J., Nusrat, A., Parkos, C.A., and Dermody, T.S. (2001a). Junction adhesion molecule is a receptor for reovirus. Cell *104*, 441–451.

Barton, E.S., Connolly, J.L., Forrest, J.C., Chappell, J.D., and Dermody, T.S. (2001b). Utilization of sialic acid as a coreceptor enhances reovirus attachment by multistep adhesion strengthening. J. Biol. Chem. *276*, 2200–2211.

Basso, A.D., Kirschmeier, P., and Bishop, W.R. (2006). Lipid posttranslational modifications: farnesyl transferase inhibitors. J. Lipid Res. *47*, 15–31.

Becker, M.M., Goral, M.I., Hazelton, P.R., Baer, G.S., Rodgers, S.E., Brown, E.G., Coombs, M., and Dermody, T.S. (2001). Reovirus σNS protein is required for nucleation of viral assembly complexes and formation of viral inclusions. J. Virol. *75*, 1459–1475.

Belanis, L., Plowman, S.J., Rotblat, B., Hancock, J.F., and Kloog, Y. (2008). Galectin-1 is a novel structural component and a major regulator of H-Ras nanoclusters. Mol. Biol. Cell *19*, 1404–1414.

Berger, A.K., and Danthi, P. (2013). Reovirus activates a caspase-independent cell death pathway. MBio *4*, e00178–13.

Bergo, M.O., Leung, G.K., Ambroziak, P., Otto, J.C., Casey, P.J., and Young, S.G. (2000). Targeted inactivation of the isoprenylcysteine carboxyl methyltransferase gene causes mislocalization of K-Ras in mammalian cells. J. Biol. Chem. *275*, 17605–17610.

Bergo, M.O., Gavino, B.J., Hong, C., Beigneux, A.P., McMahon, M., Casey, P.J., and Young, S.G. (2004). Inactivation of Icmt inhibits transformation by oncogenic K-Ras and B-Raf. J. Clin. Invest. *113*, 539–550.

Beske, O., Reichelt, M., Taylor, M.P., Kirkegaard, K., and Andino, R. (2007). Poliovirus infection blocks ERGIC-to-Golgi trafficking and induces microtubule-dependent disruption of the Golgi complex. J. Cell Sci. *120*, 3207–3218.

Bischoff, J.R., and Samuel, C.E. (1989). Mechanism of interferon action activation of the human P1/eIF-2α protein kinase by individual reovirus s-class mRNAs: s1 mRNA is a potent activator relative to s4 mRNA. Virology *172*, 106–115.

Bivona, T.G., Perez de Castro, I., Ahearn, I.M., Grana, T.M., Chiu, V.K., Lockyer, P.J., Cullen, P.J., Pellicer, A., Cox, A.D., and Philips, M.R. (2003). Phospholipase C[gamma] activates Ras on the Golgi apparatus by means of RasGRP1. Nature *424*, 694–698.

Bivona, T.G., Quatela, S.E., Bodemann, B.O., Ahearn, I.M., Soskis, M.J., Mor, A., Miura, J., Wiener, H.H., Wright, L., Saba, S.G., et al. (2006). PKC regulates a farnesyl-electrostatic switch on K-Ras that promotes its association with Bcl-XL on mitochondria and induces apoptosis. Mol. Cell *21*, 481–493.

Blanc, M., Blaskovic, S., and van der Goot, F.G. (2013). Palmitoylation, pathogens and their host. Biochem. Soc. Trans. *41*, 84–88.

Bodkin, D., Nibert, M., and Fields, B. (1989). Proteolytic digestion of reovirus in the intestinal lumens of neonatal mice. J. Virol. *63*, 4676–4681.

Boehme, K.W., Hammer, K., Tollefson, W.C., Konopka-Anstadt, J.L., Kobayashi, T., and Dermody, T.S. (2013). Nonstructural protein σ1s mediates reovirus-induced cell cycle arrest and apoptosis. J. Virol. *87*, 12967–12979.

Borsa, J., Copps, T.P., Sargent, M.D., Long, D.G., and Chapman, J.D. (1973). New intermediate subviral particles in the in vitro uncoating of reovirus virions by chymotrypsin. J. Virol. *11*, 552–564.

Borsa, J., Morash, B.D., Sargent, M.D., Copps, T.P., Lievaart, P. a, and Szekely, J.G. (1979). Two modes of entry of reovirus particles into L cells. J. Gen. Virol. *45*, 161–170.

Bos, J.L. (1989). Ras oncogenes in human cancer : a review. Cancer Res. *49*, 4682–4689.

Boyartchuk, V.L., Ashby, M.N., and Rine, J. (1997). Modulation of ras and a-factor function by carboxyl-terminal proteolysis. Science *275*, 1796–1800.

Bras, M., Queenan, B., and Susin, S.A. (2005). Programmed cell death via mitochondria: different modes of dying. Biochemistry *70*, 231–239.

Burrows, J.F., Kelvin, A.A., McFarlane, C., Burden, R.E., McGrattan, M.J., De la Vega, M., Govender, U., Quinn, D.J., Dib, K., Gadina, M., et al. (2009). USP17 regulates Ras activation and cell proliferation by blocking RCE1 activity. J. Biol. Chem. *284*, 9587–9595.

Bustinza-Linares, E., Kurzrock, R., and Tsimberidou, A.-M. (2010). Salirasib in the treatment of pancreatic cancer. Futur. Oncol. *6*, 885–891.

Cadwallader, K.A., Paterson, H., Macdonald, S.G., and Hancock, J.F. (1994). N-terminally myristoylated Ras proteins require palmitoylation or a polybasic domain for plasma membrane localization. Mol. Cell. Biol. *14*, 4722–4730.

Caloca, M.J., Zugaza, J.L., and Bustelo, X.R. (2003). Exchange factors of the RasGRP family mediate Ras activation in the Golgi. J. Biol. Chem. *278*, 33465–33473.

Calvo, F., Agudo-Ibáñez, L., and Crespo, P. (2010). The Ras-ERK pathway: understanding site-specific signaling provides hope of new anti-tumor therapies. Bioessays *32*, 412–421.

Cantley, L.C. (2002). The phosphoinositide 3-kinase pathway. Science *296*, 1655–1657.

Carew, J.S., Espitia, C.M., Zhao, W., Kelly, K.R., Coffey, M., Freeman, J.W., and Nawrocki, S.T. (2013). Reolysin is a novel reovirus-based agent that induces endoplasmic reticular stress-mediated apoptosis in pancreatic cancer. Cell Death Dis. *4*, e728.

Casey, P.J., Solski, P.A., Der, C.J., and Buss, J.E. (1989). p21ras is modified by a farnesyl isoprenoid. Proc. Natl. Acad. Sci. *86*, 8323–8327.

Castellano, E., and Santos, E. (2011). Functional specificity of ras isoforms: so similar but so different. Genes Cancer *2*, 216–231.

Chandran, K., Farsetta, D.L., and Nibert, M.L. (2002). Strategy for nonenveloped virus entry: a hydrophobic conformer of the reovirus membrane penetration protein mu1 mediates membrane disruption. J. Virol. *76*, 9920–9933.

Chandran, K., Parker, J.S.L., Ehrlich, M., Kirchhausen, T., and Nibert, M.L. (2003). The δ region of outer-capsid protein μ1 undergoes conformational change and release from reovirus particles during cell entry. J. Virol. *77*, 13361–13375.

Cheshenko, N., Trepanier, J.B., Stefanidou, M., Buckley, N., Gonzalez, P., Jacobs, W., and Herold, B.C. (2013). HSV activates Akt to trigger calcium release and promote viral entry: novel candidate target for treatment and suppression. FASEB J. *27*, 2584–2599.

Chien, Y., Kim, S., Bumeister, R., Loo, Y.-M., Kwon, S.W., Johnson, C.L., Balakireva, M.G., Romeo, Y., Kopelovich, L., Gale, M., et al. (2006). RalB GTPase-mediated activation of the IkappaB family kinase TBK1 couples innate immune signaling to tumor cell survival. Cell *127*, 157–170.

Chiu, V.K., Bivona, T., Hach, A., Sajous, J.B., Silletti, J., Wiener, H., Johnson, R.L., Cox, A.D., and Philips, M.R. (2002). Ras signalling on the endoplasmic reticulum and the Golgi. Nat. Cell Biol. *4*, 343–350.

Cho, K.-J., and Hancock, J.F. (2013). Ras nanoclusters: A new drug target? Small GTPases *1*, 57–60.

Choy, E., Chiu, V.K., Silletti, J., Feoktistov, M., Morimoto, T., Michaelson, D., Ivanov, I.E., and Philips, M.R. (1999). Endomembrane trafficking of ras: the CAAX motif targets proteins to the ER and Golgi. Cell *98*, 69–80.

Clarke, P., and Tyler, K. (2007). Down-regulation of cFLIP following reovirus infection sensitizes human ovarian cancer cells to TRAIL-induced apoptosis. Apoptosis *12*, 211–223.

Clarke, P., Meintzer, S.M., Gibson, S., Widmann, C., Garrington, T.P., Johnson, G.L., and Tyler, K.L. (2000). Reovirus-induced apoptosis is mediated by TRAIL. J. Virol. *74*, 8135–8139.

Clarke, P., Meintzer, S.M., Spalding, A.C., Johnson, G.L., and Tyler, K.L. (2001a). Caspase 8-dependent sensitization of cancer cells to TRAIL-induced apoptosis following reovirus-infection. Oncogene *20*, 6910–6919.

Clarke, P., Meintzer, S.M., Widmann, C., Johnson, G.L., and Tyler, K.L. (2001b). Reovirus infection activates JNK and the JNK-dependent transcription factor c-Jun. J. Virol. *75*, 11275–11283.

Clarke, P., Meintzer, S.M., Moffitt, L.A., and Tyler, K.L. (2003). Two distinct phases of virus-induced nuclear factor kappa B regulation enhance tumor necrosis factor-related apoptosis-inducing ligand-mediated apoptosis in virus-infected cells. J. Biol. Chem. *278*, 18092–18100.

Clarke, P., Meintzer, S., and Wang, Y. (2004). JNK regulates the release of proapoptotic mitochondrial factors in reovirus-infected cells. J. Virol. *78*, 13132–13138.

Cleveland, J.L., Jansen, H.W., Bister, K., Fredrickson, T.N., Morse, H.C., Ihle, J.N., and Rapp, U.R. (1986). Interaction between Raf and Myc oncogenes in transformation in vivo and in vitro. J. Cell. Biochem. *30*, 195–218.

Coffey, C.M., Sheh, A., Kim, I.S., Chandran, K., Nibert, M.L., and Parker, J.S.L. (2006). Reovirus outer capsid protein mu1 induces apoptosis and associates with lipid droplets, endoplasmic reticulum, and mitochondria. J. Virol. *80*, 8422–8438.

Coffey, M.C., Strong, J.E., Forsyth, P.A., and Lee, P.W. (1998). Reovirus therapy of tumors with activated Ras pathway. Science *282*, 1332–1334.

Colanzi, A., Suetterlin, C., and Malhotra, V. (2003). Cell-cycle-specific Golgi fragmentation: how and why? Curr. Opin. Cell Biol. *15*, 462–467.

Cole, N.B., Smith, C.L., Sciaky, N., Terasaki, M., Edidin, M., and Lippincott-Schwartz, J. (1996). Diffusional mobility of Golgi proteins in membranes of living cells. Science *273*, 797–801.

Coleman, R.A., Rao, P., Fogelsong, R.J., and Bardes, E.S.-G. (1992). 2-bromopalmitoyl-CoA and 2-bromopalmitate: promiscuous inhibitors of membrane-bound enzymes. Biochim. Biophys. Acta - Lipids Lipid Metab. *1125*, 203–209.

Colicelli, J. (2004). Human RAS superfamily proteins and related GTPases. Sci. STKE *250*, 1–53.

Cooper, J.M., Bodemann, B.O., and White, M.A. (2013). The RalGEF/Ral pathway: evaluating an intervention opportunity for Ras cancers. In Inhibitors of the Ras Superfamily G-Proteins, Part B, F.T. and C.J.D.B.T.-T. Enzymes, ed. (Academic Press), pp. 137–156.

Cornell, C.T., Kiosses, W.B., Harkins, S., and Whitton, J.L. (2006). Inhibition of protein trafficking by coxsackievirus B3: multiple viral proteins target a single organelle. J. Virol. *80*, 6637–6647.

Cowley, S., Paterson, H., Kemp, P., and Marshall, C.J. (1994). Activation of MAP kinase kinase is necessary and sufficient for PC12 differentiation and for transformation of NIH 3T3 cells. Cell *77*, 841–852.

Cox, A.D., and Der, C.J. (2010). Ras history: The saga continues. Small GTPases *1*, 2–27.

Dai, Q., Choy, E., Chiu, V., Romano, J., Slivka, S.R., Steitz, S.A., Michaelis, S., and Philips, M.R. (1998). Mammalian prenylcysteine carboxyl methyltransferase is in the endoplasmic reticulum. J. Biol. Chem. *273*, 15030–15034.

Danthi, P., Pruijssers, A.J., Berger, A.K., Holm, G.H., Zinkel, S.S., and Dermody, T.S. (2010). Bid regulates the pathogenesis of neurotropic reovirus. PLoS Pathog. *6*, e1000980.

Datta, S.R., Dudek, H., Tao, X., Masters, S., Fu, H., Gotoh, Y., and Greenberg, M.E. (1997). Akt phosphorylation of BAD couples survival signals to the cell-intrinsic death machinery. Cell *91*, 231–241.

Davies, H., Bignell, G.R., Cox, C., Stephens, P., Edkins, S., Clegg, S., Teague, J., Woffendin, H., Garnett, M.J., Bottomley, W., et al. (2002). Mutations of the BRAF gene in human cancer. Nature *417*, 949–954.

Dekker, F.J., Rocks, O., Vartak, N., Menninger, S., Hedberg, C., Balamurugan, R., Wetzel, S., Renner, S., Gerauer, M., Schölermann, B., et al. (2010). Small-molecule inhibition of APT1 affects Ras localization and signaling. Nat. Chem. Biol. *6*, 449–456.

De-La Vega, M., Burrows, J.F., McFarlane, C., Govender, U., Scott, C.J., and Johnston, J.A. (2010). The deubiquitinating enzyme USP17 blocks N-Ras membrane trafficking and activation but leaves K-Ras unaffected. J. Biol. Chem. *285*, 12028–12036.

Der, C.J., Krontiris, T.G., and Cooper, G.M. (1982). Transforming genes of human bladder and lung carcinoma cell lines are homologous to the ras genes of Harvey and Kirsten sarcoma viruses. Proc. Natl. Acad. Sci. *79*, 3637–3640.

Diehl, J.A., Cheng, M., Roussel, M.F., and Sherr, C.J. (1998). Glycogen synthase kinase-3beta regulates cyclin D1 proteolysis and subcellular localization. Genes Dev. *12*, 3499–3511.

Drisdel, R.C., Alexander, J.K., Sayeed, A., and Green, W.N. (2006). Assays of protein palmitoylation. Methods *40*, 127–134.

Duncan, J., and Gilman, A. (1998). A cytoplasmic acyl-protein thioesterase that removes palmitate from G protein alpha subunits and p21RAS. J. Biol. Chem. *273*, 15830–15837.

Duncan, M.R., Stanish, S.M., and Cox, D.C. (1978). Differential sensitivity of normal and transformed human cells to reovirus infection. J. Virol. *28*, 444–449.

Ebert, D.H., Deussing, J., Peters, C., and Dermody, T.S. (2002). Cathepsin L and cathepsin B mediate reovirus disassembly in murine fibroblast cells. J. Biol. Chem. *277*, 24609–24617.

Ehrlich, M., Boll, W., Van Oijen, A., Hariharan, R., Chandran, K., Nibert, M.L., and Kirchhausen, T. (2004). Endocytosis by random initiation and stabilization of clathrin-coated pits. Cell *118*, 591–605.

Elad-Sfadia, G., Haklai, R., Balan, E., and Kloog, Y. (2004). Galectin-3 augments K-Ras activation and triggers a Ras signal that attenuates ERK but not phosphoinositide 3-kinase activity. J. Biol. Chem. *279*, 34922–34930.

Esfandiarei, M., Luo, H., Yanagawa, B., Dabiri, D., Zhang, J., and McManus, B.M. (2004). Protein kinase B / Akt regulates coxsackievirus B3 replication through a mechanism which is not caspase dependent. J. Virol. *78*, 4289–4298.

Esteban, L.M., Vicario-Abejón, C., Fernández-Salguero, P., Fernández-Medarde, A., Swaminathan, N., Yienger, K., Lopez, E., Malumbres, M., Mckay, R., Ward, J.M., et al. (2001). Targeted genomic disruption of H-ras and N-ras, individually or in combination, reveals the dispensability of both loci for mouse growth and development. Mol. Cell. Biol. *21*, 1444.

Fan, F., Feng, L., He, J., Wang, X., Jiang, X., Zhang, Y., Wang, Z., and Chen, Y. (2008). RKTG sequesters B-Raf to the Golgi apparatus and inhibits the proliferation and tumorigenicity of human malignant melanoma cells. Carcinogenesis *29*, 1157–1163.

Fanger, G.R., Johnson, N.L., and Johnson, G.L. (1997). MEK kinases are regulated by EGF and selectively interact with Rac/Cdc42. EMBO J. *16*, 4961–4972.

Fehrenbacher, N., Bar-Sagi, D., and Philips, M. (2009). Ras/MAPK signaling from endomembranes. Mol. Oncol. *3*, 297–307.

Feng, L., Xie, X., Ding, Q., Luo, X., He, J., Fan, F., Liu, W., Wang, Z., and Chen, Y. (2007). Spatial regulation of Raf kinase signaling by RKTG. Proc. Natl. Acad. Sci. *104*, 14348–14353.

Fernández-Medarde, A., and Santos, E. (2011). Ras in cancer and developmental diseases. Genes Cancer *2*, 344–358.

Filippakis, H., Spandidos, D.A., and Sourvinos, G. (2010). Herpesviruses: hijacking the Ras signaling pathway. Biochim. Biophys. Acta *1803*, 777–785.

Fivaz, M., and Meyer, T. (2005). Reversible intracellular translocation of KRas but not HRas in hippocampal neurons regulated by Ca2+/calmodulin. J. Cell Biol. *170*, 429–441.

Forsyth, P., Roldán, G., George, D., Wallace, C., Palmer, C.A., Morris, D., Cairncross, G., Matthews, M.V., Markert, J., Gillespie, Y., et al. (2008). A phase I trial of intratumoral administration of reovirus in patients with histologically confirmed recurrent malignant gliomas. Mol. Ther. *16*, 627–632.

Fotiadou, P.P., Takahashi, C., Rajabi, H.N., and Ewen, M.E. (2007). Wild-type NRas and KRas perform distinct functions during transformation. Mol. Cell. Biol. *27*, 6742–6755.

Fu, X., Tao, L., Cai, R., Prigge, J., and Zhang, X. (2006). A mutant type 2 herpes simplex virus deleted for the protein kinase domain of the ICP10 gene is a potent oncolytic virus. Mol. Ther. *13*, 882–890.

Fuchs, S., Adler, V., Pincus, M.R., and Ronai, Z. (1998). MEKK1/JNK signaling stabilizes and activates p53. Proc. Natl. Acad. Sci. *95*, 10541–10546.

García, M.A., Gil, J., Ventoso, I., Guerra, S., Domingo, E., Rivas, C., and Esteban, M. (2006). Impact of protein kinase PKR in cell biology: from antiviral to antiproliferative action. Microbiol. Mol. Biol. Rev. *70*, 1032–1060.

Garcia-Rostan, G., Zhao, H., Camp, R.L., Pollan, M., Herrero, A., Pardo, J., Wu, R., Carcangiu, M.L., Costa, J., and Tallini, G. (2003). Ras mutations are associated with aggressive tumor phenotypes and poor prognosis in thyroid cancer. J. Clin. Oncol. *21*, 3226–3235.

Gentry, L., Samatar, A.A., and Der, C.J. (2013). Inhibitors of the ERK mitogen-activated protein kinase cascade for targeting RAS mutant cancers. In Inhibitors of the Ras Superfamily G-Proteins, Part B, F.T. and C.J.D.B.T.-T. Enzymes, ed. (Academic Press), pp. 67–106.

Golden, J.W., Bahe, J.A., Lucas, W.T., Nibert, M.L., and Schiff, L.A. (2004). Cathepsin S supports acid-independent infection by some reoviruses. J. Biol. Chem. *279*, 8547–8557.

Gomatos, P.J., and Tamm, I. (1963). The secondary structure of reovirus RNA. Biochemistry *49*, 707–714.

Goodwin, J.S., Drake, K.R., Rogers, C., Wright, L., Lippincott-Schwartz, J., Philips, M.R., and Kenworthy, A.K. (2005). Depalmitoylated Ras traffics to and from the Golgi complex via a nonvesicular pathway. J. Cell Biol. *170*, 261–272.

Grabocka, E., Pylayeva-Gupta, Y., Jones, M.J.K., Lubkov, V., Yemanaberhan, E., Taylor, L., Jeng, H.H., and Bar-Sagi, D. (2014). Wild-type H- and N-Ras promote mutant K-Ras-driven tumorigenesis by modulating the DNA damage response. Cancer Cell *25*, 243–256.

Gupta, S., Ramjaun, A.R., Haiko, P., Wang, Y., Warne, P.H., Nicke, B., Nye, E., Stamp, G., Alitalo, K., and Downward, J. (2007). Binding of ras to phosphoinositide 3-kinase p110alpha is required for ras-driven tumorigenesis in mice. Cell *129*, 957–968.

Gutierrez, L., Magee, A.I., Marshall, C.J., and Hancock, J.F. (1989). Post-translational processing of p21ras is two-step and involves carboxyl-methylation and carboxy-terminal proteolysis. EMBO J. *8*, 1093–1098.

Hamad, N.M., Elconin, J.H., Karnoub, A.E., Bai, W., Rich, J.N., Abraham, R.T., Der, C.J., and Counter, C.M. (2002). Distinct requirements for Ras oncogenesis in human versus mouse cells. Genes Dev. *16*, 2045–2057.

Hancock, J.F. (2003). Ras proteins: different signals from different locations. Nat. Rev. Mol. Cell Biol. *4*, 373–384.

Hancock, J.F., and Parton, R.G. (2005). Ras plasma membrane signalling platforms. Biochem. J. *389*, 1–11.

Hancock, J.F., Magee, A.I., Childs, J.E., and Marshall, J. (1989). All ras proteins are polyisoprenylated but only some are palmitoylated. Cell *57*, 1167–1177.

Hancock, J.F., Paterson, H., and Marshall, C.J. (1990). A polybasic domain or palmitoylation is required in addition to the CAAX motif to localize p21ras to the plasma membrane. Cell *63*, 133–139.

Harada, M., Kumemura, H., Bishr Omary, M., Kawaguchi, T., Maeyama, N., Hanada, S., Taniguchi, E., Koga, H., Suganuma, T., Ueno, T., et al. (2003). Proteasome inhibition induces inclusion bodies associated with intermediate filaments and fragmentation of the Golgi apparatus. Exp. Cell Res. *288*, 60–69.

Hargett, D., McLean, T., and Bachenheimer, S.L. (2005). Herpes simplex virus ICP27 activation of stress kinases JNK and p38. J. Virol. *79*, 8348–8360.

Harrington, K.J., Vile, R.G., Melcher, A., Chester, J., and Pandha, H.S. (2010). Clinical trials with oncolytic reovirus: moving beyond phase I into combinations with standard therapeutics. Cytokine Growth Factor Rev. *21*, 91–98.

Hart, K.C., and Donoghue, D.J. (1997). Derivatives of activated H-Ras lacking C-terminal lipid modifications retain transforming ability if targeted to the correct subcellular location. Oncogene *14*, 945–953.

Harvey, J.J. (1964). An unidentified virus which causes the rapid production of tumours in mice. Nature *204*, 1104–1105.

Hashiro, G., Loh, P.C., and Yau, J. (1977). The preferential cytotoxicity of reovirus for certain transformed cell lines. Arch. Virol. *54*, 307–315.

Heinemann, L., Simpson, G.R., Boxall, A., Kottke, T., Relph, K.L., Vile, R., Melcher, A., Prestwich, R., Harrington, K.J., Morgan, R., et al. (2011). Synergistic effects of oncolytic reovirus and docetaxel chemotherapy in prostate cancer. BMC Cancer *11*, 221.

Henry, D.O., Moskalenko, S.A., Kaur, K.J., Fu, M., Pestell, R.G., Camonis, J.H., and White, M.A. (2000). Ral GTPases contribute to regulation of cyclin D1 through activation of NF-kappaB. Mol. Cell. Biol. *20*, 8084–8092.

Hsu, M.-J., Wu, C.-Y., Chiang, H.-H., Lai, Y.-L., and Hung, S.-L. (2010). PI3K/Akt signaling mediated apoptosis blockage and viral gene expression in oral epithelial cells during herpes simplex virus infection. Virus Res. *153*, 36–43.

Hu, H., Bliss, J.M., Wang, Y., and Colicelli, J. (2005). RIN1 is an ABL tyrosine kinase activator and a regulator of epithelial-cell adhesion and migration. Curr. Biol. *15*, 815–823.

Ilkow, C.S., Swift, S.L., Bell, J.C., and Diallo, J.-S. (2014). From scourge to cure: tumour-selective viral pathogenesis as a new strategy against cancer. PLoS Pathog. *10*, e1003836.

Jimenez, C., Hernandez, C., Pimentel, B., and Carrera, A.C. (2002). The p85 regulatory subunit controls sequential activation of phosphoinositide 3-kinase by Tyr kinases and Ras. J. Biol. Chem. *277*, 41556–41562.

Johnson, C.W., and Mattos, C. (2013). The allosteric switch and conformational states in ras GTPase affected by small molecules. In Inhibitors of the Ras Superfamily G-Proteins, Part A, F.T.B.T.-T. Enzymes, ed. (Academic Press), pp. 41–67.

Jura, N., Scotto-Lavino, E., Sobczyk, A., and Bar-Sagi, D. (2006). Differential modification of Ras proteins by ubiquitination. Mol. Cell *21*, 679–687.

Kaelin, W.G. (2005). The concept of synthetic lethality in the context of anticancer therapy. Nat. Rev. Cancer *5*, 689–698.

Kamb, A. (2003). Consequences of nonadaptive alterations in cancer. Mol. Biol. Cell *14*, 2201–2205.

Karapanagiotou, E.M., Roulstone, V., Twigger, K., Ball, M., Tanay, M., Nutting, C., Newbold, K., Gore, M.E., Larkin, J., Syrigos, K.N., et al. (2012). Phase I/II trial of carboplatin and paclitaxel chemotherapy in combination with intravenous oncolytic reovirus in patients with advanced malignancies. Clin. Cancer Res. *18*, 2080–2089.

Karnoub, A.E., and Weinberg, R.A. (2008). Ras oncogenes: split personalities. Nat. Rev. Mol. Cell Biol. *9*, 517–531.

Kennedy, N., and Davis, R. (2002). Role of JNK in tumor development. Cell Cycle *2*, 199–201.

Kim, M., Garant, K.A., zur Nieden, N.I., Alain, T., Loken, S.D., Urbanski, S.J., Forsyth, P.A., Rancourt, D.E., Lee, P.W.K., and Johnston, R.N. (2011). Attenuated reovirus displays oncolysis with reduced host toxicity. Br. J. Cancer *104*, 290–299.

Kim, S.-E., Yoon, J.-Y., Jeong, W.-J., Jeon, S.-H., Park, Y., Yoon, J.-B., Park, Y.N., Kim, H., and Choi, K.-Y. (2009). H-Ras is degraded by Wnt/beta-catenin signaling via beta-TrCP-mediated polyubiquitylation. J. Cell Sci. *122*, 842–848.

Kirsten, W.H., and Mayer, L.A. (1967). Morphologic responses to a murine erythroblastosis virus. J. Natl. Cancer Inst. *39*, 311–335.

Kloog, Y., Elad-Sfadia, G., Haklai, R., and Mor, A. (2013). Ras chaperones: new targets for cancer and immunotherapy. In Inhibitors of the Ras Superfamily G-Proteins, Part A, F.T.B.T.-T. Enzymes, ed. (Elsevier Inc.), pp. 267–289.

Kobayashi, T., Chappell, J.D., Danthi, P., and Dermody, T.S. (2006). Gene-specific inhibition of reovirus replication by RNA interference. J. Virol. *80*, 9053–9063.

Kobayashi, T., Ooms, L.S., Chappell, J.D., and Dermody, T.S. (2009). Identification of functional domains in reovirus replication proteins muNS and mu2. J. Virol. *83*, 2892–2906.

Koera, K., Nakamura, K., Nakao, K., Miyoshi, J., Toyoshima, K., Hatta, T., Otani, H., Aiba, A., and Katsuki, M. (1997). K-ras is essential for the development of the mouse embryo. Oncogene *15*, 1151–1159.

Kominsky, D., Bickel, R., and Tyler, K. (2002a). Reovirus-induced apoptosis requires mitochondrial release of Smac/DIABLO and involves reduction of cellular inhibitor of apoptosis protein levels. J. Virol. *76*, 11414–11424.

Kominsky, D.J., Bickel, R.J., and Tyler, K.L. (2002b). Reovirus-induced apoptosis requires both death receptor- and mitochondrial-mediated caspase-dependent pathways of cell death. Cell Death Differ. *9*, 926–933.

Kranenburg, O., Verlaan, I., and Moolenaar, W.H. (2001). Regulating c-Ras function. cholesterol depletion affects caveolin association, GTP loading, and signaling. Curr. Biol. *11*, 1880–1884.

Lambert, J.M., Lambert, Q.T., Reuther, G.W., Malliri, A., Siderovski, D.P., Sondek, J., Collard, J.G., and Der, C.J. (2002). Tiam1 mediates Ras activation of Rac by a PI(3)K-independent mechanism. Nat. Cell Biol. *4*, 621–625.

Laude, A.J., and Prior, I.A. (2008). Palmitoylation and localisation of RAS isoforms are modulated by the hypervariable linker domain. J. Cell Sci. *121*, 421–427.

Lee, P.W.K., Hayes, E.C., and Joklik, W.K. (1981). Protein sigma 1 is the reovirus cell attachment protein. Virology *108*, 156–163.

Lefebvre, L., Vanderplasschen, A., Ciminale, V., Heremans, H., Dangoisse, O., Jauniaux, J., Toussaint, J.-F., Zelnik, V., Burny, A., Kettmann, R., et al. (2002). Oncoviral bovine leukemia virus G4 and human T-cell leukemia virus type 1 p13 II accessory proteins interact with farnesyl pyrophosphate synthetase. J. Virol. *76*, 1400–1414.

Lemmon, M.A., and Schlessinger, J. (2000). Cell signaling by receptor tyrosine kinases. Cell *141*, 1117–1134.

Leon, J., Guerrero, I., and Pellicer, A. (1987). Differential Expression of the ras Gene Family in Mice. Mol. Cell. Biol. *7*, 1535–1540.

Lin, H.P., Hsu, S.C., Wu, J.C., Sheen, I.J., Yan, B.S., and Syu, W.J. (1999). Localization of isoprenylated antigen of hepatitis delta virus by anti-farnesyl antibodies. J. Gen. Virol. *80*, 91–96.

Linder, M., and Deschenes, R. (2006). Protein palmitoylation. Methods *40*, 125–126.

Lommerse, P.H.M., Snaar-Jagalska, B.E., Spaink, H.P., and Schmidt, T. (2005). Single-molecule diffusion measurements of H-Ras at the plasma membrane of live cells reveal microdomain localization upon activation. J. Cell Sci. *118*, 1799–1809.

Lu, J.-Y., and Hofmann, S.L. (1995). Depalmitoylation of CAAX motif proteins. J. Biol. Chem. *270*, 7251–7256.

Lu, A., Tebar, F., Alvarez-Moya, B., López-Alcalá, C., Calvo, M., Enrich, C., Agell, N., Nakamura, T., Matsuda, M., and Bachs, O. (2009). A clathrin-dependent pathway leads to K-Ras signaling on late endosomes en route to lysosomes. J. Cell Biol. *184*, 863–879.

Maehama, T., and Dixon, J.E. (1998). The tumor suppressor, PTEN/MMAC1, dephosphorylates the lipid second messenger, phosphatidylinositol 3,4,5-trisphosphate. J. Biol. Chem. *273*, 13375–13378.

Magee, A.I., Gutierrez, L., McKay, I.A., Marshall, C.J., and Hall, A. (1987). Dynamic fatty acylation of p21N-ras. EMBO J. *6*, 3353–3357.

Maginnis, M.S., Forrest, J.C., Kopecky-Bromberg, S.A., Dickeson, S.K., Santoro, S.A., Zutter, M.M., Nemerow, G.R., Bergelson, J.M., and Dermody, T.S. (2006). Beta1 integrin mediates internalization of mammalian reovirus. J. Virol. *80*, 2760–2770.

Mainou, B.A., and Dermody, T.S. (2012). Transport to late endosomes is required for efficient reovirus infection. J. Virol. *86*, 8346–8358.

Majeau, N., Fromentin, R., Savard, C., Duval, M., Tremblay, M.J., and Leclerc, D. (2009). Palmitoylation of hepatitis C virus core protein is important for virion production. J. Biol. Chem. *284*, 33915–33925.

Malumbres, M., and Barbacid, M. (2003). RAS oncogenes: the first 30 years. Nat. Rev. Cancer *3*, 459–465.

Marais, R., Light, Y., Paterson, H.F., and Marshall, C.J. (1995). Ras recruits Raf-1 to the plasma membrane for activation by tyrosine phosphorylation. EMBO J. *14*, 3136–3145.

Marcato, P., Shmulevitz, M., Pan, D., Stoltz, D., and Lee, P.W. (2007). Ras transformation mediates reovirus oncolysis by enhancing virus uncoating, particle infectivity, and apoptosis-dependent release. Mol. Ther. *15*, 1522–1530.

Matallanas, D., Sanz-Moreno, V., Arozarena, I., Calvo, F., Agudo-Ibáñez, L., Santos, E., Berciano, M.T., and Crespo, P. (2006). Distinct utilization of effectors and biological outcomes resulting from site-specific ras activation : Ras functions in lipid rafts and golgi complex are dispensable for proliferation and transformation. Mol. Cell. Biol. *26*, 100–116.

Mattingly, R.R. (2013). Activated Ras as a therapeutic target: constraints on directly targeting Ras isoforms and wild-type versus mutated proteins. ISRN Oncol. *2013*, 1–14.

Maurer, T., Garrenton, L.S., Oh, A., Pitts, K., Anderson, D.J., Skelton, N.J., Fauber, B.P., Pan, B., Malek, S., Stokoe, D., et al. (2012). Small-molecule ligands bind to a distinct pocket in Ras and inhibit SOS-mediated nucleotide exchange activity. Proc. Natl. Acad. Sci. *109*, 5299–5304.

Mayinger, P. (2011). Signaling at the Golgi. Cold Spring Harb. Perspect. Biol. *3*, 1–14.

McKay, M.M., and Morrison, D.K. (2007). Integrating signals from RTKs to ERK/MAPK. Oncogene *26*, 3113–3121.

Mendez, I.I., Hermann, L.L., Hazelton, P.R., and Coombs, K.M. (2000). A comparative analysis of Freon substitutes in the purification of reovirus and calicivirus. J. Virol. Methods *90*, 59–67.

Mendez, I.I., Weiner, S.G., She, Y.-M., Yeager, M., and Coombs, K.M. (2008). Conformational changes accompany activation of reovirus RNA-dependent RNA transcription. J. Struct. Biol. *162*, 277–289.

Miller, S., and Krijnse-Locker, J. (2008). Modification of intracellular membrane structures for virus replication. Nat. Rev. Microbiol. *6*, 363–374.

Misaki, R., Morimatsu, M., Uemura, T., Waguri, S., Miyoshi, E., Taniguchi, N., Matsuda, M., and Taguchi, T. (2010). Palmitoylated Ras proteins traffic through recycling endosomes to the plasma membrane during exocytosis. J. Cell Biol. *191*, 23–29.

Mitchell, D.A., Vasudevan, A., Linder, M.E., and Deschenes, R.J. (2006). Protein palmitoylation by a family of DHHC protein S-acyltransferases. J. Lipid Res. *47*, 1118–1127.

Miyake, M., Mizutani, S., Koide, H., and Kaziro, Y. (1996). Unfarnesylated transforming Ras mutant inhibits the Ras-signaling pathway by forming a stable Ras-Raf complex in the cytosol. FEBS Lett. *378*, 15–18.

Mor, A., and Philips, M.R. (2006). Compartmentalized Ras/MAPK signaling. Annu. Rev. Immunol. *24*, 771–800.

Moskalenko, S., Henry, D.O., Rosse, C., Mirey, G., Camonis, J.H., and White, M.A. (2002). The exocyst is a Ral effector complex. Nat. Cell Biol. *4*, 66–72.

Mukherjee, S., Chiu, R., Leung, S.-M., and Shields, D. (2007). Fragmentation of the Golgi apparatus: an early apoptotic event independent of the cytoskeleton. Traffic *8*, 369–378.

Nakashima, S., Morinaka, K., Koyama, S., Ikeda, M., Kishida, M., Okawa, K., Iwamatsu, A., Kishida, S., and Kikuchi, A. (1999). Small G protein Ral and its downstream molecules regulate endocytosis of EGF and insulin receptors. EMBO J. *18*, 3629–3642.

Nancy, V., Callebaut, I., El Marjou, A., and de Gunzburg, J. (2002). The delta subunit of retinal rod cGMP phosphodiesterase regulates the membrane association of Ras and Rap GTPases. J. Biol. Chem. *277*, 15076–15084.

Neel, N.F., Martin, T.D., Stratford, J.K., Zand, T.P., Reiner, D.J., and Der, C.J. (2011). The RalGEF-Ral effector signaling network: the road less traveled for anti-Ras drug discovery. Genes Cancer *2*, 275–287.

Nibert, M.L., Schiff, L.A., and Fields, B.N. (1991). Mammalian reoviruses contain a myristoylated structural protein. J. Virol. *65*, 1960–1967.

Nozawa, K., Casiano, C.A., Hamel, J.C., Molinaro, C., Fritzler, M.J., and Chan, E.K.L. (2002). Fragmentation of Golgi complex and Golgi autoantigens during apoptosis and necrosis. Arthritis Res. *4*, R3.

Oberhaus, S.M., Smith, R.L., Clayton, G.H., Dermody, T.S., and Tyler, K.L. (1997). Reovirus infection and tissue injury in the mouse central nervous system are associated with apoptosis. J. Virol. *71*, 2100–2106.

Oda, K., Okada, J., Timmerman, L., Rodriguez-Viciana, P., Stokoe, D., Shoji, K., Taketani, Y., Kuramoto, H., Knight, Z.A., Shokat, K.M., et al. (2008). PIK3CA cooperates with other phosphatidylinositol 3'-kinase pathway mutations to effect oncogenic transformation. Cancer Res. *68*, 8127–8136.

Ohta, Y., Suzuki, N., Nakamura, S., Hartwig, J.H., and Stossel, T.P. (1999). The small GTPase RalA targets filamin to induce filopodia. Proc. Natl. Acad. Sci. *96*, 2122–2128.

Oncolytics Biotech Inc (2014). Reovirus clinical trials. Http://www.oncolyticsbiotech.com/clinical-Trials/default.aspx.

Otto, J.C., and Casey, P.J. (1996). The hepatitis delta virus large antigen is farnesylated both in vitro and in animal cells. J. Biol. Chem. *271*, 4569–4572.

Parker, J.S.L., Broering, T.J., Kim, J., Higgins, E., and Nibert, M.L. (2002). Reovirus core protein μ2 determines the filamentous morphology of viral inclusion bodies by interacting with and stabilizing microtubules. J. Virol. *76*, 4483–4496.

Pawson, T. (2002). Regulation and targets of receptor tyrosine kinases. Eur. J. Cancer *38*, S3–S10.

Paz, A., Haklai, R., Elad-Sfadia, G., Ballan, E., and Kloog, Y. (2001). Galectin-1 binds oncogenic H-Ras to mediate Ras membrane anchorage and cell transformation. Oncogene *20*, 7486–7493.

Pells, S., Divjak, M., Romanowski, P., Impey, H., Hawkins, N.J., Clarke, A.R., Hooper, M.L., and Williamson, D.J. (1997). Developmentally-regulated expression of murine K-ras isoforms. Oncogene *15*, 1781–1786.

Plowman, S.J., Williamson, D.J., O'Sullivan, M.J., Doig, J., Ritchie, A., Harrison, D.J., Melton, D.W., Arends, M.J., Hooper, M.L., and Patek, C.E. (2003). While K-Ras is essential for mouse development , expression of the K-Ras4A splice variant is dispensable. Mol. Cell. Biol. *23*, 9245.

Plowman, S.J., Ariotti, N., Goodall, A., Parton, R.G., and Hancock, J.F. (2008). Electrostatic interactions positively regulate K-Ras nanocluster formation and function. Mol. Cell. Biol. *28*, 4377–4385.

Poggioli, G.J., Keefer, C., Connolly, J.L., Dermody, T.S., and Tyler, K.L. (2000). Reovirus-induced G2/M cell cycle arrest requires sigma1s and occurs in the absence of apoptosis. J. Virol. *74*, 9562–9570.

Potenza, N., Vecchione, C., Notte, A., De Rienzo, A., Rosica, A., Bauer, L., Affuso, A., De Felice, M., Russo, T., Poulet, R., et al. (2005). Replacement of K-Ras with H-Ras supports normal embryonic development despite inducing cardiovascular pathology in adult mice. EMBO Rep. *6*, 432.

Prior, I.A., and Hancock, J.F. (2001). Compartmentalization of Ras proteins. J. Cell Sci. *114*, 1603–1608.

Prior, I.A., and Hancock, J.F. (2012). Ras trafficking, localization and compartmentalized signalling. Semin. Cell Dev. Biol. *23*, 145–153.

Prior, I.A., Harding, A., Yan, J., Sluimer, J., Parton, R.G., and Hancock, J.F. (2001). GTP-dependent segregation of H-ras from lipid rafts is required for biological activity. Nat. Cell Biol. *3*, 368.

Rabouille, C., Misteli, T., Watson, R., and Warren, G. (1995). Reassembly of Golgi stacks from mitotic Golgi fragments in a cell-free system. J. Cell Biol. *129*, 605–618.

Rajalingam, K., Schreck, R., Rapp, U.R., and Albert, Š. (2007). Ras oncogenes and their downstream targets. Biochim. Biophys. Acta *1773*, 1177–1195.

Rajendran, L., and Simons, K. (2005). Lipid rafts and membrane dynamics. J. Cell Sci. *118*, 1099–1102.

Ramos-Alvarez, M., and Sabin, A.B. (1954). Characteristics of poliomyelitis and other enteric viruses recovered in tissue culture from healthy American children. Proc. Soc. Exp. Biol. Med. *87*, 655–661.

Reiss, K., Stencel, J.E., Liu, Y., Blaum, B.S., Reiter, D.M., Feizi, T., Dermody, T.S., and Stehle, T. (2012). The GM2 glycan serves as a functional coreceptor for serotype 1 reovirus. PLoS Pathog. *8*, e1003078.

Resh, M.D. (2006). Use of analogs and inhibitors to study the functional significance of protein palmitoylation. Methods *40*, 191–197.

Richter, A.M., Pfeifer, G.P., and Dammann, R.H. (2009). The RASSF proteins in cancer; from epigenetic silencing to functional characterization. Biochim. Biophys. Acta *1796*, 114–128.

Rocks, O., Peyker, A., Kahms, M., Verveer, P.J., Koerner, C., Lumbierres, M., Kuhlmann, J., Waldmann, H., Wittinghofer, A., and Bastiaens, P.I.H. (2005). An acylation cycle regulates localization and activity of palmitoylated Ras isoforms. Science *307*, 1746–1752.

Rocks, O., Gerauer, M., Vartak, N., Koch, S., Huang, Z.-P., Pechlivanis, M., Kuhlmann, J., Brunsveld, L., Chandra, A., Ellinger, B., et al. (2010). The palmitoylation machinery is a spatially organizing system for peripheral membrane proteins. Cell *141*, 458–471.

Rodríguez-Escudero, I., Oliver, M.D., Andrés-Pons, A., Molina, M., Cid, V.J., and Pulido, R. (2011). A comprehensive functional analysis of PTEN mutations: implications in tumor- and autism-related syndromes. Hum. Mol. Genet. *20*, 4132–4142.

Rosen, L., Hovis, J.F., Mastrota, F.M., Bell, J.A., and Huebner, R.J. (1960). Observations on a newly recognized virus (Abney) of the reovirus family. Am. J. Hyg. *71*, 258–265.

Rotblat, B., Prior, I.A., Muncke, C., Parton, R.G., Kloog, Y., Henis, Y.I., and Hancock, J.F. (2004). Three separable domains regulate GTP-dependent association of H-ras with the plasma membrane. Mol. Cell. Biol. *24*, 6799–6810.

Rotblat, B., Belanis, L., Liang, H., Haklai, R., Elad-Zefadia, G., Hancock, J.F., Kloog, Y., and Plowman, S.J. (2010). H-Ras nanocluster stability regulates the magnitude of MAPK signal output. PLoS One *5*, e11991.

Roy, S., Wyse, B., and Hancock, J.F. (2002). H-Ras signaling and K-Ras signaling are differentially dependent on endocytosis. Mol. Cell. Biol. *22*, 5128–5140.

Roy, S., Plowman, S., Rotblat, B., Prior, I.A., Muncke, C., Grainger, S., Parton, R.G., Henis, Y.I., Kloog, Y., and Hancock, J.F. (2005). Individual palmitoyl residues serve distinct roles in H-Ras. Mol. Cell. Biol. *25*, 6722–6733.

Russell, M., Lange-Carter, C., and Johnson, G. (1995). Direct interaction between Ras and the kinase domain of mitogen-activated protein kinase kinase kinase (MEKK1). J. Biol. Chem. *270*, 11757–11760.

Russell, S.J., Peng, K.-W., and Bell, J.C. (2012). Oncolytic virotherapy. Nat. Biotechnol. *30*, 658–670.

Sabin, A.B. (1959). Reoviruses: A new group of respiratory formerly classified as ECHO type 10 is described. Science *130*, 1387–1389.

Samuels, Y., and Waldman, T. (2010). Oncogenic mutations of PIK3CA in human cancers. Curr. Top. Microbiol. Immunol. *347*, 21–41.

Santarpia, L., Lippman, S.M., and El-Naggar, A.K. (2012). Targeting the MAPK-RAS-RAF signaling pathway in cancer therapy. Expert Opin. Ther. Targets *16*, 103–119.

Sasaki, A., Carracedo, A., Locasale Jason W., Anastasiou, D., Takeuchi, K., Kahoud, E.R., Haviv, S., Asara, J.M., Pandolfi, P.P., and Cantley, L.C. (2011). Ubiquitination of K-Ras enhances activation and facilitates binding to select downstream effectors. Sci. Signal. *4*, ra13.

Schonberg, M., Silverstein, S.C., Levin, D.H., and Acs, G. (1971). Asynchronous synthesis of the complementary strands of the reovirus genome. Proc. Natl. Acad. Sci. *68*, 505–508.

Schulz, W.L., Haj, A.K., and Schiff, L.A. (2012). Reovirus uses multiple endocytic pathways for cell entry. J. Virol. *86*, 12665–12675.

Shahinian, S., and Silvius, J.R. (1995). Doubly-lipid-modified protein sequence motifs exhibit long-lived anchorage to lipid bilayer membranes. Biochemistry *34*, 3813–3822.

Shalom-Feuerstein, R., Levy, R., Makovski, V., Raz, A., and Kloog, Y. (2008). Galectin-3 regulates RasGRP4-mediated activation of N-Ras and H-Ras. Biochim. Biophys. Acta *1783*, 985–993.

Shalom-Feuerstein, R., Plowman, S.J., Rotblat, B., Ariotti, N., Hancock, J.F., and Kloog, Y. (2009). K-Ras nanoclustering is subverted by over-expression of the scaffold protein galectin-3. *68*, 6608–6616.

Sharma, S. V, Fischbach, M.A., Haber, D.A., and Settleman, J. (2006). "Oncogenic shock": explaining oncogene addiction through differential signal attenuation. Clin. Cancer Res. *12*, 4392s–4395s.

Sharpe, A.H., Chen, L.B., and Fields, B.N. (1982). The interaction of mammalian reoviruses with the cytoskeleton of monkey kidney CV-1 cells. Virology *120*, 399–411.

Sheridan, C., and Downward, J. (2013). Inhibiting the RAS–PI3K pathway in cancer therapy. In Inhibitors of the Ras Superfamily G-Proteins, Part B, F.T. and C.J.D.B.T.-T. Enzymes, ed. (Academic Press), pp. 107–136.

Shimizu, K., Goldfarb, M., Perucho, M., and Wigler, M. (1983). Isolation and preliminary characterization of the transforming gene of a human neuroblastoma cell line. Proc. Natl. Acad. Sci. *80*, 383–387.

Shirakawa, R., Fukai, S., Kawato, M., Higashi, T., Kondo, H., Ikeda, T., Nakayama, E., Okawa, K., Nureki, O., Kimura, T., et al. (2009). Tuberous sclerosis tumor suppressor complex-like complexes act as GTPase-activating proteins for Ral GTPases. J. Biol. Chem. *284*, 21580–21588.

Shmulevitz, M., Salsman, J., and Duncan, R. (2003). Palmitoylation, membrane-proximal basic residues, and transmembrane glycine residues in the reovirus p10 protein are essential for syncytium formation. J. Virol. *77*, 9769–9779.

Shmulevitz, M., Marcato, P., and Lee, P.W.K. (2005). Unshackling the links between reovirus oncolysis, Ras signaling, translational control and cancer. Oncogene *24*, 7720–7728.

Shmulevitz, M., Pan, L., Garant, K., Pan, D., and Lee, P.W.K. (2010). Oncogenic Ras promotes reovirus spread by suppressing IFN-beta production through negative regulation of RIG-I signaling. Cancer Res. *70*, 4912–4921.

Shmulevitz, M., Gujar, S. a, Ahn, D.-G., Mohamed, A., and Lee, P.W.K. (2012). Reovirus variants with mutations in genome segments S1 and L2 exhibit enhanced virion infectivity and superior oncolysis. J. Virol. *86*, 7403–7413.

Siddhanta, A., Radulescu, A., Stankewich, M.C., Morrow, J.S., and Shields, D. (2003). Fragmentation of the Golgi apparatus. A role for beta III spectrin and synthesis of phosphatidylinositol 4,5-bisphosphate. J. Biol. Chem. *278*, 1957–1965.

Silic-Benussi, M., Marin, O., Biasiotto, R., D'Agostino, D.M., and Ciminale, V. (2010). Effects of human T-cell leukemia virus type 1 (HTLV-1) p13 on mitochondrial K+ permeability: A new member of the viroporin family? FEBS Lett. *584*, 2070–2075.

Singh, A., Greninger, P., Rhodes, D., Koopman, L., Violette, S., Bardeesy, N., and Settleman, J. (2009). A gene expression signature associated with "K-Ras addiction" reveals regulators of EMT and tumor cell survival. Cancer Cell *15*, 489–500.

Smakman, N., Veenendaal, L.M., van Diest, P., Bos, R., Offringa, R., Borel Rinkes, I.H.M., and Kranenburg, O. (2005). Dual effect of Kras(D12) knockdown on tumorigenesis: increased immune-mediated tumor clearance and abrogation of tumor malignancy. Oncogene *24*, 8338–8342.

Smith, R.E., Zweerink, H.J., and Joklik, W.K. (1969). Polypeptide components of virions, top component and cores of reovirus type 3. Virology *39*, 791–810.

Smith, S.C., Baras, A.S., Owens, C.R., Dancik, G., and Theodorescu, D. (2012). Transcriptional signatures of Ral GTPase are associated with aggressive clinicopathologic characteristics in human cancer. Cancer Res. *72*, 3480–3491.

Stanley, N.F. (1961). Reovirus -- a ubiquitous orphan. Med. J. Aust. *48*, 815–818.

Stickney, B.J.T., Booden, M.A., and Buss, J.E. (2001). Targeting proteins to membranes, using signal sequences for lipid modifications. In Methods in Enzymology, Vol. 332, Part F: Regulators and Effectors of Small GTPases, (Academic Press), pp. 64–77.

Storrie, B., and Yang, W. (1998). Dynamics of the interphase mammalian Golgi complex as revealed through drugs producing reversible Golgi disassembly. Biochim. Biophys. Acta *1404*, 1271–37.

Strong, J.E., and Lee, P.W. (1996). The v-erbB oncogene confers enhanced cellular susceptibility to reovirus infection. J. Virol. *70*, 612–616.

Strong, J.E., Tang, D., and Lee, P.W.K. (1993). Evidence that the epidermal growth factor receptor on host cells confers reovirus infection efficiency. Virology *197*, 405–411.

Strong, J.E., Coffey, M.C., Tang, D., Sabinin, P., and Lee, P.W.K. (1998). The molecular basis of viral oncolysis: usurpation of the Ras signaling pathway by reovirus. EMBO J. *17*, 3351–3362.

Sturzenbecker, L.J., Nibert, M., Furlong, D., and Fields, B.N. (1987). Intracellular digestion of reovirus particles requires a low pH and is an essential step in the viral infectious cycle. J. Virol. *61*, 2351–2361.

Summy, J.M., and Gallick, G.E. (2003). Src family kinases in tumor progression and metastasis. Cancer Metastasis Rev. *22*, 337–358.

Sun, B.K., Kim, J.-H., Nguyen, H.N., Oh, S., Kim, S.Y., Choi, S., Choi, H.J., Lee, Y.J., and Song, J.J. (2011). MEKK1/MEKK4 are responsible for TRAIL-induced JNK/p38 phosphorylation. Oncol. Rep. *25*, 537–544.

Sung, P.J., Tsai, F.D., Vais, H., Court, H., Yang, J., Fehrenbacher, N., Foskett, J.K., and Philips, M.R. (2013). Phosphorylated K-Ras limits cell survival by blocking Bcl-xL sensitization of inositol trisphosphate receptors. Proc. Natl. Acad. Sci. *110*, 20593–20598.

Swarthout, J.T., Lobo, S., Farh, L., Croke, M.R., Greentree, W.K., Deschenes, R.J., and Linder, M.E. (2005). DHHC9 and GCP16 constitute a human protein fatty acyltransferase with specificity for H- and N-ras. J. Biol. Chem. *280*, 31141–31148.

Swift, a M., and Machamer, C.E. (1991). A Golgi retention signal in a membrane-spanning domain of coronavirus E1 protein. J. Cell Biol. *115*, 19–30.

Takeda, M., Leser, G.P., Russell, C.J., and Lamb, R.A. (2003). Influenza virus hemagglutinin concentrates in lipid raft microdomains for efficient viral fusion. Proc. Natl. Acad. Sci. *100*, 14610–14617.

Tamanoi, F., and Lu, J. (2013). Recent progress in developing small molecule inhibitors designed to interfere with Ras membrane association: toward inhibiting K-Ras and N-Ras functions. In Inhibitors of the Ras Superfamily G-Proteins, Part B, F.T. and C.J.D.B.T.-T. Enzymes, ed. (Academic Press), pp. 181–200.

Taveras, A.G., Remiszewski, S.W., Doll, R.J., Cesarz, D., Huang, E.C., Kirschmeier, P., Pramanik, B.N., Snow, M.E., Wang, Y.-S., del Rosario, J.D., et al. (1997). Ras oncoprotein inhibitors: the discovery of potent, Ras nucleotide exchange inhibitors and the structural determination of a drug-protein complex. Bioorg. Med. Chem. *5*, 125–133.

Thirukkumaran, C.M., Nodwell, M.J., Hirasawa, K., Shi, Z.-Q., Diaz, R., Luider, J., Johnston, R.N., Forsyth, P.A., Magliocco, A.M., Lee, P., et al. (2010). Oncolytic viral therapy for prostate cancer: efficacy of reovirus as a biological therapeutic. Cancer Res. *70*, 2435–2444.

Thissen, J.A., Gross, J.M., Subramanian, K., Meyer, T., and Casey, P.J. (1997). Prenylation-dependent association of Ki-Ras with microtubules: Evidence for a role in subcellular trafficking. J. Biol. Chem. *272*, 30362–30370.

Tian, T., Harding, A., Inder, K., Plowman, S., Parton, R.G., and Hancock, J.F. (2007). Plasma membrane nanoswitches generate high-fidelity Ras signal transduction. Nat. Cell Biol. *9*, 905–914.

Tillotson, L., and Shatkin, A.J. (1992). Reovirus polypeptide sigma3 and N-terminal myristoylation of polypeptide mu1 are required for site-specific cleavage to mu1C in transfected cells. J. Virol. *66*, 2180–2186.

Torti, D., and Trusolino, L. (2011). Oncogene addiction as a foundational rationale for targeted anti-cancer therapy: promises and perils. EMBO Mol. Med. *3*, 623–636.

Tricker, E., Arvand, A., Kwan, R., Chen, G.Y., Gallagher, E., and Cheng, G. (2011). Apoptosis induced by cytoskeletal disruption requires distinct domains of MEKK1. PLoS One *6*, e17310.

Tsai, F.-M., Shyu, R.-Y., and Jiang, S.-Y. (2006). RIG1 inhibits the Ras/mitogen-activated protein kinase pathway by suppressing the activation of Ras. Cell. Signal. *18*, 349–358.

Tucker, T.J., Abrams, M.T., Buser, C.A., Davide, J.P., Ellis-Hutchings, M., Fernandes, C., Gibbs, J.B., Graham, S.L., Hartman, G.D., Huber, H.E., et al. (2002). The synthesis and biological evaluation of a series of potent dual inhibitors of farnesyl and geranyl-geranyl protein transferases. Bioorg. Med. Chem. Lett. *12*, 2027–2030.

Tyler, K., Squier, M., Brown, A., Pike, B., Willis, D., Oberhaus, S.M., Dermody, T.S., and Cohen, J.J. (1996). Linkage between reovirus-induced apoptosis and inhibition of cellular DNA synthesis: role of the S1 and M2 genes. J. Virol. *70*, 7984–7991.

Tyler, K.L., Squier, M.K., Rodgers, S.E., Schneider, B.E., Oberhaus, S.M., Grdina, T.A., Cohen, J.J., and Dermody, T.S. (1995). Differences in the capacity of reovirus strains to induce apoptosis are determined by the viral attachment protein sigma 1. J. Virol. *69*, 6972–6979.

Veit, M. (2012). Palmitoylation of virus proteins. Biol. Cell *104*, 493–515.

Velho, S., Oliveira, C., Ferreira, A., Ferreira, A.C., Suriano, G., Schwartz, S., Duval, A., Carneiro, F., Machado, J.C., Hamelin, R., et al. (2005). The prevalence of PIK3CA mutations in gastric and colon cancer. Eur. J. Cancer *41*, 1649–1654.

Vidal, L., Pandha, H.S., Yap, T.A., White, C.L., Twigger, K., Vile, R.G., Melcher, A., Coffey, M., Harrington, K.J., and DeBono, J.S. (2008). A phase I study of intravenous oncolytic reovirus type 3 Dearing in patients with advanced cancer. Clin. Cancer Res. *14*, 7127–7137.

Vigil, D., Cherfils, J., Rossman, K., and Der, C. (2010). Ras superfamily GEFs and GAPs: validated and tractable targets for cancer therapy? Nat. Rev. Cancer *10*, 842–857.

Wagner, R., Herwig, A., Azzouz, N., and Klenk, H.D. (2005). Acylation-mediated membrane anchoring of avian influenza virus hemagglutinin is essential for fusion pore formation and virus infectivity. J. Virol. *79*, 6449–6458.

Wahlstrom, A.M., Cutts, B.A., Liu, M., Lindskog, A., Karlsson, C., Sjogren, A.-K.M., Andersson, K.M.E., Young, S.G., and Bergo, M.O. (2008). Inactivating Icmt ameliorates K-RAS induced myeloproliferative disease. Blood *112*, 1357–1365.

Wang, Y., and Seemann, J. (2011). Golgi biogenesis. Cold Spring Harb. Perspect. Biol. *3*, a005330.

Wang, M., Tan, W., Zhou, J., Leow, J., Go, M., Lee, H.S., and Casey, P.J. (2008). A small molecule inhibitor of isoprenylcysteine carboxymethyltransferase induces autophagic cell death in PC3 prostate cancer cells. J. Biol. Chem. *283*, 18678–18684.

Wang, M., Hossain, M.S., Tan, W., Coolman, B., Zhou, J., Liu, S., and Casey, P.J. (2010). Inhibition of isoprenylcysteine carboxylmethyltransferase induces autophagic-dependent apoptosis and impairs tumor growth. Oncogene *29*, 4959–4970.

Wang, Y., You, M., and Wang, Y. (2001). Alternative splicing of the K-ras gene in mouse tissues and cell lines. Exp. Lung Res. *27*, 255–267.

Wang, Y., Waldron, R.T., Dhaka, A., Patel, A., Riley, M.M., Rozengurt, E., and Colicelli, J. (2002). The RAS effector RIN1 directly competes with RAF and is regulated by 14-3-3 proteins. Mol. Cell. Biol. *22*, 916–926.

Ward, R.L., McNeal, M.M., Farone, M.B., and Farone, A.L. (2007). Reoviridae. In The Mouse in Biomedical Research, 2nd Edition, pp. 235–267.

Webb, Y., Hermida-Matsumoto, L., and Resh, M.D. (2000). Inhibition of protein palmitoylation, raft localization, and T cell signaling by 2-bromopalmitate and polyunsaturated fatty acids. J. Biol. Chem. *275*, 261–270.

Wennerberg, K., Rossman, K.L., and Der, C.J. (2005). The Ras superfamily at a glance. J. Cell Sci. *118*, 843–846.

Whyte, D.B., Kirschmeier, P., Hockenberry, T.N., Nunez-Oliva, I., James, L., Catino, J.J., Bishop, W.R., and Pai, J.-K. (1997). K- and N-Ras are geranylgeranylated in cells treated with farnesyl protein transferase inhibitors. J. Biol. Chem. *272*, 14459–14464.

Winter-Vann, A.M., Baron, R.A., Wong, W., dela Cruz, J., York, J.D., Gooden, D.M., Bergo, M.O., Young, S.G., Toone, E.J., and Casey, P.J. (2005). A small-molecule inhibitor of isoprenylcysteine carboxyl methyltransferase with antitumor activity in cancer cells. Proc. Natl. Acad. Sci. *102*, 4336–4341.

Wisniewski, M.L., Werner, B.G., Hom, L.G., Anguish, L.J., Coffey, C.M., and Parker, J.S.L. (2011). Reovirus infection or ectopic expression of outer capsid protein mu1 induces apoptosis independently of the cellular proapoptotic proteins Bax and Bak. J. Virol. *85*, 296–304.

Wohlgemuth, S., Kiel, C., Krämer, A., Serrano, L., Wittinghofer, F., and Herrmann, C. (2005). Recognizing and defining true Ras binding domains I: biochemical analysis. J. Mol. Biol. *348*, 741–758.

Wolfman, J.C., and Wolfman, A. (2000). Endogenous c-N-Ras provides a steady-state anti-apoptotic signal. J. Biol. Chem. *275*, 19315–19323.

Wolfman, J.C., Planchon, S.M., Liao, J., and Wolfman, A. (2006). Structural and functional consequences of c-N-Ras constitutively associated with intact mitochondria. Biochim. Biophys. Acta *1763*, 1108–1124.

Wortzel, I., and Seger, R. (2011). The ERK cascade: distinct functions within various subcellular organelles. Genes Cancer *2*, 195–209.

Xia, Y., Makris, C., Su, B., Li, E., Yang, J., Nemerow, G.R., and Karin, M. (2000). MEK kinase 1 is critically required for c-Jun N-terminal kinase activation by proinflammatory stimuli and growth factor-induced cell migration. Proc. Natl. Acad. Sci. *97*, 5243–5248.

Xu, L., Lubkov, V., Taylor, L.J., and Bar-Sagi, D. (2010). Feedback regulation of Ras signaling by Rabex-5-mediated ubiquitination. Curr. Biol. *20*, 1372–1377.

Yadav, S., and Linstedt, A.D. (2011). Golgi positioning. Cold Spring Harb. Perspect. Biol. *3*, a005322.

Yamakawa, M., Furuichi, Y., and Shatkin, A.J. (1982). Reovirus transcriptase and capping enzymes are active in intact virions. Virology *118*, 157–168.

Yan, J., Roy, S., Apolloni, A., Lane, A., and Hancock, J.F. (1998). Ras isoforms vary in their ability to activate Raf-1 and phosphoinositide 3-kinase. J. Biol. Chem. *273*, 24052–24056.

Zhou, Z., Mogensen, M.M., Powell, P.P., Curry, S., and Wileman, T. (2013). Foot-and-mouth disease virus 3C protease induces fragmentation of the Golgi compartment and blocks intra-Golgi transport. J. Virol. *87*, 11721–11729.